Fakultät für Medizin

Institut für Virologie

Role of the immunosuppressive environment during the course of a hepatitis B virus infection

Stefanie Graf

Vollständiger Abdruck der von der Fakultät für Medizin der Technischen Universität München zur Erlangung des akademischen Grades eines

Doktors der Naturwissenschaften

genehmigten Dissertation.

Vorsitzende(r): Univ.-Prof. Dr. P. A. Knolle

Prüfer der Dissertation:

1. Univ.-Prof. Dr. U. Protzer

2. Univ.-Prof. Dr. I. Antes

Die Dissertation wurde am 29.04.2015 bei der Technischen Universität München eingereicht und durch die Fakultät für Medizin am 15.07.2015 angenommen.

For my parents

Index

Zusammenfassung **VIII**

Summary **X**

List of abbreviations **XII**

1 Introduction **16**

1.1 Hepatitis B virus **16**

1.1.1 HBV classification and replication cycle 17

1.1.1.1 HBcAg 21

1.1.2 Clinical course of HBV infection 22

1.1.3 Animal models used in HBV research 23

1.1.3.1 AdHBV mouse model 24

1.2 Immune response against HBV **26**

1.2.1 NK and NKT cells 27

1.2.2 Antigen presenting cells 28

1.2.2.1 Mechanisms of antigen presentation 29

1.2.2.2 Variety of MHC molecules 30

1.2.2.3 HBV epitopes 31

1.2.3 $CD4^+$ T cells and $CD8^+$ T cells 32

1.2.4 Tregs 33

1.2.5 IL-10 34

1.3 Aim of this thesis **36**

2 Material and methods **38**

2.1 Material **38**

2.1.1 Instruments 38

2.1.2 Software 39

2.1.3 Consumables 40

2.1.4 Chemicals and reagents 41

2.1.5 Buffers 42

2.1.6 Medium and supplement consumables 43

2.1.7 Medium for human cells 44

2.1.8 Medium for murine cells 45

2.1.9 Antibodies 45

2.1.10 Peptide-MHC multimers 46
2.1.11 Kits 47
2.1.12 Peptides and full proteins 47
2.1.13 Primers and PCR conditions for qPCR analysis 49
2.1.14 Primers and PCR conditions for ITIB and DEREG/ITIB genotyping 50
2.1.15 Mouse lines 51
2.1.15.1 Wild type mice 51
2.1.15.2 DEREG mice 51
2.1.15.3 ITIB mice 51
2.1.15.4 DEREG/ITIB mice 52
2.1.16 Ad vectors 52
2.2 Methods 54
2.2.1 Cell culture methods 54
2.2.2 Production of Ad vector stocks 54
2.2.3 Mice experiments 55
2.2.3.1 Injection 55
2.2.3.2 Bleeding 56
2.2.3.3 Screen of DEREG and DEREG/ITIB mice 56
2.2.3.4 Genotyping of ITIB and DEREG/ITIB mice 56
2.2.3.5 Depletion of Tregs 57
2.2.3.6 Dissection and processing of organs 57
2.2.3.7 Isolation of liver-associated lymphocytes 57
2.2.3.8 Isolation of splenocytes 57
2.2.3.9 Adoptive T cell transfer 58
2.2.3.10 Ex vivo peptide stimulation 58
2.2.3.11 IL-10 reporter reaction 58
2.2.3.12 Quantitative real time PCR 59
2.2.3.13 Serological analysis 60
2.2.4 Co-culture study 61
2.2.4.1 Isolation of PBMC populations 61
2.2.4.2 Maturation of monocyte derived macrophages 62
2.2.4.3 Maturation of monocyte derived DC 62
2.2.4.4 Transduction of T cells 62
2.2.4.5 Stimulation and co-culture 63
2.2.4.6 Enzyme-linked immunosorbent assay 64
2.2.5 Flow Cytometry 64
2.2.5.1 Live/dead staining 64
2.2.5.2 Surface staining 65

2.2.5.3 Intracellular cytokine staining 65
2.2.5.4 Peptide-MHC multimer staining 66

3 Results 67
3.1 T cell priming by *in vitro* HBcAg stimulated APC 67
3.1.1 T cell activation after co-culture with stimulated APC 69
3.1.2 T cell effector function 71
3.2 Detection of Ad and HBV specific T cell responses 73
3.2.1 Epitope prediction of Ad and HBV epitopes 74
3.2.2 Detection of Ad specific T cell response during AdHBVx- infection 76
3.2.3 Detection of HBV specific T cell response during AdHBVx- infection 78
3.3 Role of Tregs and IL-10 production during AdHBVx- infection 85
3.3.1 Kinetics of IL-10 production during AdHBVx- infection 85
3.3.1.1 Kinetics of leukocyte counts during AdHBVx- infection 87
3.3.1.2 Kinetics of IL-10$^+$ leukocyte populations during AdHBVx- infection 91
3.3.1.3 Kinetics of IL-10 production on single cell level 93
3.3.2 Adoptive Treg transfer in DEREG/ITIB mice 95
3.3.2.1 Adoptive Treg transfer in Treg depleted DEREG/ITIB mice 97
3.3.2.2 IL-10 percentages and counts after adoptive Treg transfer 98
3.3.2.3 Serology and cytokine expression after adoptive Treg transfer 102

4 Discussion 104
4.1 T cell priming by *in vitro* HBcAg stimulated APC 104
4.2 Detection of Ad and HBV specific T cell responses 107
4.2.1 Identification of a new Ad hexon epitope by epitope prediction 108
4.2.2 Identification of a new HBcAg epitope 108
4.2.3 Low percentages of IFNγ$^+$ CD8$^+$ T cells 110
4.2.4 Cross-reactivity between HBV and Ad 111
4.2.5 Obstacles with Ad vectors 112
4.3 Role of Tregs and IL-10 production during AdHBVx- infection 114
4.3.1 Course of an acute AdHBVx- infection 114
4.3.2 Kinetic of IL-10 production during AdHBVx- infection 116
4.3.3 Adoptive transfer of Tregs in AdHBVx- infected DEREG/ITIB mice 119

5 Bibliography 124

6 Appendix 139
6.1 Peptides of HBc P1, HBc P2, HBc P3 139
6.2 Epitope prediction results of HBc P5 140

6.3 Sequences used for epitope prediction 141
6.3.1 Protein sequence of Ad hexon 141
6.3.2 Protein sequence of HBcAg 141
6.3.3 Protein sequence of HBsAg 142
6.4 Sequence alignments of HBcAg and pp65 protein 143
6.4.1 Sequence alignment of HBc_C18 peptide with pp65 protein 143
6.4.2 Sequence alignment of HBcAg protein with pp65 protein 144
7 Acknowledgement 145

Zusammenfassung

Das Hepatitis B Virus (HBV) ist ein behülltes Virus, das ein partiell doppelsträngiges DNA-Genom von 3.200 Basenpaaren innerhalb eines ikosaedralen Kapsids enthält. Nach der parenteralen Übertragung über Blut oder andere Körperflüssigkeiten verursacht HBV eine akute oder chronische Hepatitis B Infektion, die sich zu einer Leberzirrhose oder einem hepatozellulären Karzinom weiterentwickeln kann. Durch weltweit 240 Millionen chronisch infizierte Menschen und jährlich 780.000 durch HBV verursachte Todesfälle stellen Infektionen mit HBV ein großes Gesundheitsproblem dar. Als Ursache für die Entstehung der chronischen Hepatitis B Infektion gilt eine unzureichende HBV-spezifische T-Zellantwort, wessen zugrunde liegenden Mechanismen mithilfe von unterschiedlichen HBV-Modellen aufzuklären versucht werden.

Frühere Studien lieferten Indizien dafür, dass B Zellen in der Lage sind externe Antigene wie das HBV Kapsid zu internalisieren und zu präsentieren. Weitere Studien zeigten, dass HBV Kapside aus apoptotischen Hepatozyten freigesetzt werden und dass zudem ein Fehlen des CD95 Apoptoseweges die Aktivierung der HBV Immunantwort verhindert. Auf dieser Grundlage wurde in dem ersten Teil dieser Dissertation das Potenzial von HBV Kapsiden zur Aktivierung von T-Zellen in einer *in vitro* Co-Kultivierungsstudie untersucht. Die Funktionalität des Assays wurde durch die erfolgreiche T-Zellaktivierung durch kapsid-stimulierte Dendritische Zellen (DC) bestätigt. Im Gegensatz dazu führte die Co-Kultivierung von kapsidstimulierten B-Zellen zu keiner Aktivierung der T-Zellen. Dieses Ergebnis stimmt mit dem allgemeinen Verständnis von DC als den wichtigsten antigen-präsentierenden Zellen zur T-Zellaktivierung während einer natürlichen HBV Infektion überein.

HBV hat einen engen Wirtstropismus, sodass neben Menschen nur Menschenaffen und Spitzhörnchen infiziert werden. Durch die Verwendung eines adenoviralen (Ad) Vektors, der ein 1,3-faches Überlängengenom von HBV enthält, kann das AdHBV Mausmodel die Artengrenze überwinden und ermöglicht dadurch die Untersuchung der Immunantwort während einer selbstlimitierend verlaufenden akuten Hepatitis B Infektion im Kleintier-modell. Um die T-Zellantwort während einer AdHBVx- Infektion untersuchen zu können, sind präzise Kenntnisse von immundominanten spezifischen Epitopen notwendig, welche die separate Analyse der HBV- und Ad-spezifischen T-Zellantwort ermöglicht. Da solche Epitope für dieses Model bisher nicht identifiziert wurden, befasste sich der zweite Teil dieser

Dissertation mit der Identifizierung von HBV- und Ad-spezifischen T-Zellepitopen in AdHBVx- infizierten Mäusen. Unter Verwendung von Programmen zur Vorhersage von Epitopen konnte das neue immundominante Epitop des Ad Hexonproteins ‚RNFLYSNI' an der Aminosäureposition 470–477 identifiziert werden. Zudem konnten durch das Testen verschiedener Peptidpools, welche aus überlappenden Peptiden des ‚hepatitis B virus core antigens' (HBcAg) bestehen, immunogene HBcAg Peptide identifiziert werden. Die Kenntnis dieser HBcAg und Ad Hexon Peptide ermöglicht künftig die separate Analyse von HBV- und Ad-spezifischen T-Zellantworten in dem AdHBVx- Mausmodell.

Während einer HBV Infektion schwächt die immunsuppressive Umgebung der Leber massive Gewebeschäden ab, welche durch die antivirale Immunantwort des Wirts verursacht werden. In dem dritten Teil dieser Dissertation wurde die Rolle des antientzündlichen Zytokins Interleukin (IL)-10 bei dem Entgegenwirken der auftretenden Immunpathogenese untersucht. Mithilfe einer IL-10 Reportermaus wurde die Kinetik der IL-10 Produktion in verschiedenen Leukozytenpopulationen während einer akuten AdHBVx- Infektion untersucht. An Tag fünf nach Infektionsstart korrelierte der auftretende Leberschaden mit einer starken Infiltration von antigenunspezifischen mononukleären Zellen, wovon $CD8^+$ T-Zellen und B-Zellen als die Hauptproduzenten von IL-10 identifiziert wurden. Des Weiteren wurde die Rolle von regulatorischen T Zellen (Treg) in der Regulation der IL-10 Produktion von Zellen der angeborenen und adaptiven Immunantwort in neu gezüchteten DEREG/ITIB Mäusen untersucht, welche die Untersuchung der IL-10 Produktionslevel in An- und Abwesenheit von Tregs ermöglichen. Der adoptive Treg-Transfer in AdHBVx- infizierte Mäuse mit vorheriger Depletion von Tregs, zeigte, dass die Anwesenheit von Tregs zu Beginn der Infektion eine essentielle Voraussetzung für die Rekrutierung von Leukozyten in die Leber ist. Darüber hinaus wurde gezeigt, dass die Abwesenheit von Tregs die IL-10 Produktion von $CD8^+$ T-Zellen und $CD4^+$ T-Zellen, jedoch nicht die von Monozyten und Makrophagen, beeinträchtigt. Die verminderte IL-10 Produktion von $CD8^+$ T-Zellen sowie $CD4^+$ T-Zellen konnte durch einen adoptiven Transfer von Tregs behoben werden. Dieses Ergebnis indiziert, dass die zu Beginn der Infektion anwesenden Tregs eher Einfluss auf die Zellen des adaptiven als auf die des angeborenen Immunsystems ausüben.

Zusammenfassend ermöglichen die Ergebnisse dieser Dissertation die separate Analyse der HBV- und Ad-spezifischen T-Zellantwort während einer AdHBVx- Infektion, sowie liefern sie neue Erkenntnisse über die durch Treg-vermittelte Regulation der IL-10 Produktion zur Abschwächung der antiviralen Immunantwort.

Summary

The hepatitis B virus (HBV) is an enveloped virus with an icosahedral capsid that contains the partially double stranded DNA genome of 3,200 base pairs. HBV is transmitted parenterally via infected blood or other body fluids inducing an acute or chronic viral hepatitis B infection, which can progress to liver cirrhosis or hepatocellular carcinoma. The world health organization reports of annually 780,000 HBV related deaths and of more than 240 million people, which are chronically infected with HBV worldwide. In order to address the health burden that is caused by HBV, more research is needed to elucidate the interactions of HBV with the host immune system in order to provide a good basis for the development of new and more effective treatment strategies.

Previous studies have shown that B cells are able to take up and present external antigens like HBV capsids. Further studies provide evidence that HBV capsids are released from apoptotic hepatocytes and that ablation of the CD95 pathway of apoptosis prevents the induction of the anti-HBV immune response. Therefore, the potential of HBV capsids in T cell priming was examined in an *in vitro* co-culture study in the first part of this thesis. The functionality of the assay was demonstrated, as capsid stimulated dendritic cells (DC) successfully primed T cells. To the contrary, co-culture of capsid stimulated B cells with T cells did not result in T cell priming, thus supporting the notion of DC being the most important antigen presenting cells for T cell priming during an HBV infection.

HBV has a narrow host tropism, infecting apart from humans only humanoid primates and tree shrews. By making use of an adenoviral (Ad) vector, which contains a 1.3-fold overlength genome of HBV, the AdHBV mouse model is able to overcome the species barrier and allows to examine the immune response during a self-limiting acute hepatitis B infection in a small animal model. In order to monitor the T cell response during the AdHBV infection, precise knowledge of immunodominant specific epitopes is required to allow the accurate separation of HBV specific T cell responses and Ad specific T cell responses. As such epitopes have not yet been identified in this model, the second part of this thesis was dedicated to identify HBV and Ad specific T cell epitopes in AdHBVx- infected mice. By means of epitope prediction software, the new immunodominant Ad hexon epitope ‘RNFLYSNI’ on amino acid position 470–477 was identified. Furthermore, testing of overlapping peptide pools revealed immunogenic peptides, which are derived from the hepatitis B virus core antigen (HBcAg). Owing to the identification of this Ad hexon and the

HBcAg peptides, it will be from now on possible to accurately separate HBV and Ad specific T cell responses in the AdHBV mouse model.

During HBV infection, the immunosuppressive environment of the liver prevents massive tissue damage, which is induced by the antiviral host immune response. In order to examine the role of the anti-inflammatory cytokine Interleukin (IL)-10 in counteracting the occurring immunopathogenesis, a new IL-10 reporter mouse was used during the third part of this thesis, which allowed monitoring of the IL-10 production kinetic in various leukocyte populations during an acute AdHBVx- infection. On day five post infection, the established liver damage correlated with the large infiltrate of non-antigen specific mononuclear cells, from which $CD8^+$ T cells and B cells were identified to be the main producers of IL-10. Furthermore, the role of regulatory T cells (Treg) in regulation of IL-10 production by cells of the innate and adaptive immune response was examined in newly crossbred DEREG/ITIB mice, which enable the detection of IL-10 production levels in presence and absence of Tregs. An adoptive Treg transfer in previously Treg depleted AdHBVx- infected mice showed the need of Tregs being present at the very onset of the infection for recruitment of leukocytes into the liver. Moreover, the absence of Tregs impaired the IL-10 production of $CD8^+$ T cells and $CD4^+$ T cells, but not of monocytes and macrophages. This reduced IL-10 production by $CD8^+$ T cells and $CD4^+$ T cells was rescued after the adoptive transfer of Tregs, suggesting that the initial presence of Tregs rather affects cells of the adaptive than cells of the innate immune response.

Taken together, the findings of this thesis enable the separate readout of HBV and Ad specific T cell responses during AdHBVx- infection and furthermore consolidate the understanding of the role of Tregs in mitigation of the anti-HBV immune response via regulation of the IL-10 production.

List of abbreviations

aa	amino acid
AAV	Ad associated viral
Ad	adenoviral
Ad5	adenovirus type 5
AdEmpty	adenoviral vector construct without insert
AdH #	Ad hexon derived peptide
AdH P	Ad hexon derived peptide pool
AdHBV	adenoviral vector construct with HBV insert
AdHBVx-	adenoviral vector construct with HBVx- insert
AdOVA	adenoviral vector construct with OVA insert
AFP	alpha-fetoprotein
ALT	alanine aminotransferase
APC	antigen presenting cell(s)
ARD	arginine-rich domain
BAC	bacterial artificial chromosome
BCR	B cell receptor
BFA	brefeldin A
bla	β-lactamase gene
Bla	β-lactamase
bp	base pairs
Bregs	regulatory B cells
BSA	bovine serum albumine
°C	degree Celsius
cccDNA	covalently closed circular DNA
CD	cluster of differentiation
CCF4-AM	coumarin-cephalosporin-flourescin-acetoxymethyl
CCF4	coumarin-cephalosporin-flourescin
CO_2	carbon dioxide
CsCl	cesium chloride
CSIF	cytokine synthesis inhibitory factor
CTL	cytotoxic T cells
DEREG/ITIB	crossbred mouse derived from DEREG and ITIB mice
DC	dendritic cells
DEREG	depletion of regulatory T cell mouse
DHV	duck hepatitis virus
DMSO	dimethyl sulfoxide
DNA	desoxyribonucleic acid
DT	diphtheria toxin
DTR	diphtheria toxin receptor
E	early region
EBV	Epstein Barr virus
EDTA	ethylenediaminetetraacetic acid
eGFP	enhanced green flourescent protein
ELISA	enzyme-linked immunosorbent assay
EMA	ethidium monoazid
ER	endoplasmatic reticulum
FACS	fluorescence-activated cell sorting

Foxp3	factor forkhead box protein 3
fwd	forward
FRET	fluorescence resonance energy transfer
GAPDH	glyceraldehyde 3-phosphate dehydrogenase
h	hour(s)
HBcAg	hepatitis B virus core antigen
HBc #	HBcAg derived peptide
HBc P	HBcAg derived peptide pool
HBeAg	hepatitis B virus e antigen
HBsAg	hepatitis B virus surface antigen
HBs P	HBsAg derived peptide pool
HBV	hepatitis B virus
HBVx-	hepatitis B virus with stop codon in the HBxAg ORF
HBxAg	hepatitis B virus x protein
HCC	hepatocellular carcinoma
HCMV	human cytomegalovirus
HCl	hydrochloric acid
HCV	hepatitis C virus
HDI	hydrodynamic injection
HEK cells	human embryonic kidney cells
HLA	human leukocyte antigen
HPRT	Hypoxanthine-guanine phosphoribosyltransferase
hTCM	human T cell medium
ICS	intracellular cytokine staining
IEDB	Immune Epitope Database and Analysis Resource
IFN	interferon
Ii	invariant chain
IL	interleukin
i.p.	intraperitoneally
IRES	internal ribosome entry side
ITIB	IL-10–bla reporter mouse
iTreg	induced Treg
IU	infectious units
i.v.	intravenously
l	liter
L-protein	large surface envelope protein
LAL	liver associated lymphocytes
LSEC	liver sinusoidal endothelial cells
M	mol per liter
M-protein	middle surface envelope protein
MACS	magnetic activated cell sorting
MCMV	murine cytomegalovirus
mDC	myeloid DC
$MgCl_2$	magnesium chloride
MIIC	MHC class II loading compartment
min	minute(s)
MHC	major histocompatibility complex
mg	milligram
µM	mikromol per liter

ml	milliliter
mM	millimol per liter
MOI	multiplicity of infection
mRNA	messenger RNA
mTCM	murine T cell medium
µl	microliter
mRNA	messenger RNA
NaCl	sodium chloride
nd	not determined
NF-κB	nuclear factor kappa-light chain-enhancer of activated B cells
NIR	Near-IR
NK	natural killer cells
NH_4Cl	ammonium chloride
NKT	natural killer T cells
nm	nanometer
NTCP	sodium taurocholate cotransporting polypeptide
nTreg	natural Treg
ORF	open reading frame
OVA	ovalbumin
PBMC	peripheral blood mononuclear cells
PBS	phosphate buffered saline
pDC	plasmacytoid DC
PFA	paraformaldehyde
pgRNA	pregenomic RNA
p.i.	post infection
PI	propidium iodide
PRR	pattern-recognition receptors
qPCR	quantitative real time PCR
rcDNA	relaxed circular DNA
rec	recombinant
rev	reverse
RNA	ribonucleic acid
RPM	revolutions per minute
RT	room temperature
s	second(s)
S-protein	small surface envelope protein
U/l	units per liter
U/mg	units per milligram
T	triangulation number
T_H	T helper cells
TAP	transporter associated with antigen processing
TCCl_pp65	T cell clone with specificity for HCMV_pp65 epitope
TCR	T cell receptor(s)
TCR_core	T cells equipped with TCR with specificity for HBV_C18
TCR_surface	T cells equipped with TCR with specificity for HBV_S20
TGF	transforming growth factor
TLR	toll-like receptors
TNF	tumor necrosis factor
Treg	regulatory T cells

Tr1	T regulatory type 1
V	volt
v/v	volume per volume
WHV	woodchuck hepatitis virus
WHO	world health organization
w/v	weight per volume

1 Introduction

1.1 Hepatitis B virus

Although an effective prophylactic vaccine is available, hepatitis B virus (HBV) remains the cause of a most common virus infection, occurring as acute or chronic hepatitis B. Most adults with an acute infection can eliminate the virus. Nevertheless, 5–10 % of infected adults and even 90 % of infected children and newborns fail to eliminate the virus and thus develop a chronic disease, which may lead to liver cirrhosis and hepatocellular carcinoma (HCC). The world health organization (WHO) reports of annually 780,000 HBV related deaths and of more than 240 million people, which are chronically infected with HBV worldwide (WHO 2014). Understanding the immunopathogenesis of HBV infection is an essential pre-requisite for the development of new, more effective treatment strategies (Lavanchy 2005, WHO 2014).

HBV is transmitted by parenteral route via infected blood or other body fluids. The route of transmission is shown to correlate with the seroprevalence of the HBV marker hepatitis B virus surface antigen (HBsAg). HBsAg is an indicator of hepatitis B endemicity in a defined population (Shepard *et al.* 2006). High endemic regions (≥ 8 %) are sub-Saharan Africa and East Asia, where transmission of the virus occurs mainly from mother to child at birth or person-to-person contact during childhood. In regions with intermediate HBsAg prevalence (2–7 %) like Latin America, Mediterranean countries or the Middle East, or low HBsAg prevalence (< 2 %) like Western Europe and North America, transmission occurs more often sexually or by the use of contaminated syringes or medical equipment (Liaw *et al.* 2009, Ott *et al.* 2012).

Since 1969, a prophylactic HBV vaccine is available and since the early 1990s worldwide vaccination programs aim to prevent further HBV infections. In addition to this, an effort is made to raise awareness of HBV transmission and the importance of HBV screenings using accurate diagnostic assays (Fung *et al.* 2012, WHO 2009). Treatment with antiviral agents such as the nucleoside and nucleotide analogues Entecavir and Tenofovir as well as interferon injections are used to alleviate the progression of liver cirrhosis and HCC formation of chronically HBV infected patients but do not succeed to eliminate HBV and bear the risk of resistance (Hadziyannis 2011, Liaw *et al.* 2009). New therapeutic approaches including inhibition of viral replication, therapeutic vaccinations and activation of the host's innate and

adaptive immune response are being tested in order to eliminate infected cells and ultimately eradicate HBV (Grimm *et al.* 2013, Pourkarim *et al.* 2014, Shimizu 2012).

1.1.1 HBV classification and replication cycle

Discovered in 1967 by B.S. Blumberg, HBV is a noncytopathic, enveloped virus with a partially double stranded desoxyribonucleic acid (DNA) enclosed by an icosahedral capsid (Blumberg *et al.* 1967). HBV belongs to the genus of the orthohepadnaviruses within the family of the *Hepadnaviridae* replicating through reverse transcription of a ribonucleic acid (RNA) intermediate. HBV is classified into 8 genotypes (A–H) plus two tentative genotypes I and J that differ by at least 7.5 % of their genome, which again can be further subdivided into various subgenotypes (Pourkarim *et al.* 2014, Schaefer 2007). The HBV genome is ~3.2 kb in size and encodes for four genes in partially overlapping open reading frames (ORF) including regulatory elements for transcription (Rehermann *et al.* 2005) (Figure 1). The pre-C/core ORF encodes the hepatitis B virus core antigen (HBcAg) and the hepatitis B virus e antigen HBeAg. While HBcAg is required for formation of viral capsid and replication, HBeAg is not needed for infection or replication of HBV. The second ORF encodes the hepatitis B virus x protein (HBxAg), which is involved in HBV gene expression and replication. Furthermore HBxAg interacts with the host immune response as well as with the host gene expression hence promoting HBV pathogenesis (Feitelson *et al.* 2014). The preS/S ORF encodes for the large (L), middle (M) and small (S) surface envelope proteins (HBsAg) dependent on the respective initiation sites of pre-S1, pre-S2 or S. All surface proteins consist of the same carboxyl-terminal S domain but vary in the length of their amino-terminal domain. The different functions in HBV entry, morphogenesis and release of the envelope proteins are related to their transmembrane topology (Bruss 2007, Heermann *et al.* 1984, Pollicino *et al.* 2014). The fourth ORF encodes the viral polymerase, which is covalently linked to the full-length negative DNA strand. The polymerase is responsible for the genetic variability of HBV due to both its high replication capacity and error prone reverse transcriptase activity (Pollicino *et al.* 2014).

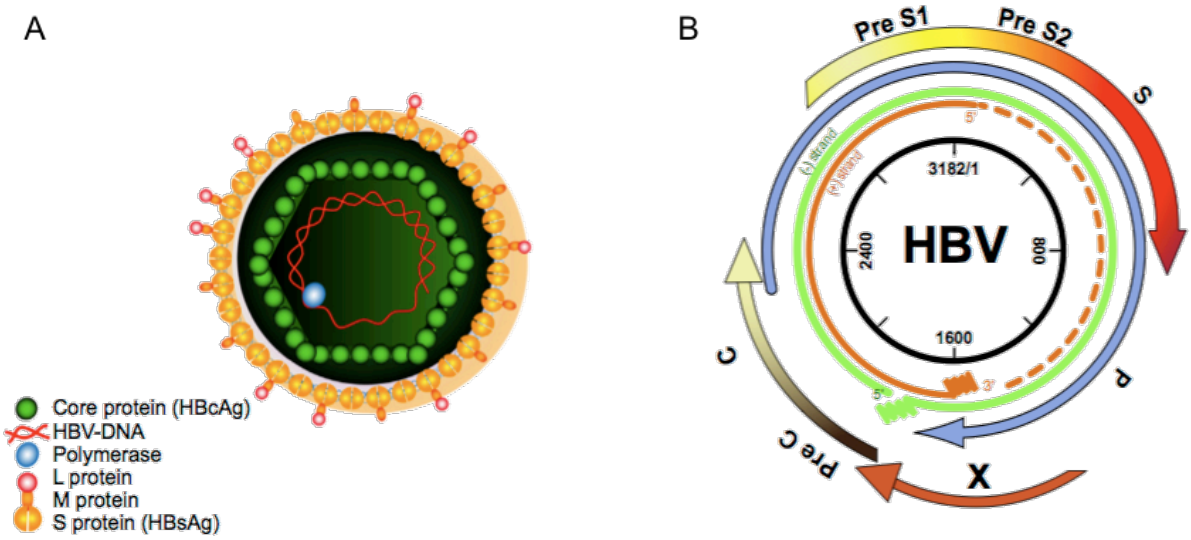

Figure 1: Overview of HBV virion and genome structure. (A) Schematic representation of the HBV virion consisting of a partially double stranded DNA linked to the viral polymerase, encapsidated by an icosahedral capsid of self-assembled core proteins which again is surrounded by an envelope containing the three related surface proteins S-, M- and L-protein. (B) Schematic representation of the HBV genome structure indicating the size and position of the HBV genes in the innermost circle. The full length minus strand is depicted as green circle, while the incomplete plus strand is depicted as orange circle in the middle. The outer circle depicts the overlapping open reading frames of the viral genes X, Pre C/C, P, Pre S1/Pre S2/S. (Pollicino *et al.* 2014)

HBV has a very narrow host and cell tropism infecting only hepatocytes of humans, humanoid primates and tree shrews (Schieck *et al.* 2013, Walter *et al.* 1996). HBV virions are trapped on the surface of hepatocytes by interactions with heparan sulfate proteoglycans (Schulze *et al.* 2007). Attachment of the virion is mediated by the pre-S1 domain of the large envelope protein interacting specifically with the sodium taurocholate co-transporting polypeptide (NTCP) and leading via an yet unknown mechanism to internalization of the HBV virion in the hepatocyte (Leistner *et al.* 2008, Yan *et al.* 2012). Following entry, which might be mediated by clathrin dependent endocytosis or viral membrane fusion, uncoating and release of the capsid into the cytosol occurs (Huang *et al.* 2012, Liu *et al.* 2014). The capsid is able to bind to the nuclear pore and therefore allows the viral relaxed circular (rc) DNA to enter the nucleus, where the missing plus-strand is repaired with the help of the viral polymerase. Cellular polymerases ligate both DNA strands and convert the viral DNA to an episomal minichromosome in form of covalently closed circular (ccc) DNA. cccDNA serves as transcription template for four capped and polyadenylated messenger (m) RNAs (Nassal 2008, Urban *et al.* 2010). Following nuclear export, the three envelope proteins as well as HBxAg are translated from the subgenomic mRNAs, whereupon the envelope proteins are co-translationally translocated into the endoplasmatic reticulum (ER) membrane

(Bruss 2007). HBeAg, HBcAg and the polymerase are translated from greater-than-genome-length mRNAs one of which that also serves as the template for replication. This pregenomic (pg) RNA is encapsidated together with the polymerase within the self-assembled capsid wherein after reverse transcription the plus-strand DNA synthesis takes place (Beck *et al.* 2007, Zlotnick *et al.* 1999). Some of the capsids are recycled to the nucleus in order to establish and maintain persistent infection by filling up the cccDNA pool, whereas other capsids bud into the ER via interaction with the large envelope protein and are secreted as matured virions via multivesicular bodies. DNA-free subviral particles as well as HBeAg on the other hand are secreted via the Golgi pathway (Bruss *et al.* 1995, Patient *et al.* 2009, Werle-Lapostolle *et al.* 2004). The replication cycle of HBV is depicted in Figure 2.

The mature virion has a size of 42–47 nm is called after is discoverer Dane particle (Dane *et al.* 1970). Fast spread of HBV in the liver is enabled due to an estimated release of 50–300 virions per day per infected hepatocytes in patients or more than 500 virions per day per infected primary human hepatocyte (Cohen *et al.* 2010, Quasdorff *et al.* 2008). Capsid-free non-infectious quasi-spherical or filamentous lipoprotein particles are released by secretion at a 1,000 to 10,000-fold higher concentration than the Dane particles. The superior number of these subviral particles is assumed to be advantageous for the virus by interacting with the host immune response (Bruss 2007, Kondo *et al.* 2013, Rehermann *et al.* 2005). The incidence of HBeAg and HBsAg as diagnostic markers of HBV during an acute hepatitis B infection is described in the chapter 1.1.2.

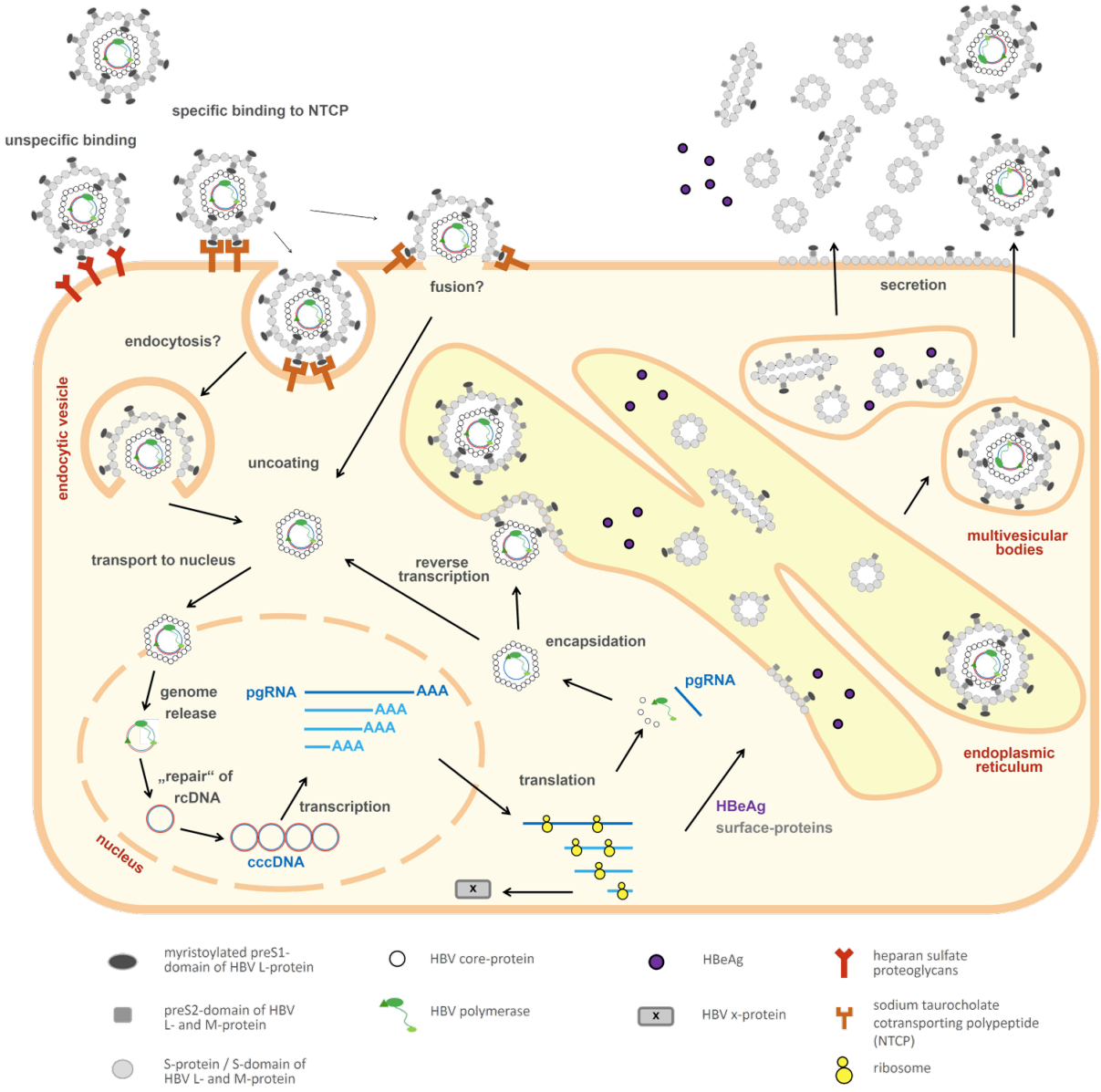

Figure 2: Schematic representation of the HBV replication cycle. The HBV virion enters the hepatocyte after unspecific and specific binding steps that are followed by endocytosis or fusion with the cell membrane to enable uncoating of the virion and release of the capsid into the cytosol. After transport of the capsid, the HBV genome is released into the nucleus where the rcDNA is repaired to cccDNA which serves as transcription template for pgRNA as well as messenger RNAs that are translocated into the cytosol where translation of the HBV polymerase, HBV x-protein, HBV core-protein, HBeAg and S-, M-, L-surface proteins takes place. Encapsidation of the pgRNA and polymerase enables reverse transcription to rcDNA resulting in the HBV capsid that either recycles back to the nucleus or buds into the endoplasmatic reticulum. Mature virions are secreted via multivesicular bodies, while subviral particles and HBeAg are secreted via the Golgi pathway. (cccDNA: covalently closed circular DNA, L: large, M: middle, pgRNA: pre-genomic RNA, rcDNA: relaxed circular DNA, S: small). (Jäger 2015)

1.1.1.1 HBcAg

Self-assembly of HBcAg dimers forms icosahedral particles containing 180 or 240 protein subunits corresponding to the triangulation number (T) of T=3 or T=4 respectively (Crowther *et al.* 1994). The HBcAg monomer consists of an amino-terminal assembly domain (amino acid (aa) 1-140), a linker region (aa 141-146) and a carboxyl-terminal arginine-rich domain (ARD; aa 147-183), whereupon the latter is not required for assembly of the capsid (Chu *et al.* 2014) (Figure 3). In the assembled capsid, the amino- and carboxyl-terminal domains of the HBcAg monomers are arranged in two layers with the assembly domain on the outside and the ARD facing inwards the capsid (Yu *et al.* 2013). The assembly domain regulates assembly kinetics and capsid stability, whereas the ARD interacts with the viral DNA and is associated with nucleic acid chaperone activity (Chu *et al.* 2014, Tan *et al.* 2015). Mutations in the pre-C/core gene can result in alterations of the secondary amino acid (aa) structure and the tertiary protein structure as well as in changes of antigenicity and biological function of HBeAg and HBcAg (Wu *et al.* 2014).

Figure 3: Schematic representation of the HBV core-protein. The numbers are amino acid positions. The dark grey box indicates the amino-terminal assembly domain. The light grey box indicates the linker region and the white box with + indicates the four arginine clusters in the arginine-rich domain. (Chu *et al.* 2014)

HBcAg is both a T cell-dependent and T cell-independent antigen that is highly immunogenic and hence elicits a strong immune response in patients with an acute HBV infection (Chisari *et al.* 1995, Milich *et al.* 1986). HBcAg further binds to specific membrane immunoglobulin antigen receptors on B cells, which may take up, process and present HBcAg to naïve T cells (Milich *et al.* 1997). Moreover it is shown, that apoptosis of hepatocytes interrupts the viral life cycle resulting in the release of nonenveloped and noninfectious HBV capsids (Arzberger *et al.* 2010). Due to the self-assembly capacity and high immunogenicity of HBcAg during HBV infection in humans, HBcAg-based virus like particles are used as a vaccine carrier in order to present heterologous epitopes (Roose *et al.* 2013, Whitacre *et al.* 2009).

1.1.2 Clinical course of HBV infection

Although the severity of HBV induced hepatitis B varies greatly from person to person, a general course of infection can be monitored via diagnostic markers (Ganem et al. 2004). While an acute hepatitis B is characterized by the presence of HBsAg, HBeAg and at later stages of anti-HBcAg antibodies, chronic infections are characterized by persisting HBsAg levels over more than six months (WHO 2014).

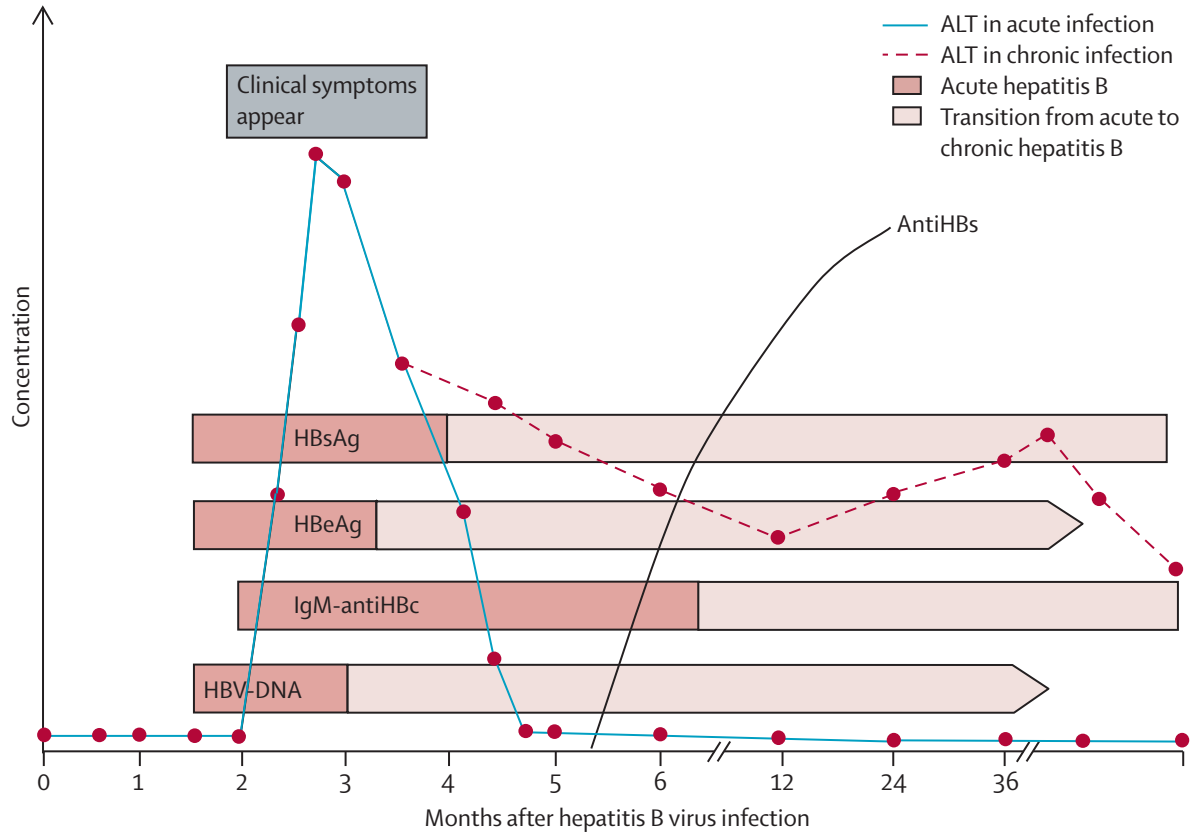

Figure 4: Schematic representation of the serological and clinical course after acute HBV infection. The marker levels for ALT, HBsAg, HBeAg, IgM-anti-HBc, anti-HBs and HBV-DNA are shown for the acute hepatitis B and the transition from acute to chronic hepatitis B. (ALT: alanine aminotransferase). (Liaw *et al.* 2009)

After HBV transmission, a nonsymptomatic incubation time of 1–6 months is observed in patients (Figure 4). During an acute phase of infection, HBV DNA levels rise according to viral spread in the liver. At the same time, seropositivity of HBeAg as marker of viral replication and HBsAg indicates infection that can be detected before the manifestation of clinical symptoms. IgM anti-HBcAg antibodies appear 1–2 weeks after the rise of HBsAg and persist until after anti-HBs seroconversion. One to six weeks after detection of HBsAg, a rise in serum of alanine aminotransferase (ALT) levels is detectable. ALT is a marker of

hepatocellular injuries that is induced by a cytolytic immune response rather than by the non-cytopathic HBV (Guidotti *et al.* 1999). Decline of HBV DNA and HBeAg levels occur simultaneously with the peak of ALT levels. One to two months later, seroconversion from HBsAg to anti-HBs positivity signifies the recovery from acute HBV infection. The progression to chronic HBV infection is characterized by persistence of HBeAg (for > 10 weeks) and HBsAg (for > 6 months) that are followed by high viral loads as well as increased ALT levels (Liaw *et al.* 2009).

1.1.3 Animal models used in HBV research

Cell culture models are not sufficient to fully analyze the establishment of HBV infection, the subsequent anti-HBV immune response as well as to monitor the success of vaccines, therapeutic vaccinations and agents counteracting HBV infection, so that the use of animal models is inevitable for HBV research. Due to the narrow host tropism, besides humans only humanoid primates and tree shrews can be infected with HBV (Barker *et al.* 1973, Walter *et al.* 1996). However, studies in these animals are problematic because of high costs, difficulties in keeping of the animals or analyzing tools as well as ethical issues. Even though HBV-like viruses like the woodchuck hepatitis virus (WHV) and the duck hepatitis virus (DHV) could provide insights into HBV replication and immune pathology, these models are not satisfactory due to their differences in genome structure and replication cycle compared to HBV (Di *et al.* 1997, Roggendorf *et al.* 1995, Summers 1981).

Mice are genetically well described as mammalian animal model and easy to handle at low-cost in the laboratory environment. Moreover, HBV can replicate in murine hepatocytes provided that the species barrier preventing the infection of the hepatocytes is overcome. Therefore, mouse models are advantageous to the previous described models of WHV and DHV (Guidotti *et al.* 1995). The species barrier of HBV is overcome by using HBV transgenic mice or by HBV genome delivery into immunocompetent mice via hydrodynamic injection (HDI), adenoviral (Ad) or Ad associated viral (AAV) gene transfer (Araki *et al.* 1989, Sprinzl *et al.* 2001, Warrington *et al.* 2006, Yang *et al.* 2002). Due to HBV replication from the integrated genome, transgenic mice are immunotolerant to HBV and therefore not able to clear HBV infection and moreover neither allow to study the establishment nor the viral dynamics of an acute HBV infection (Oberwinkler *et al.* 2005). Given that the infection in HDI mice is not easily reproducible and induces severe liver damage and that AAV/HBV1.2 vectors favor HBV persistence, a mouse model with Ad gene

transfer of the HBV genome (AdHBV) is used in this study in order to analyze the immune response during an acute, self-resolving HBV infection (Dembek *et al.* 2015, Huang *et al.* 2006, von Freyend *et al.* 2011).

1.1.3.1 AdHBV mouse model

First-generation Ad vectors carry deletions in the regions of the early regions 1A (E1A), E1B and E3 in order to prevent Ad replication and immune evasion strategies (Blair *et al.* 2004, Windheim *et al.* 2004). The transgene is inserted into the E1 region of the Ad vector derived from Ad serotype 5 (Figure 5). Production of Ad vectors takes place in human embryonic kidney (HEK) 293 cells, in which replication of the Ad vector is enabled by trans-complementation of the E1 region (Zhang 1999). The Ad vector with the inserted transgene is encapsidated with seven Ad structural proteins, whereof the hexon and the fiber capsid proteins are the major antigenic determinants of the Ad virion (Kinloch *et al.* 1984). After harvesting and purification, the Ad particles can then be injected intravenously into mice for liver-directed gene transfer (Benihoud *et al.* 1999, Hegenbarth *et al.* 2000).

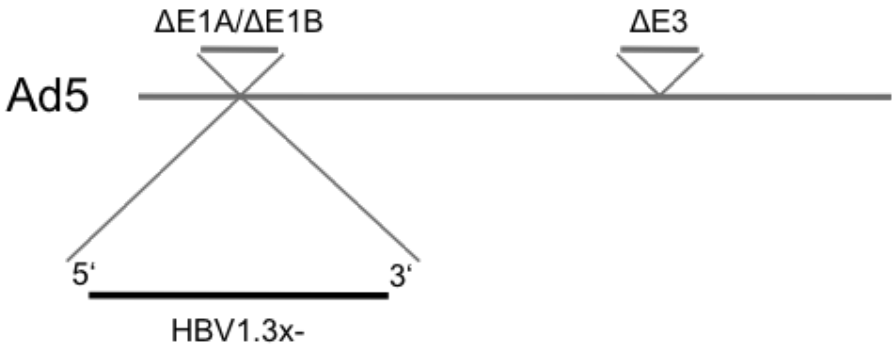

Figure 5: Schematic representation of the AdHBVx- vector construct. First-generation adenoviral vector derived from Ad5 with deletions Δ in the early regions of E1A, E1B and E3. The HBV1.3-fold-overlength genome of HBV contains a stop codon in the open reading frame of HBxAg and is inserted into the region of ΔE1A/E1B. (Ad5: adenovirus type 5). (von Freyend *et al.* 2011)

Using the AdHBV mouse model, the murine liver is transduced with an Ad vector containing a replication competent 1.3-fold-overlength genome of HBV, that is organized as extra-chromosomal template similar to cccDNA in infected human hepatocytes (Sprinzl *et al.* 2001, Untergasser *et al.* 2006, von Freyend *et al.* 2011). In presence of hepatic transcription factors, HBV replication takes place and HBV particles are released from the murine hepatocytes (Quasdorff *et al.* 2008). Furthermore, peaks of HBsAg and HBeAg as well as elevated ALT levels, which are followed by a cellular and humoral immune response, show the

characteristic features of an acute HBV infection. Due to differences in the NTCP receptor between human and mice, HBV cannot spread in mouse livers resulting in a self-revolving infection (von Freyend *et al.* 2011, Yan *et al.* 2013). Therefore, the AdHBV mouse model is a valuable tool for investigating the role of different immune modulators during HBV infection (Stross *et al.* 2012). In this thesis, AdHBVx- with a stop codon in the ORF of HBxAg, that does not affect HBV replication in mice, is used in order to induce the acute phase of HBV infection (von Freyend *et al.* 2011).

1.2 Immune response against HBV

The immune response against pathogens like HBV is composed of an innate immune response and an adaptive immune response. The innate immune response is triggered directly after the first contact with the virus and is furthermore important for both controlling the spread of the infection and initiating the development of the adaptive immune response. The adaptive immune response is composed of a cellular and humoral immune response that results in clearance of the HBV from the host and in the establishment of memory immune cells preventing further infections with HBV. Dysfunction and obstruction of the immune response result in a failed elimination of HBV and a subsequent persistent infection (Bertoletti *et al.* 2013, Murphy 2011). The following is focused on the immune response during the acute HBV infection.

The viral inoculum influences the outcome of the HBV infection with regard to kinetics of viral spread and immunological priming. A weak induction of the innate immune response is associated with a following weak induction of the adaptive immune response against HBV infection, which favors viral persistence (Asabe *et al.* 2009, Bauer *et al.* 2011). Recently, the role of the innate immune response against HBV infection was re-evaluated due to findings that HBV actively induces immunosuppression and that HBV does not evade the innate immune response by acting as a stealth virus (Busca *et al.* 2014, Wieland *et al.* 2005). Activation of the innate immune response is thought to be achieved by pattern-recognition receptors (PRR), including the toll-like receptors (TLR), which induce pro-inflammatory cytokines in the infected cell via signaling cascades mediated by the production of nuclear factor kappa-light chain-enhancer of activated B cells (NF-κB) (Akira *et al.* 2006, Isogawa *et al.* 2005b). Secretion of type I and type II interferons (IFN) as well as other cytokines including interleukin (IL)-6, IL-12, IL-18 and tumor necrosis factor (TNF) α are observed by infected cells as well as by immune cells, resulting in an antiviral immune response controlling the replication of HBV (Bauer *et al.* 2011, Busca *et al.* 2014). This antiviral response is counteracted by the HBV proteins polymerase, HBxAg, HBeAg, HBsAg as well as by virions that interfere with the host cell signaling (Bertoletti *et al.* 2013, Busca *et al.* 2014, Wu *et al.* 2009). Moreover, HBeAg may modulate the respiratory burst and migration of monocytes and neutrophils (Leu *et al.* 2014). Furthermore, immunosuppressive strategies of HBV are supported by secretion of anti-inflammatory cytokines like IL-10 (Hyodo *et al.* 2004).

Secretion of type I IFNs recruits dendritic cells (DC) as well as other antigen presenting cells (APC), which consecutively recruit inflammatory cells to the liver as site of infection. In addition, DC prime effector T and B cells via presentation of HBV derived peptides in order to inhibit HBV replication (Kimura *et al.* 2002). Presence of HBV or HBsAg during myeloid DC (mDC) maturation is shown to result in a more tolerogenic mDC phenotype and thus reduced T cell stimulation (Op den Brouw *et al.* 2009). Plasmacytoid DC (pDC) fail to induce cytolytic activity of natural killer (NK) cells, presumably due to high levels of HBeAg and HBsAg (Martinet *et al.* 2012). Furthermore, NK cells and natural killer T (NKT) cells are thought to sense HBV infection (Durantel *et al.* 2009, Gregoire *et al.* 2007, Trobonjaca *et al.* 2002). The kinetics of NK and NKT cells are faster than of HBV specific T cell and decline with the viral load indicating the timely induction of the adaptive immune response (Fisicaro *et al.* 2009, Webster *et al.* 2000).

During an acute HBV infection, B cells contribute to viral clearance via production of neutralizing anti-HBsAg antibodies. HBV specific $CD4^+$ and $CD8^+$ T cell responses are multispecific and polyfunctional. Therefore, noncytopathic cytokine mediated inhibition of viral replication as well as killing of infected hepatocytes are induced whereupon resolution of the acute HBV infection is achieved (Guidotti *et al.* 1996, Guidotti *et al.* 1999, Rehermann *et al.* 2005). The establishment of HBV persistence otherwise is associated with defective T cell function due to long-term exposure to high quantities of viral antigen and by the tolerogenic environment of hepatocytes (Maini *et al.* 2010). Moreover, Tregs are shown to actively suppress the immune response against HBV infection, counteracting liver injuries and in return prolong clearance of HBV (Franzese *et al.* 2005, Stross *et al.* 2012). Previous studies also showed that the ablation of the cluster of differentiation (CD) 95 pathway of apoptosis prevents the induction of the anti-HBV immune response by deficient priming of HBV specific B cells and T cells (Arzberger 2009).

1.2.1 NK and NKT cells

NK cells are an early effector component of the innate immune system that are activated in response to IFNs and other cytokines that are secreted by DC and macrophages. NK cells possess cytoplasmic granules containing cytotoxic granzymes and the pore forming protein perforin, which after release onto the cell surface induce the lysis or apoptosis of the target cells (Bryceson *et al.* 2008). ‘Altered self’ changes of the expression of major histocompatibility complex (MHC) class I molecules, which is ubiquitously expressed on all

nucleated cells, indicate that the cells are stressed due to infection, are sensed by NK cells and hence lead to the killing of the infected cell. Removal of harmful cells missing MHC class I is important because they cannot be detected by T cells (Karre 2008). Moreover, NK cells exert their antiviral activity through immunoregulatory cytokines such as IFNγ, TNFα and IL-10 or by cell mediated cytotoxicity that induces liver damage. NKT cells express a T cell receptor recognizing glycolipid antigens that are presented by the MHC-like molecule CD1. Antigen stimulation of NKT cells results in rapid cytokine secretion including IFNγ and IL-10 (Bendelac *et al.* 2007, Nakagawa *et al.* 2001). As highly heterogeneous effector cells, NKT cells serve immune and regulatory functions by inducing liver damage and hence removing of the virus from the host (Li *et al.* 2011).

NK and NKT cells are very abundant in the human and murine liver with 10–20 % and 50 % of total murine intrahepatic lymphocytes for NK cells and NKT cells respectively, which therefore can exert their antiviral functions without prior recruitment to the liver (Kakimi *et al.* 2000, Li *et al.* 2011, Tian *et al.* 2013). Moreover, their activity initially controls the acute HBV infection and enables timely and efficient induction of the adaptive immune response (Fisicaro *et al.* 2009, Zeissig *et al.* 2012).

1.2.2 Antigen presenting cells

In order to prime and activate lymphocytes, antigen presentation as well as expression of co-stimulatory molecules is required. Professional APC like B cells, DC and macrophages can efficiently internalize and present antigens for T cell priming. DC are thought to be the most important APC initiating the adaptive immune response via priming of T cells, whereas the antigen presenting function of macrophages and B cells is needed at another time during infection, when T cells have acquired effector activities (Lazdina *et al.* 2003, Murphy 2011, Pozzi *et al.* 2005).

Activation of PRR and cytokines activate DC after capturing and procession of exogenous infectious agents and inflammatory products at the site of infection. Thereupon, DC migrate to the lymph nodes and spleen as local lymphoid organ, where DC mature into highly active APC. Antigen presentation by mDC activates naïve T cells that recirculate through the peripheral lymphoid tissues, as well as cytolytic $CD8^+$ T cells, $CD4^+$ helper T cells and B cells that reenter the circulation in order to execute their effector function at the site of infection. pDC on the other hand sense viral infections and produce high amounts of

type I IFNs that have antiviral potential and furthermore support the activation of cells of the innate and adaptive immune system (Banchereau *et al.* 1998, Lambotin *et al.* 2010).

Macrophages and B cells process and present exogenous antigens and interact with already primed effector $CD4^+$ T cells. Macrophages scavenge pathogens and subsequently recruit IFNγ producing $CD4^+$ T cells by antigen presentation. B cells are very efficient in taking up and internalizing extracellular antigens via receptor mediated endocytosis resulting in antigen presentation to $CD4^+$ T helper cells that stimulate the differentiation of B cells into antibody producing plasma cells. The secretion of high quantities of antigen specific antibodies is an important part of the adaptive immune response during the course of infection (Constant 1999, Watts 2012, Whitmire 2011).

During HBV infection, DC as well as liver resident macrophages (Kupffer cells), liver sinusoidal endothelial cells (LSEC) and hepatocytes act as intrahepatic APC. These cells, however, rather contribute to the tolerogenic hepatic microenvironment by acting as scavenger cells and actively modulating the immune response (Knolle *et al.* 2014).

1.2.2.1 Mechanisms of antigen presentation

In order to activate antigen specific immune responses during an infection, self or non-self antigens in form of peptides need to be presented to T cells and B cells by the MHC class I or class II molecules. Endogenous antigens derived from viral proteins that are degraded by the proteasome, are translocated into the ER by the transporter associated with antigen processing (TAP). After assembly of the MHC class I molecule with the peptide, the peptide-MHC class I complex is released from the ER and transported via the Golgi pathway to the cell surface for antigen presentation to $CD8^+$ T cells. The peptide-MHC class I complex is recognized specifically by the T cell receptor (TCR) of effector $CD8^+$ T cells, which induce cell death of the infected cell and cytokine secretion after binding to the complex (Malmstrom *et al.* 2013, Neefjes *et al.* 2011) (Figure 6A).

The MHC class II molecule is mainly expressed on professional APC and is used for presentation of extracellular antigens taken up via phagocytosis, receptor mediated endocytosis or macropinocytosis into vesicles. MHC class II molecules assemble in the ER with the invariant chain (Ii) to the MHC class II loading compartment (MIIC). MIIC is transported to the late endosome, where Ii is replaced by a peptide that is derived from an exogenous protein degraded in the endosomal pathway. The peptide-MHC class II complex is

then transported to the cell surface in order to present the peptide to effector $CD4^+$ T cells that either activate the presenting cell to kill the pathogen or activate B cells for antigen specific antibody production (Malmstrom *et al.* 2013, Neefjes *et al.* 2011).

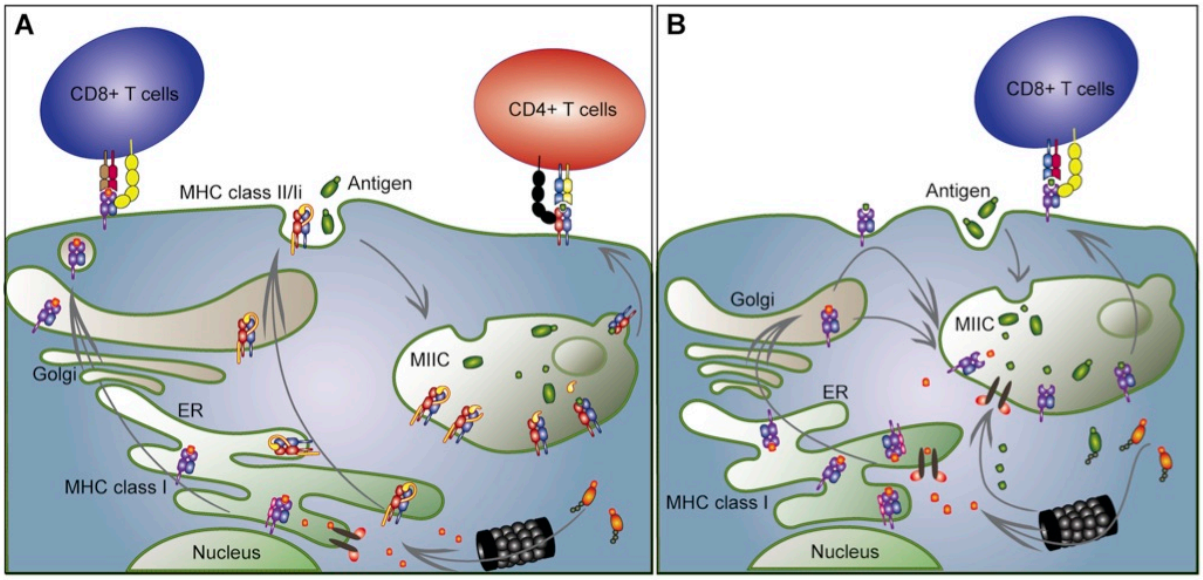

Figure 6: Schematic representation of the antigen presentation pathways. (A) Classical antigen presentation of endogenous antigens on the MHC class I molecule to $CD8^+$ T cells and presentation of exogenous antigens on the MHC class II molecule to $CD4^+$ T cells. (B) Cross-presentation of exogenous antigen on the MHC class I molecule to $CD8^+$ T cells. (MHC: major histocompatibility complex). (Malmstrom *et al.* 2013)

In addition to the classical antigen presentation pathways, an alternative pathway of antigen presentation exists, where extracellular antigens taken up by phagocytosis are presented on MHC class I molecules to effector $CD8^+$ T cells in a process called cross-presentation. Here, the MHC class I molecule is transported to the endosomal pathway where it can be loaded with peptides degraded in the endosomal pathway (Joffre *et al.* 2012) (Figure 6B). Aside from DC, B cells and macrophages, but also LSEC are also able to cross-present exogenous peptides on their MHC class I molecules to $CD8^+$ T cells (Debrick *et al.* 1991, Heit *et al.* 2004, Limmer *et al.* 2000).

1.2.2.2 Variety of MHC molecules

The genetic organization of the MHC in human and mouse is similar with separate clusters of MHC class I and class II genes. In this work, the focus will be on MHC class I alleles of the human leukocyte antigen (HLA)-A2 and the murine H-2Kb. The HLA-A2 haplotype is chosen due to its prevalence in the human population, whereas the H-2Kb haplotype is expressed by the popular C57BL/6 inbred strain that is widely used in mouse models in our

laboratory. The genetic polymorphism and polygyny of MHC molecules are responsible for the expression of diverse MHC molecules that show different affinities for the same peptide between individuals (Gao *et al.* 2000, Murphy 2011). Screening of a panel of overlapping peptides, which span the aa sequence of viral antigens, are used to identify peptides binding to a certain MHC molecule that subsequently enables the readout of antigen specific $CD8^+$ T cell responses (Penna *et al.* 1991).

1.2.2.3 HBV epitopes

Monitoring of T cell responses during an infection and the further identification of epitopes allow the understanding of the *in vivo* immune response and the design of novel immunotherapeutic strategies like antigen specific vaccines (Bercovici *et al.* 2000, Gajewski 2000). In order to monitor antigen specific $CD8^+$ T cell responses, single peptides, peptide pools consisting of overlapping peptides or carbamylated (urea modified) proteins can be used (Barabas *et al.* 2008, Desmond *et al.* 2008, Penna *et al.* 1991). While single peptides are loaded exogenously onto MHC molecules, carbamylated proteins are naturally processed and presented on MHC molecules and moreover display the functionality and the ability for cross-presentation of the APC (Barabas *et al.* 2008).

The site of an antigen, which is recognized by an antibody or an antigen receptor, like a TCR or a B cell receptor (BCR), is called epitope. B cell epitopes are composed of three-dimensional protein structures, whereas T cell epitopes are immunogenic peptides of different lengths (Murphy 2011). HBV T cell epitopes from HBcAg or HBsAg, that are described as immunodominant in HLA-$A2^+$ humans, are HBV_C18 (FLPSDFFPFV), HBV_S20 (FLLTRILTI) as well as the peptide pools HBc P4 and HBs P1 (Desmond *et al.* 2008), whereas for H-$2Kb^+$ DNA immunized or HBV transgenic mice the epitopes HBV_C93 (MGLKFRQL), HBV_S190 (VWLSVIWM) and HBV_S208 (ILSPFLPLL) (Backes *et al.* submitted, Kuhober *et al.* 1996, Schirmbeck *et al.* 2003a) are described. The detection of activated T cells is performed after intracellular cytokine staining (ICS) and flow cytometry measurement of *ex vivo* peptide stimulated lymphocytes.

Computational epitope prediction methods are used to supplement limited experimental data, which results from the diversity of both MHC molecules and peptide epitopes (Bordner 2013). Epitope prediction software contain machine learning algorithms that make use of sequence or binding affinity data entered in the database in order to do binding

prediction for epitope discovery (Lundegaard *et al.* 2010, Roomp *et al.* 2010). In this thesis, epitope prediction is based on the database of SYFPEITHI (Rammensee *et al.* 1999), the Immune Epitope Database and Analysis Resource (IEDB) (Peters *et al.* 2005) and netMHC (Lundegaard *et al.* 2008). SYFPEITHI contains mapped epitopes and naturally processed peptides, whereas the bigger IEDB database contains additional peptide binding data and also annotates the immunogenic context of the epitopes. netMHC uses affinity data and elution data from the before mentioned databases and is rated among the best predictors available (Lin *et al.* 2008).

1.2.3 $CD4^+$ T cells and $CD8^+$ T cells

The adaptive immune response consists of antigen specific antibody production mediated by B cells and further by T cells, which aim to fight and finally eliminate HBV by various effector functions. Since T cells are not able to recognize pathogens, they rely on the presentation of pathogen derived peptides via APC. After contact with antigen presenting DC in the lymphoid tissue, naïve T cells are activated to undergo clonal expansion and differentiate into effector $CD4^+$ T cells and $CD8^+$ T cells that are recruited to the site of infection. These T cells carry a TCR with specificity for a certain antigen in form of a peptide that is presented on MHC molecules. An immunological synapse is formed upon interaction between the peptide-MHC complex on the cell presenting the antigen and the TCR as well as the CD4 or CD8 co-receptor of the T cell, thus resulting in subsequent T cell signaling (Murphy 2011). However, TCR binding degeneracy allows cross-reactivity of T cells, where numerous peptides are thought to be recognized by one T cell in order to cope with the vast number of potential foreign peptide-MHC complexes (Sewell 2012).

$CD4^+$ T cells comprise several subsets of functionally different effector T cells including among others T helper (T_H) 1 cells activating macrophages and thus supporting cell mediated immune response, T_H2 cells inducing B cell differentiation into antibody producing plasma cells and Tregs executing immune regulatory functions that are described further in 1.2.4 (Whitmire 2011). $CD8^+$ T cells are also called cytotoxic T cells (CTL) due to their abilities to induce killing of infected cells via perforin/granzyme or Fas mediated apoptosis. Along with their cytotoxic abilities, $CD8^+$ T cells exert antiviral functions in a noncytopathic way via secretion of cytokines like IFNγ and TNFα (Guidotti *et al.* 1996). Interaction of T cell activation markers like CD137 and CD134 with their respective ligands on APC, enhance T cell survival and proliferation, which is also supported by IL-2 cytokine secretion

(Taraban *et al.* 2002). On the contrary, sustained presence of antigen results in T cell exhaustion characterized by failing cytokine production and expansion as well as loss of cytolytic activity (Bauer *et al.* 2011).

During the course of an acute HBV infection large quantities of virus are eliminated via noncytopathic cytokine secretion of HBV specific $CD8^+$ T cells preceding the induction of liver damage. This consecutively recruits many antigen nonspecific mononuclear cells that amplify the formation of necroinflammation (Guidotti *et al.* 1999, Sitia *et al.* 2004). Like $CD4^+$ T cell dependent B cell responses, $CD4^+$ T cells are required to promote strong and multispecific $CD8^+$ T cell responses that are associated with resolution of the HBV infection (Rehermann *et al.* 2005).

1.2.4 Tregs

$CD4^+$ $CD25^+$ $Foxp3^+$ Tregs are a functionally distinct subpopulation of $CD4^+$ T cells that suppress and mitigate effector T and B cell function as well as that of DC, NK cells and NKT cells. Moreover, Tregs maintain tolerance to self-antigens in order to prevent autoimmunity and enhancement of the host defense (Billerbeck *et al.* 2007, Manigold *et al.* 2007). The transcription factor forkhead box protein 3 (Foxp3) is a master control gene for the generation and function of Tregs. Foxp3 expressing natural Tregs (nTreg) originate from the thymus, whereas Tregs with induced $Foxp3^+$ expression (iTreg) derive from mature naïve $CD4^+$ T cells in the periphery. Natural Tregs act synergistically with overlapping effector functions and represent 5–10 % of the human or murine $CD4^+$ T cell population (Haribhai *et al.* 2011, Sakaguchi 2005).

Tregs were originally characterized among $CD4^+$ T cells by their expression of the alpha chain of the IL-2 receptor (CD25). Later it was shown that mature T and B lymphocytes also express CD25 upon activation, what is crucial for their survival and function (Willerford *et al.* 1995). The TCR diversity of Tregs is larger than that of effector T cells resulting in a bias of Tregs for self-peptides (Hsieh *et al.* 2004). Tregs exert their suppressive activity by expression of the anti-inflammatory cytokines transforming growth factor (TGF) β, IL-10, IL-35 and galectin 1 as well as by cytolysis, targeting DC, competition for critical cytokines or metabolic disruption (Caridade *et al.* 2013, Veiga-Parga *et al.* 2013). Dysfunction of Tregs leads to several autoimmune or inflammatory disorders (Sakaguchi 2004).

Tregs counteract liver damage and actively suppress HBV specific T cell functions indicating their anti-inflammatory role during an acute HBV infection at the cost of prolonged viral clearance (Bertoletti *et al.* 2013, Stross *et al.* 2012). The role of Tregs in the development of a persistent HBV infection remains elusive (Billerbeck *et al.* 2007). Furthermore, depletion of Tregs results in an increase of HBV specific T cell proliferation in chronic hepatitis B patients (Stoop *et al.* 2005). In acute hepatitis B patients increasing numbers of circulating Tregs are only detectable during the convalescent phase, whereby Treg numbers are restored to normal levels upon resolution of infection (Yang *et al.* 2007). Moreover, HBV antigen specific Tregs are observed in acutely infected patients (Xu *et al.* 2006). Although Tregs are thought to play a critical role in priming of the immune response, only little is known about Tregs during the acute phase of HBV, which is also due to the lack of adequate models or the availability of liver biopsies of acutely infected patients (Alatrakchi *et al.* 2009, Pace *et al.* 2012). Accordingly, the mechanisms by which Tregs influence the immune response against HBV still need to be further elucidated.

1.2.5 IL-10

The anti-inflammatory cytokine IL-10 was first discovered in 1989 as the cytokine synthesis inhibitory factor (CSIF) from T_H2 cells (Mosmann *et al.* 1990). Nowadays, it is known that IL-10 excites multiple immunoregulatory effects and thereby plays a crucial role in preventing inflammatory and autoimmune pathologies. Several cells of the innate and adaptive immune system express IL-10 including NK cells, NKT cells, monocytes, macrophages, DC, T and B cells as well as Tregs (Sag *et al.* 2014, Saraiva *et al.* 2010, Shouval *et al.* 2014). In mice, IL-10 deficiency is described as the cause for the development of inflammatory bowel disease and microbial colonization of the gut (Sellon *et al.* 1998). By signaling through the IL-10 receptor, IL-10 regulates growth and differentiation – amongst others – of B cells, NK cells, DC, cytotoxic and helper T cells (Moore *et al.* 2001). During infection, the effect of IL-10 by suppressing DC and macrophage function results in impaired T_H1 and T_H2 effector functions. The suppressive effects of IL-10 are thought to be irrespective of the cell producing this cytokine, due to the potential of IL-10 producing cells to regulate each other (Couper *et al.* 2008). Though, the timing and site of IL-10 production are crucial to determine the immunoregulatory impact of IL-10 (Couper *et al.* 2008, Rouse *et al.* 2010). Moreover, the strength of the regulatory IL-10 response, which is mediated by various cell types, is claimed to reflect the preceding inflammatory response during an

infection (Couper *et al.* 2008). In recent years, the limitations of experimental tools in the detection of IL-10 in single cells are attempted to be overcome e.g. by the generation of the IL-10 β-lactamase (Bla) reporter (ITIB) mouse that allows the specific detection of IL-10 production levels even at low concentrations in different cell populations of the innate and adaptive immune system (Bouabe 2012, Muris *et al.* 2012). The ITIB mouse was generated by homologous recombination mediated insertion of two copies of internal ribosome entry side (IRES)-bla cassette at the end of the last exon of IL-10 and before the 3' polyadenylation signal of the IL-10 gene (Bouabe *et al.* 2011).

During the acute HBV infection, elevated IL-10 levels occur at the peak of viremia coinciding with the transient inhibition of NK and T cell responses (Dunn *et al.* 2009, Keating *et al.* 2014). Furthermore, IL-10 expression is also associated with the presence of HBeAg and HBsAg in the liver or HBcAg stimulation of peripheral blood mononuclear cells (PBMC) (Bertoletti *et al.* 2013, Hyodo *et al.* 2004). Moreover, IL-10 was shown to be necessary for the humoral tolerance that is initiated by Kupffer cells (Xu *et al.* 2014). Since IL-10 acts in multiple ways, its anti-inflammatory influence, that potentially counteracts tissue damage and pathogen clearance during HBV infection, will be an object of further investigations.

1.3 Aim of this thesis

My work aims to contribute to the further understanding of immunological basics during HBV infection that would provide crucial knowledge for the establishment of new therapy strategies in the future. In particular I have investigated three different but related aspects of this process. Previous studies have shown that non-enveloped HBV capsids are released if apoptosis is induced and that ablation of the CD95 pathway of apoptosis prevents the induction of an anti-HBV immune response (Arzberger *et al.* 2010). Furthermore, HBV capsids are shown to directly stimulate B cells more efficiently than macrophages or DC (Milich *et al.* 1997). The aim of the first part of this thesis was therefore to examine the potential of HBV capsids, which are taken up and presented by B cells, in T cell priming. This hypothesis was tested by an *in vitro* co-culture study of T cells with capsid stimulated B cells, macrophages and DC.

Monitoring of T cell responses requires precise knowledge of immunodominant specific epitopes. Using the mouse model of self-limiting AdHBVx- infection, T cell epitopes are required that accurately separate HBV specific T cell responses and Ad specific T cell responses. Such epitopes have not yet been defined although they are important in order to analyze immune responses in this model (von Freyend *et al.* 2011). The second aim of my thesis was therefore to identify Ad and HBV specific T cell epitopes in AdHBVx- infected mice. Determination of immunodominant epitopes was performed by testing of peptide pools as well as by screening of epitope predicted peptides from HBcAg, HBsAg or the Ad hexon protein.

The immunosuppressive environment of the liver prevents massive tissue damage during HBV infection in order to maintain organ function (Protzer *et al.* 2012). The mechanism how the HBV specific immune response is counteracted remains elusive, but it is hypothesized that the cytokine IL-10 that is expressed in vast amounts early during AdHBVx- infection (von Freyend *et al.* 2011) plays an important role in the anti-inflammatory response. In order to overcome the difficulties of IL-10 detection, a new IL-10 reporter mouse was used in this thesis, which allows monitoring of the kinetic of IL-10 production by various leukocyte populations during acute AdHBVx- infection (Bouabe *et al.* 2011). Since Tregs counteract the HBV specific immune response by mitigating the immune mediated liver damage as well as T cell effector functions (Stross *et al.* 2012), the aim of the third part of this thesis is to further investigate the regulatory role of Tregs in the establishment of the anti-HBV immune

response. An IL-10 reporter mouse was used, which enables the detection of IL-10 production by Tregs and of other cells of the innate and adaptive immune response during the course of an acute AdHBVx- infection. Furthermore, a mouse model was established, which allows examining IL-10 production levels in presence and absence of Tregs during an acute AdHBVx- infection. Restoration of Treg mediated effects on the anti-HBV immune response in Treg depleted mice are examined during an adoptive Treg transfer experiment.

2 Material and methods

2.1 Material

The materials were part of the inventory of AG Protzer, Institute of Virology, TUM unless indicated otherwise.

2.1.1 Instruments

Table 1: Instruments used during this thesis.

Instrument name	Manufacturer
Architect	Abbott
Centrifuge 4K15	Sigma-Aldrich
Cryo freezing container	Thermo Scientific
Dissecting set	Haeberle
FACSCanto II	Becton Dickinson
FACSFortessa	Becton Dickinson
Fusion Fx7	Peqlab
Gel system (S, M)	Peqlab
Hemocytometer (Neubauer impoved)	Brand
Incubator Hera cell 150	Thermo Scientific
Infinite F200	Tecan
Infrared lamp	Petra
Laminar flow	Heraeus
Light microscope Axiovert 40C	Zeiss
LightCycler480 II	Roche
Magnetic stirrer IKA Ret basic	Sigma-Aldrich
MoFlo cell sorter	Beckman Coulter
Optima L-90K Ultracentrifgue	Beckman Coulter
pH meter	Mettler Toledo
Pipetboy	Brand
Pipettes	Eppendorf
Power Pac basic power supply	Bio-Rad
Precision balance 572	Kern
Reflotron Reflovet Plus	Roche
Spectrophotometer NanoVue	GE Healthcare
Stainless steal beads	Qiagen
Table top centrifuge 5417C	Eppendorf
T3000 Thermocycler	Biometra
Thermomixer comfort	Eppendorf
Tissue Lyser LT	Qiagen
Vortex mixer	Neo-Lab
Water bath	GLF

2.1.2 Software

Table 2: Software used during this thesis.

Software name	Company
FACSDiva	Becton Dickinson
FlowJo	Tree Star Inc.
GraphPad Prism5	Graph Pad Software
IEDB	www.iedb.org
LightCycler 480 Software	Roche
Magellan Software	Tecan
MS Office 2011	Microsoft
netMHC 3.4 Server	www.cbs.dtu.dk
Roche Universal Probe Library	Roche
Serial Cloner	serialbasics
SYFPEITHI	www.syfpeithi.de

2.1.3 Consumables

Table 3: Consumables used during this thesis.

Consumable name	Manufacturer
AloeCare gloves	Meditrade
Blood lancets	Marienfeld
Cell scraper	TPP
Cell strainer (100 µm)	Corning
Cellstar centrifuge tube (15 ml, 50 ml)	VWR
Costar reagent reservoir	Sigma-Aldrich
F96 Maxisorp Nunc-Immuno Plate	Thermo Scientific
FACS micro test tube	Bio-Rad
Filter tip (10 µl)	Biozym
Filter tip (20 µl, 200 µl, 1000 µl)	Star Lab
Filtropur S 0.2 µm, S 0.45 µm	Sarstedt
FrameStar 480/96 plate with seal for LightCycler	4titude
Illustra PuRe Taq Ready To Go PCR beads	GE Healthcare
Injekt syringe (10 ml, 20 ml)	B. Braun
MACS Columns (LS)	Miltenyi Biotech
Micro tube 1.1 ml Z-gel	Sarstedt
Non-tissue culture treated plates (24-well)	Corning
Nunclon delta-surface flask (75 cm^3)	Nunc
Original perfusor 50 ml syringe	Braun
PCR tubes	Thermo Scientific
Perform	Schülke
Pipettes (2 ml, 5 ml, 10 ml, 25 ml, 50 ml)	Greiner Bio-One
Reaction tube (1.5 ml, 2.0 ml)	Greiner Bio-One
Rotilabo micro test plate (96-well V-profile)	Roth
Safety-Multifly needle (21 G)	Sarstedt
Slide-A-Lyzer dialysis cassette 10 K MWCO, (3 ml, 12 ml)	Thermo Scientific
Sterican needles (20 G, 27 G)	B. Braun
Sterilium (Virugard)	Bode
Surgical disposable scalpels	B. Braun
Syringe 1 ml TBC with needle	Dispomed
Syringe with Luer-Lock connector (1 ml)	Becton Dickinson
Tissue culture dish (4 cm, 6 cm)	TPP
Tissue culture flask (25 cm^3, 75 cm^3, 150 cm^3)	TPP
Tissue culture test plate (6-well,12-well, 24-well)	TPP
Tissue culture test plate (96-well U-profile)	TPP
UZ centrifuge tube (25x89 mm)	Seton

2.1.4 Chemicals and reagents

Table 4: Chemicals and reagents used during this thesis.

Chemical or reagent name	Catalog number	Manufacturer
Acetic acid	CP28.1	Roth
Ammonium chloride (NH_4Cl)	K298.1	Roth
AutoMACS rinsing solution	130-091-222	Miltenyi Biotec
BD Cytofix/Cytoperm	51-2090KZ	Becton Dickinson
BD Perm/Wash	554723	Becton Dickinson
BD PharmLyse (10x)	555899	Becton Dickinson
CD14 micro beads, human	130-050-201	Miltenyi Biotec
CD19 micro beads, human	130-050-301	Miltenyi Biotec
Cesium cloride (CsCl)	7878.2	Roth
Collagenase type 4 (240 U/mg)	43E14252	Worthington
Dimethyl sulfoxide (DMSO)	D2650	Sigma-Aldrich
Diphteria Toxin (DT; 10µg/ml)	322326	Merck
Ethanol	9065.2	Roth
Ethylenediaminetetraacetic acid (EDTA)	8043.2	Roth
FACS Stain Buffer	554656	Becton Dickinson
Foxp3 staining buffer set	00-5523-00	eBioscience
Glycerin Rotipuran	3783.1	Roth
Heparin-Natrium-25000	PZN-03029843	Ratiopharm
Hydrochloric acid (HCl)	X942.1	Roth
LightCycler480 SYBR Green I Master	04887352001	Roche
Lipofectamine 2000	11668-019	Life Technologies
Lymphocyte separation medium LSM 1077	J15-004	PAA
Magnesium chloride ($MgCl_2$) Hexahydrat	A537.1	Roth
Paraffin oil	9190.1	Roth
peqGOLD universal agarose	35-1020	Peqlab
Percoll	17-0891-02	GE Healthcare
Poly-L-lysine solution	P8920	Sigma-Aldrich
Quick-load 1 kb DNA ladder	N0468G	New England Biolabs
RedTaq ready PCR mix	R2523	Sigma-Aldrich
RetroNectin (1 mg/ml)	T100B	Takara Clontech
RNAlater	76154	Qiagen
Rotifix 4 % paraformaldehyde (PFA)	P087.3	Roth
Smart ladder 100 bp	MW-1800-02	Eurogentec
Sodium chloride (NaCl) 0.9 %	PZN 3079870	B. Braun
Sucrose	S0389	Sigma-Aldrich
Tris	4855.3	Roth
Trizol reagent	15596018	Life Technologies
Trypan blue stain (0.4 %)	15250-061	Life Technologies
Water for moleculary biology	A7398,1000	AppliChem

2.1.5 Buffers

Table 5: Buffers used during this thesis.

Buffer	Ingredients
Coating buffer	PBS (1x) OKT3 5 µg/ml anti-hCD28 0.05 µg/ml
1.2 CsCl solution	Tris-HCl 10 mM at pH 8.0 CsCl 26.8 % (w/v)
1.4 CsCl solution	Tris-HCl 10 mM at pH 8.0 CsCl 53.0 % (w/v)
Dialysis buffer	Tris-HCl 10 mM at pH 8.0 $MgCl_2$ hexahydrat 2 mM Sucrose 4 % (w/v)
Erythrocyte lysis buffer	NH_4Cl (0.16 M stock) 90 % (v/v) Tris HCl (0.17 M stock, pH 7.7) 10 % (v/v)
FACS buffer (murine cells)	PBS Fetal bovine serum 1 % (v/v)
FACS buffer (IL-10 reporter)	PBS EDTA 2 mM BSA 0.5 % (v/v)
FACS buffer (human cells)	PBS Human serum 0.5 % (v/v)
90 % Percoll solution	Percoll PBS (10x) 11,1 % (v/v)
80 % Percoll solution	90 % Percoll solution PBS (1x) 12.5 % (v/v)
40 % Percoll solution	PBS (1x) 90 % Percoll solution 80 % (v/v) Heparin 100 IU/ml
TAE buffer (50x)	Tris 2 M Acetic acid 2 M EDTA 50 mM at pH 8.0

2.1.6 Medium and supplement consumables

Table 6: Medium and supplement consumables used during this thesis.

Medium or supplement name	Catalog number	Manufacturer
0.5 % Trypsin-EDTA (10x)	15400-054	Life Technologies
2-Mercaptoethanol	4227.1	Roth
Anti-hCD28	16-0289-85	eBioscience
Brefeldin A (BFA; stock 1 mg/ml)	B7651	Sigma-Aldrich
Bovine serum albumine (BSA; stock 10 % (w/v) in PBS)	15100	Berva
CCF4-AM (stock 1 mM in DMSO)	K1096	Life Technologies
Diphteria Toxin (DT; stock 10µg/ml)	322326	Merck
DMEM	11960-044	Life Technologies
Fetal bovine serum	16000-044	Life Technologies
Gentamicin	G1397	Sigma-Aldrich
Glucose (40 %)	2357742	B. Braun
GM-CSF (stock 800 IU/µl in H_2O)	NDC 58468-0180-1	Genzyme
HEPES (1 M)	15630-080	Life Technologies
Human albumin (200 g/l)	717158	Baxter
Human serum	self-made	AG Protzer
Hyclone fetal bovine serum	SH30071.03	Thermo Scientific
IL-1β (0.1µg/µl)		R&D
IL-2 (180 IU/µl in H_2O)	L03AC01	Novartis
IL-4 (0.1 µg/µl)		CellGenix
L-Glutamine (100x; 200 mM)	25030-024	Life Technologies
MEM NEAA (100x)	11140-035	Life Technologies
anti-hCD3:OKT3 hybridoma supernatant (1.8 mg/ml)	in-house	E. Kremmer, HelmholtzZentrum Munich
OptiMEM (1x)	31985-070	Life Technologies
PBS Dulbecco (1x)	L1825	Biochrom
PBS pH 7.4 (10x)	70011-036	Life Technologies
Pen Strep	15140-122	Life Technologies
PGE_2 (stock 1 mg/ml)		Pfizer
Probenicid (stock 180 mM in NaOH)	P-8761	Sigma-Aldrich
RPMI medium 1640	21875-034	Life Technologies
Sodium pyruvate (100x; 100 mM)	11360-039	Life Technologies
TNFα ($1x10^7$ IU/ml)		Miltenyi Biotec
VLE-RPMI 1640 medium	F1415	Biochrom
William's medium E	22551-022	Life Technologies
Sodium chloride (NaCl) 0.9 %	PZN 3079870	B. Braun
Sucrose	S0389	Sigma-Aldrich
Tris	4855.3	Roth
Trizol reagent	15596018	Life Technologies
Trypan blue stain (0.4 %)	15250-061	Life Technologies
Water for moleculary biology	A7398,1000	AppliChem

2.1.7 Medium for human cells

Table 7: Medium for human cells used during this thesis.

Medium for human cells	Ingredients
DC medium	VLE-RPMI 1640 medium Human serum 1.5 % (v/v) Pen Strep 1 % (v/v)
DC freezing medium	Human albumin 55 % (v/v) Glucose 25 % (v/v) DMSO 20 % (v/v)
DC maturation mix I	DC medium IL-4 20 ng/ml GM-CSF 100 ng/ml
DC maturation mix II	DC medium TNFα 10 ng/ml IL-1β 10 ng/ml PGE_2 250 ng/ml GM-CSF 100 ng/ml IL-4 20 ng/ml
DMEM complete medium	DMEM Fetal bovine serum 10 % (v/v) Pen Strep 1 % (v/v) L-Glutamine, 1 % (v/v) MEM NEAA 1 % (v/v) Sodium pyruvate 1 % (v/v)
DMEM medium without antibiotics	DMEM Fetal bovine serum 10 % (v/v) L-Glutamine, 1 % (v/v) MEM NEAA 1 % (v/v) Sodium pyruvate 1 % (v/v)
Human T cell medium (hTCM)	RPMI medium 1640 Human serum 10 % (v/v) Pen Strep 1 % (v/v) L-Glutamine, 1 % (v/v) MEM NEAA 1 % (v/v) Sodium pyruvate 1 % (v/v) HEPES 1% (v/v) Gentamicin 0.4 % (v/v)
hTCM for growth	hTCM IL-2 300 U/ml
Leukocyte medium	VLE-RPMI 1640 medium Pen Strep 1 % (v/v) Hyclone fetal bovine serum 10 % (v/v) GMCSF 100 ng/ml
Leukocyte wash medium	RPMI medium 1640 Pen Strep 1 % (v/v)
Macrophage maturation mix	Leukocyte medium GM-CSF 100 ng/ml

2.1.8 Medium for murine cells

Table 8: Medium for murine cells used during this thesis.

Medium for murine cells	Ingredients
CCF4-AM loading medium	mTCM CCF4-AM 1.5 µM Probenicid 3.5 mM
Freezing medium	Fetal bovine serum DMSO 20 % (v/v)
Murine T cell medium (mTCM)	RPMI medium 1640 Fetal bovine serum 10 % (v/v) Pen Strep 1 % (v/v) L-Glutamine, 1 % (v/v) MEM NEAA 1 % (v/v) Sodium pyruvate 1 % (v/v) β-Mercaptoethanol 0.1 % (v/v)
RPMI complete medium	RPMI medium 1640 Fetal bovine serum 10 % (v/v) Pen Strep 1 % (v/v) L-Glutamine, 1 % (v/v) MEM NEAA 1 % (v/v) Sodium pyruvate 1 % (v/v)
RPMI wash medium	RPMI medium 1640 Pen Strep 1 % (v/v)
William's medium	William's medium E $CaCl_2$ 2.5 M Collagenase 0.1 % (w/v)

2.1.9 Antibodies

Table 9: Fluorescent-labeled antibodies and reagents for human samples used during this thesis.

Anti-human antibody name	Use	Catalog number	Manufacturer
CD134-APC	1:8	17-1347-42	eBioscience
CD137-Alexa Flour700	1:19	BLD-309815	Biozol
CD14-PE	1:33	21270144	Immutech
CD4-ECD	1:1000	6604727	Beckman Coulter
CD8-PeCy7	1:2400	25-0088-42	eBioscience
CD8-Pacific Blue	1:50	PB984	Dako
CD80-FITC	1:25	1853	Immutech
CD83-APC	1:25	17-0839-41	eBioscience
Streptactin-APC	1:50	6-5000-005	iba

Table 10: Fluorescent-labeled antibodies and reagents for murine samples used during this thesis.

Anti-mouse antibody name	Use	Catalog number	Manufacturer
CD11b-PeCy7	1:300	101216	BioLegend
CD11c-PeCy5	1:250	15-0114	eBioscience
CD19-PE	1:300	12-0193	eBioscience
CD25-APC	1:100	17-0251-82	eBioscience
CD3-V500	1:50	560771	Becton Dickinson
CD4-Pacific Blue	1:250	48-0042-82	eBioscience
CD4-PE	1:200	22150044	Immutech
CD4-PeCy7	1:300	25-0042	eBioscience
CD64-PE	1:150	139304	BioLegend
CD8a-Pacific Blue	1:250	48-0081	eBioscience
CD8a-PerCP-Cy5.5	1:200	45-0081	eBioscience
Ethidium monoazide (EMA; 2 mg/ml in DMSO)	1:5000	E1374	Life Technologies
F4/80-PerCP-Cy5.5	1:50	45-4801	eBioscience
Foxp3-PE	1:150	12-5773	eBioscience
IFNγ-FITC	1:300	554411	Becton Dickinson
IL-2-APC	1:200	17-7021	eBioscience
Ly6C-APC	1:300	128010	BioLegend
Ly6C-APC	1:300	128010	BioLegend
Near-IR (NIR; in 50 µl DMSO)	1:200	L10119	Life Technologies
NK1.1-PerCP-Cy5.5	1:100	45-5941-82	eBioscience
Propidium iodide (PI; 6 µg/ml in mTCM)	1:21	CN74.3	Roth
Streptactin-PE	1:50	6-5000-005	iba
TNFα-PeCy7	1:200	557644	Becton Dickinson
anti-mCD16/CD32	1:1000	553141	Becton Dickinson

2.1.10 Peptide-MHC multimers

Table 11: Peptide-MHC multimers used during this thesis. H2-kb restricted peptide-MHC class I multimers were used for *ex vivo* labeling of murine lymphocytes. All HBV derived multimers were obtained from working group Busch, whereas the AFP-MHC multimer was derived from IBA. Peptide-MHC multimers were used at 0.4 µg/50 µl for labeling with Streptactin-PE.

Multimer name	Position (aa)	Sequence
HBV_C18	18-27	FLPSDFFPFV
HBV_C93	93-100	MGLKFRQL
HBV_S20	20-28	FLLTRILTI
HBV_S172	172-191	WLSLLVPFVQWFVGLSPTVW
HBV_S190	190-197	VWLSVIWM
Unspecific (AFP)	325-334	GLSPNLNRFL

2.1.11 Kits

Table 12: Kits used during this thesis.

Kit name	Catalog number	Manufacturer
Allprep DNA/RNA	80204	Qiagen
ELISA max standard set human IFNγ	430103	Biolegend
M&N Nucleo spin tissue	740952250	Macherey-Nagel
SuperScript III first strand synthesis supermix	18080-400	Life Technologies

2.1.12 Peptides and full proteins

Table 13: Previously described peptides used for *ex vivo* stimulation of murine lymphocytes or for stimulation of human APC in co-culture study.

Peptide name	Position (aa)	Sequence	Remark	Use
HBV_C18	18-27	FLPSDFFPFV	Desmond, *et al.* 2008	5 µM/ml
HBV_C93	93-100	MGLKFRQL	Kuhober, *et al.* 2006	8 µM/ml
HCMV_pool		Pool of 138 HCMV 15-mer peptides each with an 11 aa overlap	Immunmonitoring HelmholtzZentrum Munich	1 µg/ml
OVA_SIIN	257-264	SIINFEKL	Carbone, *et al.* 1992	1 µg/ml
HBV_S20	20-28	FLLTRILTI	Desmond, *et al.* 2008	5 µM/ml
HBV_S190	190-197	VWLSVIWM	Schirmbeck, *et al.* 2003	8 µM/ml
HBV_S208	208-216	ILSPFLPLL	Schirmbeck, *et al.* 2003	8 µM/ml
Unspecific (A3L)	270-277	KSYNYMLL	Moutaftsi, *et al.* 2006	1 µg/ml

Table 14: Proteins used for stimulation of human APC during co-culture study.

Protein name	Description	Remark	Use
Capsid	NP40-denatured HBV virions derived from HepG2.2.15 cells	Provided by J.H. Bockmann	MOI = 10
Capsid rec	E. coli derived recombinant HBcAg (genotype D, subtype adw)	Biochemical research center, University of Lativa in Riga	1 µg/ml
HCMV *pp65	Carbamylated HCMV pp65 protein	Immunmonitoring HelmholtzZentrum Munich	3 µg/ml

Table 15: HBcAg derived peptides and peptide pools used for *ex vivo* stimulation of murine lymphocytes. Origin of peptides and peptide pools are indicated by numbers: 1 = Thinkpeptides; 2 = Immunmonitoring HelmholtzZentrum Munich; 3 = Peptide& Elephants. Peptides of pools were used with different concentrations: HBc P1 to P3 with 2 µg/ml; HBc P4 to P7 with 8 µM/ml each. (HBc P = HBcAg derived peptide pool, HBc # = HBcAg derived peptide).

Peptide name		Position (aa)	Sequence	Remark	Origin
HBc P1		1-71		pool of 15-mer peptides each with an 11 aa overlap	1
HBc P2		61-117	see Appendix		
HBc P3		121-183			
	HBc #33	129-143	PQAYRPPNAPILSTL	from HBc P3	1
	HBc #42	165-179	RRRSQSPRRRRSQSR		
HBc P4				pool of peptides described previously (Desmond, *et al.* 2008)	2
HBc P5		20-27	PTDFFPSV	epitope prediction from HBc P1	3
		86-93	VNYVNTNM	epitope prediction from HBc P2	
		136-143	NAPILSTL		
		133-140	RPPNAPIL	epitope prediction from HBc P3	
		140-147	LSTLPETT		
		137-144	APILSTLP		
HBc P6		93-100	MGLKFRQL	epitope prediction from HBcAg	3
		86-93	VSYVNTNM		
		120-131	VSFGVWIRTPPA	previously described peptides (Milich, *et al.* 1995)	
		130-140	PAQRPPNAPIL		
HBc P7	HBc #1	1*-10	LCLGWLWGMDIDPYKEFG	pool of 18-mer peptides each with an 11 aa overlap	2
	HBc #2	1*-17	GMDIDPYKEFGATVELLS		
	HBc #3	7-24	KEFGATVELLSFLPSDFF		
	HBc #4	14-31	ELLSFLPSDFFPSVRDLL		
	HBc #5	21-38	SDFFPSVRDLLDTASALY		
	HBc #6	28-45	RDLLDTASALYREALESP		
	HBc #7	35-52	SALYREALESPEHCSPHH		
	HBc #8	42-59	LESPEHCSPHHTALRQAI		
	HBc #9	49-66	SPHHTALRQAILCWGELM		
	HBc #10	56-73	RQAILCWGELMTLATWVG		
	HBc #11	63-80	GELMTLATWVGGNLEDPI		
	HBc #12	70-87	TWVGGNLEDPISRDLVVS		
	HBc #13	77-94	EDPISRDLVVSYVNTNMG		
	HBc #14	84-101	LVVSYVNTNMGLKFRQLL		
	HBc #15	91-108	TNMGLKFRQLLWFHISCL		
	HBc #16	98-115	RQLLWFHISCLTFGRETV		
	HBc #17	105-122	ISCLTFGRETVIEYLVSF		
	HBc #18	112-129	RETVIEYLVSFGVWIRTP		

Table 16: Ad Hexon derived peptides and peptide pools used for *ex vivo* stimulation of murine lymphocytes. Origin of peptides and peptide pools are indicated by numbers: 3 = Peptides&Elephants. Peptides were used at 8 µM/ml each. (AdH P = Ad hexon derived peptide pool, AdH # = Ad hexon derived peptide).

Peptide name		Position (aa)	Sequence	Remark	Origin
AdH P1	AdH #1	470-477	RNFLYSNI	epitope prediction from Ad hexon	3
	AdH #2	676-683	RGWAFTRL		
	AdH #3	64-71	LTRRFIPV		

Table 17: HBsAg derived peptide pools used for *ex vivo* stimulation of murine lymphocytes. Origin of peptides and peptide pools are indicated by numbers: 2 = Immunmonitoring HelmholtzZentrum Munich; 3 = Peptides&Elephants. Peptides were used at 8 µM/ml each. (HBs P: HBsAg derived peptide pool).

Peptide name	Position (aa)	Sequence	Remark	Origin
HBs P1			pool of peptides described previously (Desmond, *et al.* 2008)	2
HBs P2	81-88	IIFLFILL	epitope prediction from HBsAg	3
	179-186	ASARFSWL		

2.1.13 Primers and PCR conditions for qPCR analysis

Table 18: Forward (fwd) and reverse (rev) primers for qPCR synthesized by Invitrogen.

Target		Sequence (5'-3')	Program
Ad	fwd	TAAGCGACGGATGTGG	Ad
	rev	CCACGTAAACGGTCAAAG	
HBV	fwd	GTTGCCCGTTTGTCCTCTAATTC	HBV
	rev	GGAGGGATACATAGAGGTTCCTTGA	
mGAPDH	fwd	ACCAACTGCTTAGCCC	C3
	rev	CCACGACGGACACATT	
mHPRT	fwd	AGGACCTCTCGAAGTG	C3
	rev	AACAGGACTCCTCGTAT	
mIFNg	fwd	GTGGACCACTCGGATGA	C3
	rev	ATGGTGACATGAAAATCCTG	
mIL-10	fwd	CAGAGCCACATGCTCCTAGA	C3
	rev	GTCCAGCTGGTCCTTTGTTT	
mIntron	fwd	GGATCAAGGTCAGAGGACCA	Ad + HBV
	rev	CCACGTAAACGGTCAAAG	

Table 19: Cycling conditions for the LightCycler480.

		Ad			C3			HBV	
Activation		95 °C	5 min		95 °C	5 min		95 °C	5 min
Denaturation	45 cycles	95 °C	15 s	45 cycles	95 °C	15 s	45 cycles	95 °C	25 s
Annealing		55 °C	10 s		60 °C	10 s		60 °C	15 s
Elongation		72 °C	25 s		72 °C	25 s		72 °C	30 s
Melting curve		65-95 °C	0.11°C/ s		65-95 °C	0.11°C/ s		65-95 °C	0.11°C/ s
Cooling		40 °C	hold		40 °C	hold		40 °C	hold

2.1.14 Primers and PCR conditions for ITIB and DEREG/ITIB genotyping

Table 20: Fwd and rev primers for PCR synthesized by Invitrogen.

Target		Sequence (5‘-3‘)	Program
bla	fwd	GGTCTTTCCCCTCTCGCCAAAGGAATGC	ITIB
	rev	CCCACTCGTGCACCCAACTGATCTTCAGC	
IL-10	fwd	GCTGGGAGAAGGTATAGGAGAAACAGGGG	ITIB
	rev	GCTAAGATCCCTGGATCAGATTTAGAGAGCTCTG	

Table 21: Cycling conditions for the thermocycler.

		ITIB	
Activation		95 °C	6:50 min
Denaturation	40 cycles	95 °C	30 s
Annealing		60 °C	20 s
Elongation		72 °C	30 s
Elongation		72 °C	5 min
Cooling		4 °C	hold

2.1.15 Mouse lines

All mice were bred and kept in the animal facilities of the institute of virology or of the Helmholtz Zentrum Munich unless indicated otherwise.

2.1.15.1 Wild type mice

C57BL/6 mice are an inbreed strain with the H2-kb MHC allele. C57BL/6 mice were obtained from Charles River Laboratories or Harlan Laboratories and were used as wild type mice.

CD45.1 mice are congenic mice on C57BL/6 background, which carry the leukocyte marker CD45.1. CD45.1 mice were obtained from in-house breeding and used as wild type mice.

2.1.15.2 DEREG mice

Depletion of regulatory T cells (DEREG) mice have a C57BL/6 background and furthermore carry a bacterial artificial chromosome (BAC) that enables the detection and inducible depletion of Tregs with diphtheria toxin (DT). DEREG mice are heterozygous for the diphtheria toxin receptor (DTR) and enhanced green fluorescent protein (eGFP) under control of the Treg specific FOXP3 promoter (Lahl *et al.* 2007). In order to prevent sterile offspring, DEREG mice were bred by using male DEREG mice and female C57BL/6 mice. A protocol for screening of the heterozygous offspring is described in 2.2.3.3. During this thesis, DEREG mice were exclusively used for crossbreeding with ITIB mice in order to obtain DEREG/ITIB mice.

2.1.15.3 ITIB mice

IL-10–Bla reporter (ITIB) mice are transgenic mice with C57BL/6 background that enable the detection of IL-10 on single cell level in all lymphoid and myeloid cells. The ITIB mouse was generated by homologous recombination mediated insertion of two copies of internal ribosome entry side (IRES)-bla cassette at the end of the last exon of IL-10 and before the 3’ polyadenylation signal of the IL-10 gene.

For the reporter reaction, cells are loaded with the lipophilic, esterified form of the substrate coumarin-cephalosporin-flourescin-acetoxymethyl (CCF4-AM) that enters the cells efficiently. Cytoplasmic esterases hydrolyze the ester groups of CCF4-AM and release the

negatively charged form CCF4 that is trapped in the cytosol. Excitation of the CCF4 at 405 nm allows for sensitive detection of the fluorescence resonance energy transfer (FRET) from the coumarin donor to the flourescin acceptor, which emits green light at 520 nm. Bla activity cleaves CCF4 to CCF4* thus separates the two fluorophores resulting in the disruption of FRET and the emission of blue light at 447 nm. The amount of the substrate CCF4 and the cleaved product CCF4* can be measured via flow cytometry in the green and blue channel respectively (Bouabe *et al.* 2011, Held 2007). Mice were obtained originally from Hicham Bouabe, Babraham Institute in Cambridgeshire and used for experiments and in-house crossbreeding with DEREG mice in order to obtain DEREG/ITIB mice.

2.1.15.4 DEREG/ITIB mice

DEREG/ITIB mice are a newly crossbred transgenic mouse strain with combined features of DEREG and ITIB mice enabling the inducible depletion of GFP^+ Tregs and the detection of IL-10 via the Bla reporter reaction (see 2.1.15.2 and 2.1.15.3). The DEREG/ITIB mice are heterozygous for the DTR-eGFP BAC and homozygous for the IL-10–Bla reporter enzyme. DEREG/ITIB mice were obtained from in-house crossbreeding by using a male DEREG/ITIB and a female ITIB mouse in order to avoid sterile offspring.

2.1.16 Ad vectors

Recombinant adenoviruses expressing HBV and variants, that were used in this thesis, are based on the Gateway/AdEasy pENTR system from Invitrogen (see Table 22). The Ad vector is derived from adenovirus type 5 (Ad5) and carries deletions in the region encoding for the Ad proteins E1 and E3 disabling Ad replication and interaction with the host immune response. The insert is inserted into the deleted E1 region. Linearized Ad vectors are transfected into human embryonic kidney (HEK) 293 cells, which complement the missing E1 region and therefore allow for replication of the Ad vector.

Table 22: Overview of Ad vector constructs with their characteristics that were used during this thesis.

Vector name	Description
AdHBVx-	Insert of HBV1.3 overlength genome (subtype ayw) under the HBV promoter with a premature stop codon in the HBx ORF preventing HBx expression (see Freyend *et al.* 2011).
AdHBVk/o	Insert of HBV1.3 overlength genome (subtype ayw) under the HBV promoter with premature stop codons in all HBV ORF preventing expression of all HBV proteins (see Freyend *et al.* 2011).
AdOVA	Insert of the antigen ovalbumine under the CMV promoter
AdEmpty	No insert

2.2 Methods

2.2.1 Cell culture methods

HEK 293A cells or HEK 293T cells were cultured in a 150 cm^2 tissue culture flask with DMEM complete medium and incubated at 37 °C and 5 % carbon dioxide (CO_2). At 90 % confluence, the cells were passaged by adding 3 ml of 1x Trypsin-EDTA to the previously PBS washed cells. As soon as cells detached from the flask, the cells were resuspended with medium counted and in a next step split or seeded in the desired concentration.

The number of live cells in the suspension was determined by Trypan blue staining, which passes the impaired membranes of dead cells but not the intact membranes of viable cells. The number of live cells was determined by using a hemocytometer, in which the number of cells counted in one large square corresponds to the number of cells per milliliter multiplied by 10^4, i.e. the number of 127 cells in one large square corresponds to $1.27x10^6$ cells/ml.

In order to freeze cells of an early passage, cells of one confluent tissue culture flask were split in ten parts, pelleted for 5 min at 1,300 RPM at RT and resuspended in 0.5 ml FBS to which 0.5 ml freezing medium were added dropwise. The aliquots were quickly placed in the freezing container and stored at -80 °C. Thawing of cells was performed by 1:10 dilution of the cells with DMEM complete medium, followed by two wash steps and counting. The thawed cells needed generally two passages to grow quickly again.

2.2.2 Production of Ad vector stocks

Production of Ad vector stocks was performed according to the protocol of Andreas Untergasser (Untergasser *et al.* 2008a, b, c). Changes and additions to this protocol are described below.

In order to produce an animal stock of Ad vector, HEK 293A cells were cultured in 18 tissue culture flasks (150 cm^2). At 80 % confluence, the cells were infected with a multiplicity of infection (MOI) of 7 of the respective Ad glycerol stock. The detaching cells were harvested after approximately 48 h post infection (p.i.), centrifuged, frozen and thawed as described in the Untergasser protocol.

Purification by a CsCl density gradient was performed by ultracentrifugation with the SW32Ti rotor at 24,200 RPM for 90 min without brake at 10 °C. For removal of CsCl, the

collected Ad solution was filled into a Slide-A-Lyzer dialysis cassette and incubated under stirring in dialysis buffer at RT with renewed buffer after 1 h, 2 h and 3 h consecutively. After dialysis, the Ad stock was stored at 4 °C for maximal 7 days until titration was completed. Long-term storage of the animal stock was performed at -80 °C. The aliquot for titration was also frozen at -80 °C prior to use.

The amount of functional Ad vectors was determined as infectious units (IU)/ml by titration. HEK 293A were seeded in a 12 well tissue culture test plate with a concentration of $1x10^6$ cells/ml and well in DMEM complete medium. Before titration, 100 µl medium were removed from the wells in the middle and lower row. In the top row 100 µl, 30 µl, 10 µl and 3 µl of the Ad stock (derived from the frozen aliquot) were added to the DMEM complete medium and mixed by gentle pipetting. In the next step, a 1:10 dilution was prepared by transferring 100 µl of each well in the top row to the subjacent well in the middle row. After mixing by gentle pipetting, 100 µl of the three highest concentrations in the middle row were transferred to the subjacent well in the bottom row. The fourth well in the bottom row served as control without virus. 48 h p.i. the Ad titer of the animal stock was determined with help of the table in the Untergasser protocol.

Mice were injected intravenously (i.v.) with $1x10^9$ IU/mouse of the AdHBVx- animal stock (with a maximal volume of 200 µl) in order to induce an acute hepatitis B infection. Other Ad vectors were also used at concentrations of $1x10^9$ IU/mouse. Highly concentrated Ad animal stocks were diluted with NaCl solution prior to injection.

2.2.3 Mice experiments

Mice experiments were performed after approval by the local authorities. Mice were kept in the animal facilities of the institute of virology or of the Helmholtz Zentrum Munich.

2.2.3.1 Injection

Prior to i.v. injection of the respective Ad vector into the tail vein, the mice were warmed under an infrared lamp in order to dilate the veins. The mice were placed in a mouse holder box enabling the fixation of the mouse. The tail was disinfected with 70 % ethanol before 200 µl Ad vector were injected. After the injection, mild pressure was applied on the site of injection for approximately 5 s in order to stop bleeding, before the mice were placed back into the cage.

For intraperitoneal (i.p.) injection, the mice were grasped gently but firmly in one hand for fixation displaying the ventral side. Up to 200 µl were injected with the syringe placed in a 45 ° angle at knee height, right to the middle line in order to avoid puncture of the bladder. The peritoneum was rubbed gently before the mice were placed back into the cage.

2.2.3.2 Bleeding

The mice were grasped gently but firmly in one hand for fixation and bled by puncture of the facial vein with a lancet.

For the screen of DEREG and DEREG/ITIB mice (2.2.3.3), six drops of blood were collected in a reaction tube, which contained 50 µl of 1:5 diluted heparin in PBS. For serological analysis, 8 drops of blood were collected in a reaction tube and further processed as described in 2.2.3.13.

2.2.3.3 Screen of DEREG and DEREG/ITIB mice

Heparinized blood was diluted with 1 ml murine T cell medium (mTCM) and stored at 4 °C until further processing. After centrifugation at 1,300 RPM for 5 min at room temperature (RT), the supernatant was discarded and the cell pellet was resuspended in 1 ml of 1x PharmLysis buffer and incubated for 15 min at RT. The cells were washed twice with FACS buffer for murine cells, before subjected to FACS surface staining with the anti-mouse CD4-Pacific Blue antibody as described in 2.2.5.2. DEREG or DEREG/ITIB mice that carry the DTR-eGFP BAC can be detected as $CD4^+$ Foxp3-GFP^+ cells in flow cytometry.

2.2.3.4 Genotyping of ITIB and DEREG/ITIB mice

The murine DNA of tails was purified with the Macherey-Nagel NucleoSpin Tissue Kit according to the manufacturer's instructions for mouse tails (40 µl eluate). Two reactions with each 7.5 µl RedTaq mix, 30 ng DNA, 1 µM fwd and rev primers for bla and IL-10 respectively were set up in a total volume of 14 µl in PCR tubes. Primers and cycling conditions for the thermocycler are described in 2.1.14. The PCR products were loaded next to a DNA ladder onto a 2 % (w/v) agarose gel with 1x TAE buffer. After the run for 45 min at 80 V, gels were analyzed with the Fusion Fx7. The product of wild type IL-10 has a size of 360 base pairs (bp) and the product of IL-10–bla has a size of 500 bp. For breeding, only mice that are homozygous for IL-10–bla were used.

2.2.3.5 Depletion of Tregs

Depletion of Tregs in DEREG/ITIB mice was achieved by daily i.p. administration of 1 µg/mouse DT on three subsequent days. The DT stock solution was diluted with NaCl solution.

2.2.3.6 Dissection and processing of organs

Mice were sacrificed with CO_2 for collection of whole blood and organs. The spleen was dissected and placed on ice in a 4 cm tissue culture dish filled with RPMI wash medium until further processing. The liver was perfused with ice-cold PBS before dissection. Liver pieces of approximately 1 mm^3 were stored in reaction tubes with 200 µl RNAlater or 1 ml Trizol for qPCR analysis (2.2.3.12). The remaining liver was placed on ice in a 4 cm tissue culture dish filled RPMI wash medium until further processing.

2.2.3.7 Isolation of liver-associated lymphocytes

The dissected liver was grinded in a cell strainer placed in a 6 cm tissue culture dish with the plunger of a 10 ml syringe. The liver cells were resuspended in 25 ml RPMI wash medium and pelleted by centrifugation for 10 min at 1,300 RPM at RT. After careful decanting of the supernatant, the pellet was resuspended in pre-warmed 12.5 ml William's medium and incubated for 20 min at 37 °C in the water bath with occasional shaking. Afterwards, the tube with the collagenase-digested liver cells was filled up to 45 ml with RPMI wash medium and centrifuged at 1,300 RPM for 10 min at RT. The pellet was resuspended in 3 ml of 40 % percoll solution and layered carefully onto 3 ml of 80 % percoll solution in a 15 ml centrifuge tube. The percoll gradient was centrifuged at 2,600 RPM for 20 min without brakes at RT. The liver-associated lymphocytes (LAL) were carefully collected from the interphase of the percoll media layer, diluted with RPMI wash medium and pelleted for 3 min at 1,300 RPM at RT. Remaining erythrocytes were removed from the cell pellet during incubation with 3 ml erythrocyte lysis buffer for 2 min in a water bath at 37 °C. Afterwards, LAL were washed three times, counted and seeded with $2x10^6$ cells/well in mTCM in an U-profile 96-well tissue culture test plate.

2.2.3.8 Isolation of splenocytes

The dissected spleen was grinded with the plunger of a 10 ml syringe in a cell strainer, which was placed in a 6 cm tissue culture dish. The cells were resuspended in 15 ml RPMI wash

medium and pelleted by centrifugation for 5 min at 1,300 RPM at RT. After careful decanting of the supernatant, the pellet was resuspended in 3 ml erythrocyte lysis buffer and incubated for 2 min at 37 °C in the water bath with occasional shaking. Splenocytes were washed three times, counted and seeded with $2x10^6$ cells/well in mTCM in an U-profile 96-well tissue culture test plate.

2.2.3.9 Adoptive T cell transfer

For the adoptive Treg transfer, splenocytes of wild type mice were isolated as described in 2.2.3.8. The splenocytes were surface stained (see 2.2.5.2) and sorted on the MoFlo cell sorter by the group of Matthias Schiemann for $CD4^+$ $CD25^{high}$ T cells. The sorted cells were diluted in NaCl solution and i.p. injected in Treg depleted DEREG/ITIB mice.

2.2.3.10 Ex vivo peptide stimulation

LAL and splenocytes were seeded with $2x10^6$ cells/well in 200 µl in an U-profile 96-well tissue culture test plate in mTCM and stored at 37 °C with 5 % CO_2. The single peptides, peptide pools or proteins were added in the respective dilution (see 2.1.12) in 50 µl mTCM to the before seeded cells and stored in the incubator. After 1 h of stimulation, 20 µl of a 13.5 µg/ml Brefeldin A (BFA) predilution in mTCM were added to the cells and stored over night in the incubator. On the next day, the cells were transferred to a V-profile 96-well micro test plate. After live/dead staining, the cells were subjected to surface staining of CD4-PE and CD8-Pacific Blue as well as to ICS of IFNγ-FITC, TNFα-PeCy7 and IL-2-APC (see 2.2.5.1, 2.2.5.2 and 2.2.5.3).

Murine 8-mer peptides for H2-kb molecules were determined by epitope prediction with the SYFPEITHI (www.syfpeithi.de), IEDB (www.iedb.org) or netMHC 3.4 Server (www.cbs.dtu.dk) database. The sequences of Ad hexon, HBcAg and HBsAg that were used for epitope prediction are derived from the AdHBV vector sequence and are depicted in chapter 6.3.

2.2.3.11 IL-10 reporter reaction

The IL-10 reporter reaction enables the detection of IL-10 in all lymphoid and myeloid cells derived from ITIB and DEREG/ITIB mice, which carry the IL-10–bla transgene. Cells were seeded with $1x10^6$ cells/well in a V-profile 96-well tissue culture test plate in mTCM and pelleted at 1,300 RPM for 3 min at RT. Cells were resuspended in 100 µl/well CCF4-AM

loading medium and incubated in a thermomixer at 150 RPM for 90 min at 29 °C in the dark. After washing with PBS, the cells were NIR stained as described in 2.2.5.1.

In case of macrophage staining, the macrophages were stained with anti-CD64 antibody for 20 min at 4 °C in the dark, washed twice with PBS and then incubated with Fc-Block 1:1000 diluted in 10 µl/well in PBS for further 10 min on ice in the dark. Afterwards the NIR staining was performed.

After live/dead staining, the cells were washed in the following steps with the FACS buffer for the IL-10 reporter reaction. Surface staining and in the case of staining of Tregs, surface staining followed by ICS, was performed like described in 2.2.5.2 and 2.2.5.3. The different leukocyte populations were stained in three groups: T cells ($CD8^+$ T cells: $CD8^+$, $CD4^+$ $Foxp3^-$ T cells : $CD4^+$ $Foxp3^-$, Tregs: $CD4^+$ $CD25^+$ $Foxp3^+$), B cells; NK cells and NKT cells (B cells: $CD19^+$, NK cells: $CD3^-$ $NK1.1^+$ cells, NKT cells: $CD3^+$ $NK1.1^+$ cells) and monocytes, macrophages and DC (macrophages: $F4/80^{high}$ $CD11b^{low}$, monocytes: $F4/80^-$ $CD11b^{high}$, DC: $CD11c^+$). Except the T cells, which were fixed during ICS, all cells were fixed after surface staining with 0.2 % (v/v) PFA in FACS buffer. After fixation of cells and storage at 4 °C, the reporter reaction was stable for several days. Due to selection of antibodies, the group of monocytes, macrophages and DC was measured on the FACS Fortessa, whereas T cells, B cells, NK cells and NKT cells were measured on the FACS Canto II.

The ratio of the CCF4 substrate (denominator in FITC) and the cleaved CCF4* pruduct (numerator in Pacific Blue) was set on the FACS Canto II and the FACS Fortessa to a scaling of 11 %. In order to set the gate for the IL-10–Bla^+ cells correctly, the staining for the IL-10 reporter reaction had to be performed also on a wild type mouse, which lacks the IL-10–bla transgene.

2.2.3.12 Quantitative real time PCR

Quantitative real time PCR (qPCR) is used to amplify and quantify a defined section of a DNA template at the same time by measuring the emission of an intercalating SYBR Green dye. In order to isolate genomic DNA and total RNA of liver pieces, which were stored in RNAlater (2.2.3.6), the tissue was homogenized by using the Tissue Lyser LT according to the manufacturer's handbook. Further homogenization was achieved by using a 20 G needle. Isolation of genomic DNA and total RNA was performed with the Allprep DNA/RNA kit

according to the manufacturer's instructions for simultaneous purification of genomic DNA (100 µl eluate) and total RNA (40 µl eluate) from animal tissues.

For the detection of HBV copy numbers in the liver, 5 µl SYBR Green mix, 1.25 ng/µl genomic DNA and 1 µM of each fwd and rev HBV primer were pipetted in a total volume of 10 µl/well in a Frame Star plate. The same was performed with murine intron primers on the same plate, whereas the mix with Ad and murine intron primers respectively was pipetted on a different plate. A relative quantification of Ad and HBV copy numbers was achieved by normalization of the values with the murine intron as endogenous target that was measured in the same sample. For each primer pair, a six step dilution series (1:2 to 1:64) of the template and a sample with water instead of the DNA template was pipetted in order to control PCR efficiency. Primers and cycling conditions for the LightCycler480 II are described in 2.1.13.

For detection of expression levels of IFNγ and IL-10 in the liver, the purified total RNA was reversely transcribed to cDNA using the SuperScript III kit according to manufacturer's instructions. The cDNA was diluted 1:12 in water for qPCR analysis, for which 5 µl SYBR Green mix, 4 µl of the diluted cDNA and 1 µM of each fwd and rev IFNγ primer were pipetted in a total volume of 10 µl/well in a Frame Star plate. The same was performed with IL-10, GAPDH and HPRT primers on the same plate. A relative quantification of IFNγ and IL-10 copy numbers was achieved by normalization of the values with GAPDH and HPRT as endogenous targets measured in the same sample. For each primer pair, a six step dilution series (1:2 to 1:64) of the template and a sample with water instead of DNA template was pipetted in order to control PCR efficiency. Primers and cycling conditions for the LightCycler480 II are described in 2.1.13.

2.2.3.13 Serological analysis

Murine whole blood was transferred to micro tube and centrifuged at 10,000 RPM for 10 min at RT. After centrifugation the serum, that was located above the gel matrix, was transferred to a new reaction tube and used for serological analysis.

In order to determine liver damage, 32 µl of fresh serum diluted 1:2 in PBS were pipetted onto an ALT stripe that was inserted into the Reflotron machine for measurement. In order to determine the levels of HBeAg, HBsAg and anti-HBsAg antibody, the serum was diluted in PBS and measured with the diagnostic Architect immunoassay analyzer.

2.2.4 Co-culture study

For the co-culture study, B cells, monocyte derived DC and monocyte derived macrophages were isolated and matured from HLA-A2$^+$ primary blood mononuclear cells (PBMC). Furthermore, the PBMC served as source for T cells, which were transduced with a TCR specific for either HBV_C18 (TCR_core) or HBV_S20 (TCR_surface) on HLA-A2$^+$ APC.

2.2.4.1 Isolation of PBMC populations

In order to isolate PBMC for the co-culture study, 100 ml peripheral blood of one healthy HLA-A2$^+$ donor were drawn in two 50 ml syringes, each with 1 ml of heparin and were diluted 1:1 with prewarmed leukocyte wash medium. The diluted blood was split in six parts, layered onto 15 ml Lymphocyte separation medium in a 50 ml centrifuge tube and centrifuged at 1,800 RPM for 20 min without brake at RT. The white lymphocyte layer was carefully collected from the interphase between the plasma and the separation medium. The collected cells of each 50 ml centrifuge tube were diluted 1:1 with leukocyte wash medium and centrifuged at 1,300 RPM for 10 min at RT. Afterwards, the cell pellets were pooled and washed three times. For the removal of thrombocytes, the cells were centrifuged at 600 RPM for 20 min at RT with the brake speed set to 5. The cell pellet was resuspended in PBS, washed once and counted before used for magnetic activated cell sorting (MACS).

PBMC were sorted by MACS for CD19$^+$ cells on a LS column according to manufacturer's instructions. The flow-through was collected on ice, while the isolated CD19$^+$ B cells were counted. The cells were resuspended in 0.5 ml human albumin to which 0.5 ml DC freezing medium was added dropwise. Afterwards, the cells were quickly placed in the freezing container at -80 °C.

The monocytes of the CD19$^-$ flow-through were divided in half. One half was used for maturation of monocyte derived DC (see 2.2.4.3), while the other half was sorted by MACS for CD14$^+$ cells on a LS column according to manufacturer's instructions. The flow-through was collected on ice, while the isolated CD14$^+$ monocytes were counted and seeded with $1.9x10^5$ cells/well in a 24 well tissue culture test plate in Leukocyte medium. The monocytes were stored at 37 °C and 5 % CO_2 for maturation (see 2.2.4.2).

The CD19$^-$ monocyte$^-$ PBMC were used as source for T cells that were transduced with HBV specific TCR (see 2.2.4.4). After counting of the surplus CD19$^-$ monocyte$^-$ PBMC, the cells

were resuspended in 0.5 ml human albumin, to which 0.5 ml DC freezing medium was added dropwise. Afterwards, the cells were quickly placed in the freezing container at -80 °C.

2.2.4.2 Maturation of monocyte derived macrophages

For maturation of monocyte derived macrophages, monocytes were cultured with the Macrophage maturation mix for three days at 37 °C with 5 % CO_2. After a renewal of the mix and culturing of the cells for additional four days, the monocyte derived macrophages developed the characteristic shape of macrophages. The cells were scraped from the bottom of the plate and counted. Afterwards, the cells were resuspended in 0.5 ml human albumin, to which 0.5 ml DC freezing medium was added dropwise. The cells were quickly placed in the freezing container at -80 °C.

2.2.4.3 Maturation of monocyte derived DC

In order to maturate monocyte derived DC from the monocytes of the $CD19^-$ flow-through, the cells were resuspended in 12 ml DC medium, transferred to a Nunclon delta-surface flask (75 cm^3) and incubated at 37 °C with 5 % CO_2. The cells were cultured in DC maturation mix I for 2 days and in DC maturation mix II for an additional day. A small aliquot of monocyte derived DC was surface stained for NIR, CD14-PE, CD80-FITC and CD83-APC (see 2.2.5.1, 2.2.5.2), as control for successful maturation of $CD14^-$ $CD80^+$ $CD83^+$ DC. After counting, the DC were resuspended in 0.5 ml human albumin to which 0.5 ml DC freezing medium was added dropwise. Afterwards, the cells were quickly placed in the freezing container at -80 °C.

2.2.4.4 Transduction of T cells

In preparation for transduction of T cells with a TCR specific for either HBV_C18 (TCR_core) or HBV_S20 (TCR_surface) on $HLA\text{-}A2^+$ APC, 24 well non-tissue culture treated plates were coated with 250 µl/well coating buffer and incubated for 2 h at 37 °C with 5 % CO_2. After removal of the coating buffer, the wells were covered with 500 µl/well of 2 % BSA (v/v) in PBS for 30 min in the incubator, after which the plate was washed twice with 2 ml PBS. In the next step, the remaining $CD19^-$ $monocyte^-$ PBMC from 2.2.4.1 were seeded with $6x10^5$ cells/well in hTCM for growth and incubated for 2 days in the incubator in order to expand the T cell population.

In preparation for culturing of HEK 293 T cells, 6-well tissue culture test plates were coated with 1 ml/well of 1:20 diluted poly-L-lysine solution in PBS for 60 min in the incubator and afterwards washed twice with 2 ml/well PBS. In a next step, HEK 293 T cells were seeded with $2x10^6$ cells/well in 2 ml DMEM medium without antibiotics. The cells were transfected with lipofectamin and either pcDNA3.1-gag-pol, pALF10.a1env and MP71_TCR_5E_co (TCR_core) or MP71_TCR_D1_co (TCR_surface) according to manufacturer's instructions in order to produce retroviral supernatant. One day after transfection, the medium was replaced by DMEM complete medium. Two days after transfection, 1.5 ml of the retroviral supernatant of the TCR_core or TCR_surface respectively were pooled and filtered through a 0.45 µm filter, whereas fresh 1.5 ml DMEM complete medium were added to the plate with the transfected HEK 293 T.

In order to prepare the retroviral transducing agent for transduction of T cells, 24-well non-tissue culture treated plates were coated with 250 µl/well of a 1:50 dilution of Retronectin in PBS for 2 h at RT under the hood. After removal of the Retronectin solution, which is stored at 4 °C for the next day, the wells were covered with 500 µl/well of 2 % BSA (v/v) in PBS for 30 min in the incubator, after which the plate was washed twice with 2 ml PBS. The filtered retroviral transducing agent was transferred to the Retronectin coated plates (1 ml/well), which were centrifuged at 3,100 RPM for 2 h at 32 °C. After centrifugation, the plates were blocked with 500 µl/well 2 % (v/v) BSA in PBS for 30 min in the incubator and washed twice with 2 ml PBS. For transduction of T cells, the expanded T cells were counted and seeded with $0.8x10^6$ cells/well in 0.5 ml/well of the medium in which they were grown in, combined with 1 ml/well of fresh hTCM for growth. The T cells were spun onto the Retronectin/ retrovirus coated plate at 3,100 RPM for 10 min at 32 °C and stored in the incubator over night. On the next day, the procedure of the transfer of retroviral supernatant and of T cells to a new Retronectin coated plates was repeated. 24 h after the second T cell transduction, NIR stained T cells were subjected to peptide-MHC multimer staining with CD8-Pacific Blue, C18-MHC-Streptactin-APC or S20-MHC-Streptactin-APC in order to control the transduction rate of TCR_core and TCR_surface (see 2.2.5.1 and 2.2.5.4).

2.2.4.5 Stimulation and co-culture

For the co-culture study of capsid stimulated APC with the transduced T cells of 2.2.4.4, B cells, DC and macrophages were thawed, counted and seeded with $5x10^4$ cells/well in

U-profile 96-well tissue culture test plates. APC were stimulated in triplets with capsid, recombinant (rec) capsid, HBV_C18, HBV_S20, HCMV *pp65, HCMV pool (see 2.1.12) and without peptide for 16 h at 37 °C with 5 % CO_2. After stimulation, the transduced T cells TCR_core, TCR_surface or the T cell clone with specificity for HCMV_pp65 epitope (TCCl_pp65) were added in a 1:1 ratio to the respective APC and stored in the incubator.

Table 23: Overview of characteristics of transduced T cells provided by Karin Wisskirchen and the T cell clone provided by Andreas Moosmann, HelmholtzZentrum Munich for the co-culture study.

Name	Type	Epitope origin	Targeted epitope	Position epitope
TCR_core	TCR	HBV D	FLPSDFFPFV	HBV_HBcAg 18-27
TCR_surface	TCR	HBV D	FLLTRILTI	HBV_HBsAg 20-28
TCCl_pp65	T cell clone	HCMV 7	NLVPMVATV	HCMV_pp65 495-503

After 22 h of co-culture, the supernatant was collected in a new 96-well plate and stored at -20 °C for an IFNγ ELISA (2.2.4.6), whereas the cells were subjected to surface staining of CD4-ECD, CD8-PeC7, CD134-APC and CD137-Alexa Flour700 (2.2.5.2).

2.2.4.6 Enzyme-linked immunosorbent assay

The enzyme-linked immunosorbent assay (ELISA) was used to identify the secreted IFNγ derived from activated T cells after 22 h of co-culture with capsid stimulated APC. The ELISA was performed according to manufacturer's instruction on Nunc-Immuo plates and analyzed with the Infinite 200 detection system.

2.2.5 Flow Cytometry

Flow Cytometry is a way to measure single cells according to their size and granularity. By the use of fluorochrome-conjugated antibodies it is furthermore possible to stain cells for their surface markers and after fixation and permeabilization also for intracellular proteins such as transcription factors and cytokines.

2.2.5.1 Live/dead staining

For live/dead staining with EMA, the cells were resuspended in 100 µl EMA diluted in FACS buffer for murine cells and incubated for 20 min on ice in close proximity of a light source, in order to allow crosslinking of the dye with the genomic DNA. After two rounds of washing with FACS buffer, the cells were stained for their surface markers as described in 2.2.5.2.

For live/dead staining without prior fixation of surface stained lymphocytes, which were isolated from murine blood for the DEREG or DEREG/ITIB screen (see 2.2.3.3), 10 µl of PI solution were added to each FACS tube prior to measurement.

For the IL-10 reporter reaction (see 2.2.3.11) and the co-culture study (see 2.2.4), the cells were stained with NIR 1:200 diluted in 50 µl PBS and were incubated for 20 min on ice in the dark. This live/dead staining was suitable for human and murine cells.

2.2.5.2 Surface staining

For surface staining of murine LAL and splenocytes, cells were transferred to a V-profile 96-well micro test plate. The cells were pelleted at 1,300 RPM for 3 min at 4 °C. The supernatant was discarded, while the cell pellet was resuspended in 200 µl FACS buffer for murine cells. Staining of murine cells was performed in a volume of 50 µl/well of the respective fluorochrome conjugated anti-mouse antibody (see 2.1.9) that was diluted in FACS buffer for 30 min on ice in the dark. The cells were washed twice with FACS buffer and in case of no further ICS (see 2.2.5.3), the cells were transferred to the FACS tubes in a final volume of 200 µl FACS buffer with 0.2 % (v/v) PFA and measured with the FACS Canto II. Data were analyzed with FlowJo and GraphPad Prism software.

For surface staining of human cells isolated from PBMC for the co-culture study, cells were transferred to a V-profile 96-well micro test plate. The cells were pelleted at 1,300 RPM for 3 min at 4 °C. The supernatant was discarded, while the cell pellet was resuspended in 200 µl FACS buffer for human cells. Staining of murine cells was performed in a volume of 19 µl/well of the respective fluorochrome conjugated anti-human antibody (see 2.1.9) that was diluted in FACS buffer for 30 min on ice in the dark. The cells were washed twice with FACS buffer and were transferred to the FACS tubes in a final volume of 300 µl FACS buffer and measured with the FACS Fortessa. Data were analyzed with FlowJo and GraphPad Prism software.

2.2.5.3 Intracellular cytokine staining

After surface staining and double wash steps, cells were fixed in 50 µl Cytofix and incubated for 20 min on ice in the dark. In the subsequent steps, the fixed cells were washed with 200 µl 1x PermWash (diluted in water). The ICS was performed in 50 µl volume of the respective fluorochrome conjugated anti-mouse antibody (see 2.1.9) that was diluted in 1x PermWash

and incubated for 30 min on ice in the dark. Afterwards, cells were washed twice with 1x PermWash and once with FACS buffer for murine cells. ICS stained cells were transferred to the FACS tube in a final volume of 200 µl FACS buffer and measured with the FACS Canto II. Data were analyzed with FlowJo and GraphPad Prism software.

2.2.5.4 Peptide-MHC multimer staining

For peptide-MHC multimer staining of murine splenocytes, 0.4 µg peptide-MHC multimer (peptide-MHC class I complex) and 1:50 dilution of Streptactin-PE in 50 µl/well FACS buffer for murine cells were incubated for 25 min on ice in the dark. Afterwards, the cells were resuspended in the multimer-Streptactin-PE mix and incubated for 30 min on ice in the dark. For surface staining, cells were stained with CD8-Pacific Blue as described in 2.2.5.2. Prior to measurement on the FACS Canto II, 10 µl PI were added to the FACS tube for live/dead staining. $CD8^+$ T cells that recognize the peptide presented by the MHC class I molecule could be detected as $CD8^+$ $multimer^+$ cells in flow cytometry. Data were analyzed with FlowJo and GraphPad Prism software.

3 Results

3.1 T cell priming by *in vitro* HBcAg stimulated APC

HBcAg is described to act as highly immunogenic antigen, which elicits strong T cell effector functions in HBV infected patients. Furthermore, it was shown that apoptosis of HBV infected hepatocytes released great amounts of non-enveloped HBV capsids that were speculated to prime T cells and B cells. In order to examine the potential of HBV capsids for T cell priming via B cells an *in vitro* co-culture study of T cells with capsid stimulated B cells and other APC was designed as described in the following.

The process of leukocyte isolation as well as APC stimulation and their co-culture with the different T cells is schematically depicted in Figure 7A. PBMC from a HLA-$A2^+$ donor were purified by density gradient and sorted by MACS for $CD19^+$ cells in order to obtain B cells. The monocytes of the $CD19^-$ PBMC were either used for maturation of monocyte derived DC or sorted by MACS for $CD14^+$ cells for maturation of monocyte derived macrophages. In the following monocyte derived DC and macrophages are referred to as DC or macrophages respectively. In the next step, the remaining $CD19^-$ $monocyte^-$ PBMC were used as source for T cells that were transduced with a TCR specific for either HBV_C18 (TCR_core) or HBV_S20 (TCR_surface) on HLA-$A2^+$ APC. The two TCR were kindly provided by Karin Wisskirchen. T cells equipped with the TCR_core were expected to recognize all capsid derived antigens, whereas T cells equipped with the TCR_surface served as negative control for capsid derived antigens. Andreas Moosmann provided a T cell clone with specificity for NLVPMVATV on position aa 495–503 of the human cytomegalovirus (HCMV) pp65 protein (TCCl_pp65) on HLA-$A2^+$ APC that served as control for cross-presenting abilities of the respective APC. For detailed information about purification and maturation see chapter 2.2.4.

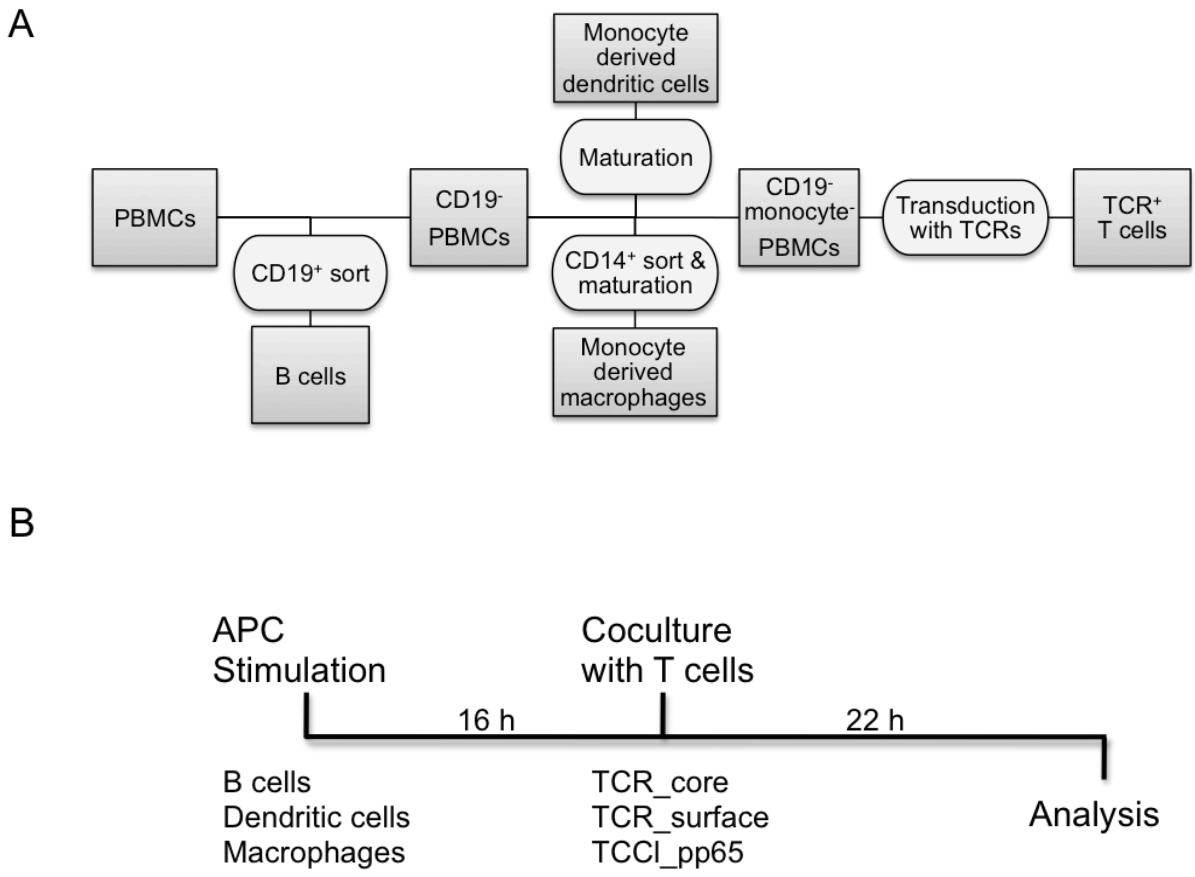

Figure 7: Co-culture of capsid stimulated APC with T cells. Leukocyte populations were isolated and matured from human PBMC in order to obtain APC (B cells, dendritic cells and macrophages) as well as T cells that were transduced with TCR. APC were stimulated with variably antigens for 16 h, followed by co-culture with T cells for 22 h. The T cells were equipped with different specificities of TCR or TCCl. Analysis was performed via flow cytometry and ELISA. (A) Flow chart of B cell, DC, macrophage and T cell isolation from PBMC. The maturation process of DC and macrophages as well as transduction of T cells with TCR was started on the same day after leukocyte isolation of PBMC. (B) Flow chart of APC stimulation and co-culture with T cells with different specificities. (ELISA: enzyme-linked immunosorbent assay, PBMC: peripheral blood mononuclear cells, TCR: T cell receptor, TCCl: T cell clone).

The candidate APC were stimulated with capsids derived from envelope denatured HBV virions produced by the HBV producing HepG2.2.15 cells or with recombinant HBV capsids produced in *Escherichia coli*. APC were also stimulated with the single peptides HBV_C18 or HBV_S20 as positive control for the respective TCR specificity. Moreover the APC were stimulated with carbamylated-pp65 protein of HCMV (HCMV *pp65), which is cross-presented by APC. Candidate APC were stimulated with a peptide pool containing 138 HCMV derived peptides with an 11 aa overlap (HCMV pool) in order to control the specificity of TCCl_pp65. Unstimulated APC (without peptide) were used to determine background levels of T cell activation.

B cells, DC or macrophages were stimulated for 16 h with the different antigens before co-culture with either one of the three types of T cells carrying the different TCR referred to as TCR_core, TCR_surface and TCCl_pp65 in the following. After 22 h of co-culture, the cells were stained for flow cytometric analysis of T cell activation markers CD137 and CD134 on $CD4^+$ T cells and $CD8^+$ T cells whereas the co-culture supernatant was used for detection of secreted IFNγ via ELISA (Figure 7B).

3.1.1 T cell activation after co-culture with stimulated APC

T cell activation after 22 h co-culture with the variably stimulated APC was measured by staining of the activation markers CD137 and CD134 on $CD4^+$ and $CD8^+$ T cells. In general, CD137 is stronger expressed in activated $CD8^+$ than $CD4^+$ T cells and CD134 is vice versa stronger expressed in activated $CD4^+$ T cells than $CD8^+$ T cells. $CD4^+$ and $CD8^+$ T cell activation is shown in Figure 8. $CD137^+$ $CD134^+$ double positive $CD4^+$ and $CD8^+$ T cells were not detected during this study (data not shown).

Co-culture of TCR_core and B cells that were stimulated with capsid, recombinant capsid or HBV_C18 did not result in significant increase of the activation marker CD137 on the surface of $CD8^+$ T cells or CD134 on the surface of $CD4^+$ T cells (Figure 8A and D). In contrast, TCR_core co-culture with recombinant capsid stimulated DC and to a lesser extend with HBV_C18 stimulated DC resulted in an increase of CD137 expression levels on $CD8^+$ and $CD4^+$ T cells. Furthermore, CD134 levels increased on $CD4^+$ and $CD8^+$ T cells after TCR_core co-culture with recombinant capsid stimulated DC (Figure 8B and E). Interestingly, TCR_core co-culture with macrophages resulted only in increased levels of CD137 on $CD8^+$ and $CD4^+$ T cells or increased levels of CD134 on $CD4^+$ T cells when macrophages were stimulated with HBV_C18 (Figure 8C and F). Unspecific $CD4^+$ and $CD8^+$ T cell activation with increased CD137 level was mainly observed after TCR_core co-culture with HCMV *pp65 or HCMV pool stimulated APC.

TCR_surface $CD4^+$ and $CD8^+$ T cell activation was solely observed after co-culture with HBV_S20 stimulated APC, indicating high specificity of this setting. Co-culture of TCCl_pp65 with HCMV pool but not with HCMV *pp65 stimulated APC resulted in $CD8^+$ T cell activation, especially after co-culture with macrophages. Similarly $CD4^+$ T cell activation was observed after TCCl_pp65 co-culture with HCMV pool stimulated APC. However, $CD137^+$ $CD4^+$ T cells were only observed after TCCl_pp65 co-culture with

HCMV *pp65 stimulated B cells and DC but not macrophages where solely high level of $CD134^+$ $CD4^+$ T cells were observed. Unspecific activation of T cells was detected after TCCl_pp65 co-culture with recombinant capsid stimulated DC as well as with capsid, recombinant capsid and HBV_C18 stimulated B cells.

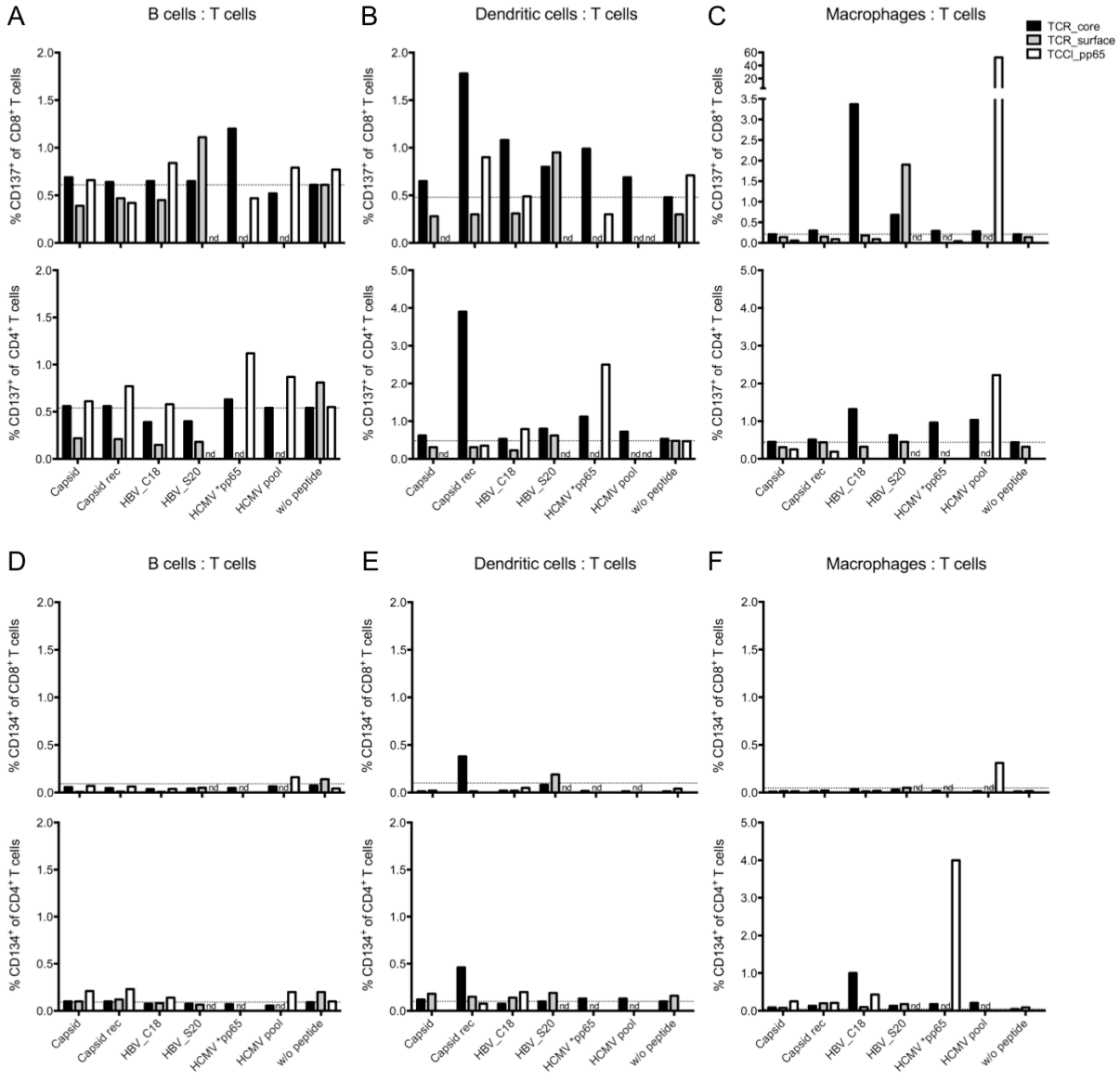

Figure 8: Activation marker expression on $CD4^+$ and $CD8^+$ T cells after co-culture with stimulated APC. Flow cytometric analysis of T cells with different TCR specificities after 22h co-culture with variably stimulated APC. Percentages of $CD137^+$ $CD8^+$ T cells (top row) and $CD137^+$ $CD4^+$ T cells (2nd row) are shown after co-culture with (A) B cells, (B) DC and (C) macrophages. Percentages of $CD134^+$ $CD8^+$ T cells (3rd row) and $CD134^+$ $CD4^+$ T cells (bottom row) are shown after co-culture with (D) B cells, (E) DC and (F) macrophages. The dotted line shows the level of T cell activation after co-culture with unstimulated APC (without peptide). (TCR: T cell receptor, TCCl: T cell clone).

Taken together these results indicate that the three receptors TCR_core, TCR_surface and TCCl_pp65 were functional and able to recognize their designated target peptides. Unspecific

antigen recognition and subsequent T cell activation was detected for TCR_core and TCCl_pp65 but not for TCR_surface. HCMV *pp65 stimulation resulted in $CD4^+$ T cell activation, but not in $CD8^+$ T cell activation indicating that no cross-presentation occurred in the used APC which could be detected with TCCl_pp65. Nevertheless cross-presentation was detected in DC stimulated with recombinant capsids and to a lesser extent with capsids. At the same time cross-presentation abilities were observed for macrophages and B cells when stimulated with the carbamylated HCMV *pp65 protein but not with capsids.

3.1.2 T cell effector function

IFNγ secretion as standard T cell effector function was measured by ELISA 22h after co-culture with differentially stimulated B cells, DC or macrophages, which is shown in Figure 9. In line with the increased expression levels of activation markers on $CD4^+$ T cells and $CD8^+$ T cells, high IFNγ secretion was detected after TCR_core co-culture with macrophages stimulated with HBV_C18, whereas TCR_core co-culture with B cells stimulated with HBV_C18 resulted only in IFNγ secretion slightly above background level. Unspecific IFNγ secretion was observed after TCR_core co-culture with HBV_S20, HCMV *pp65 and HCMV pool stimulated APC. TCR_surface co-culture with HBV_S20 stimulated APC resulted in high IFNγ secretion that reflects the increase of activation markers described above. IFNγ secretion was observed to a lesser extent after TCR_surface co-culture with capsid and recombinant capsid stimulated B cells. For TCCl_pp65 IFNγ secretion was only observed after co-culture with HCMV *pp65 and HCMV pool stimulated APC.

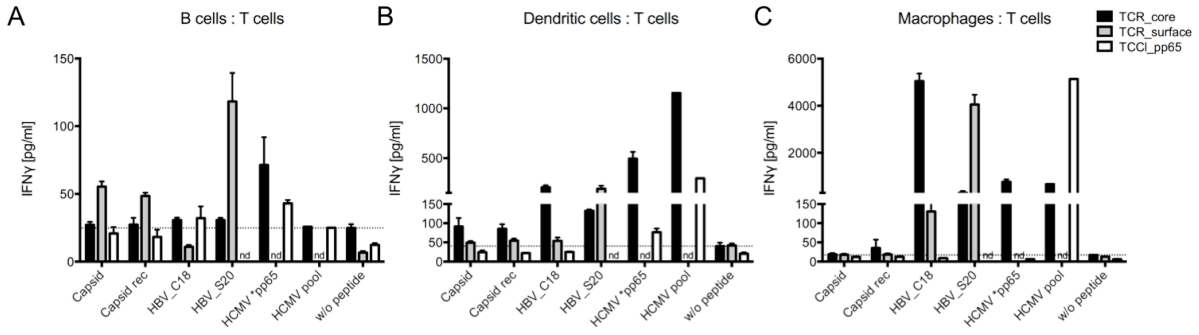

Figure 9: IFNγ secretion of T cells after co-culture with stimulated APC. IFNγ secretion of T cells, which are equipped with different TCR specificities, was detected by ELISA after 22 h of co-culture with (A) B cells, (B) dendritic cells and (C) macrophages. Data are shown as mean values with standard deviation for n=3, otherwise as mean values only. (ELISA: enzyme-linked immunosorbent assay, TCR: T cell receptor).

In summary, peptide presentation by DC and macrophage resulted in IFNγ secretion indicating $CD4^+$ and $CD8^+$ T cell activation. In addition, cross-presentation of capsid derived antigen by DC resulted in $CD8^+$ T cell activation. For capsid stimulated B cells, however, no T cell activation and no further IFNγ secretion was detected. Thus, capsid stimulation of B cells is not sufficient to activate T cells.

3.2 Detection of Ad and HBV specific T cell responses

The AdHBV mouse model was shown to be a good model in order to establish an acute hepatitis B during which liver damage, HBV replication, secretion of the HBV markers HBeAg and HBsAg as well as the corresponding antibodies were detected in the course of a self-limiting AdHBV infection. However, detection of HBV specific $CD8^+$ or $CD4^+$ T cell responses has not been specific enough yet in this model due to a lack of epitope characterization in AdHBV infected mice.

In order to test for HBV specific $CD8^+$ T cell responses, C57BL/6 mice were intravenously (i.v.) infected with $1x10^9$ IU AdHBVx- or the control virus AdEmpty and sacrificed on day 28 post infection (p.i.) for flow cytometric ICS after *ex vivo* peptide stimulation of leukocytes. Due to limited amounts of isolated leukocytes at late points during AdHBVx- infection (compare Figure 19A), more peptides could be tested on leukocytes isolated from the spleen than from liver. In the following these cells will be referred to as splenocytes or LAL since the analysis in this chapter is focused on $CD4^+$ and $CD8^+$ lymphocytes. An overview of the tested peptides is shown in chapter 2.1.12.

In general, higher $CD8^+$ T cell responses were detected in the liver than in the spleen due to increased infiltration of antigen specific $CD8^+$ T cells to the liver as site of infection. ICS after stimulation with peptides that were described as immunogenic in HBV DNA immunized mice, HBV transgenic mice (HBV_C93, HBV_S190) or HBV infected humans (HBc P4) as well as stimulation with recombinant HBcAg protein (capsid rec) did not result in a detectable $CD8^+$ T cell response (Figure 10B and C) in AdHBVx- infected mice. Stimulation with HBV_S208 and HBs P1 resulted only in a slight $CD8^+$ T cell response above background level. In contrast, a strong $IFN\gamma^+$ $CD8^+$ response in liver (23 %) and spleen (9 %) on day 28 p.i. was observed after stimulation with the peptide pool HBc P3 consisting of 15-mer peptides each with an 11 aa overlap covering the carboxyl-terminal last 62 amino acids of the HBcAg protein (Figure 10B and C; see 6.1). However, the *ex vivo* stimulation of LAL and splenocytes isolated from AdEmpty infected mice resulted also in the detection of $IFN\gamma^+$ $CD8^+$ T cells indicating cross-reactivity to the Ad5 vector (5 % in LALs, 7 % in splenocytes; Figure 10B and C). Silke Arzberger identified regions within the single peptides HBc #33 and HBc #42 of the HBc P3 peptide pool that could be responsible for Ad cross-reactivity (Figure 10D). The SYFPEITHI database was used for the prediction of H-2Kb (MHC class I allele in C57BL/6 mice) binding epitopes derived from the

carboxyl-terminal end of HBcAg. This epitope prediction resulted in four HBc 8-mer peptides that partially covered the sequence of HBc #33 and two 8-mer peptides outside of the HBcAg sequence covered by HBc P3 (see 6.2). *Ex vivo* stimulation of LAL and splenocytes with a pool of these six HBcAg peptides (HBc P5), however, did not result in any IFNγ$^+$ CD8$^+$ response (Figure 10C).

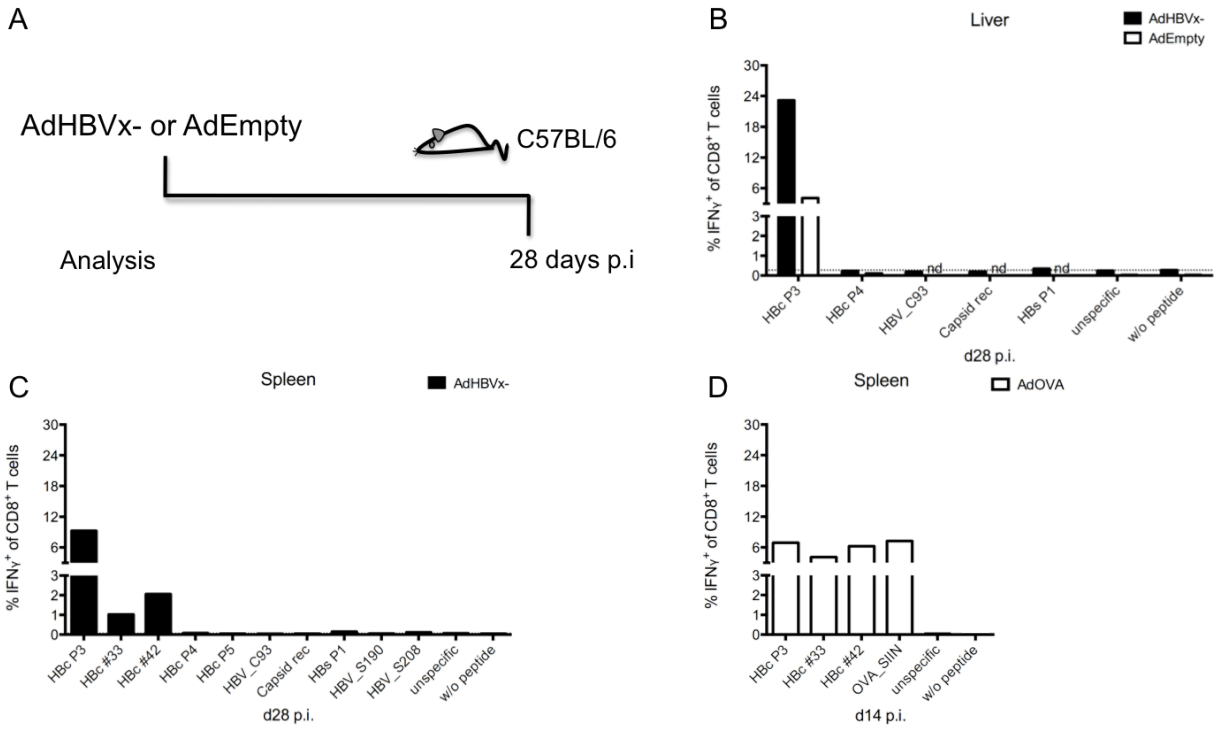

Figure 10: Characterization of epitopes for detection of HBV specific CD8$^+$ T cell responses. C57BL/6 mice (n=2) were infected intravenously with 1x10^9 IU of AdHBVx- or the control virus AdEmpty and sacrificed on day 28 p.i. for flow cytometric ICS analysis. (A) Experimental setup. (B) Percentages of IFNγ$^+$ CD8$^+$ T cells derived from LAL and (C) splenocytes. (D) Percentages of IFNγ$^+$ CD8$^+$ T cells derived from splenocytes of AdOVA infected mice on day 14 p.i.. Data are shown as mean values. (ICS: intracellular cytokine staining, LAL: liver associated lymphocytes, nd: not determined).

3.2.1 Epitope prediction of Ad and HBV epitopes

The purpose of the following experiments was to identify epitopes that enabled separate detection of Ad and HBV specific CD8$^+$ T cell responses during AdHBVx- infection in C57BL/6 mice carrying the H-2kb molecule. Extension of the SYFPEITHI epitope prediction with the output of further epitope prediction software tools based on the IEDB and netMHC databases for the HBcAg, HBsAg and Ad hexon proteins was implemented in order to identify Ad and HBV epitopes that were immunogenic in the AdHBV mouse model enabling a separate readout of CD8$^+$ T cell responses directed against the Ad vector and the HBV

transgene. The predicted epitopes with the two (HBcAg and HBsAg) or three (Ad hexon) best scores of the netMHC prediction were pooled respectively (Table 24) and used for stimulation of LAL on day 7 and day 28 p.i. (Figure 11A). On day 7 p.i., an apparent $CD8^+$ T cell response against the Ad hexon peptide pool AdH P1 was detected for both AdHBV and the control AdHBVk/o infected mice. The Ad hexon specific response was still detectable on day 28 p.i.. Conversely, stimulation of LAL with the peptide pools HBc P6 and HBs P2 consisting of the predicted epitopes did not result in $CD8^+$ T cell responses detectable above background level. Further analysis of the Ad specific $CD8^+$ T cell response is shown in 3.2.2, whereas further testing of HBcAg derived epitopes is described in 3.2.3.

Table 24: Overview of selected 8-mer peptides after epitope prediction for H-2Kb using the netMHC databases. Outputs of netMHC are in IC50 [nM] compared to IEDB [percentile rank] and SYFPEITHI [Score]. Epitopes predicted by netMHC were rated as strong binders (values <50) and weak binders (values <500). (Epitopes predicted by IEDB were rated as high affinity (values <0.3) and intermediate affinity (values <1.0) binding peptides; SYFPEITHI predicted strong binders within the top 2% of the score (values in brackets are below the top 2%)).

Position	Sequence	SYFPEITHI	IEDB	netMHC	Nomenclature	
HBV_C93	MGLKFRQL	24	0.15	7		HBc P6
HBV_C86	VSYVNTNM	15	0.15	28		
HBV_S81	IIFLFILL	23	0.10	3		HBs P2
HBV_S179	ASARFSWL	24	0.35	72		
Ad_H470	RNFLYSNI	(20)	0.10	3	AdH #1	
Ad_H676	RGWAFTRL	23	0.15	8	AdH #2	AdH P1
Ad_H64	LTRRFIPV	(19)	0.30	36	AdH #3	

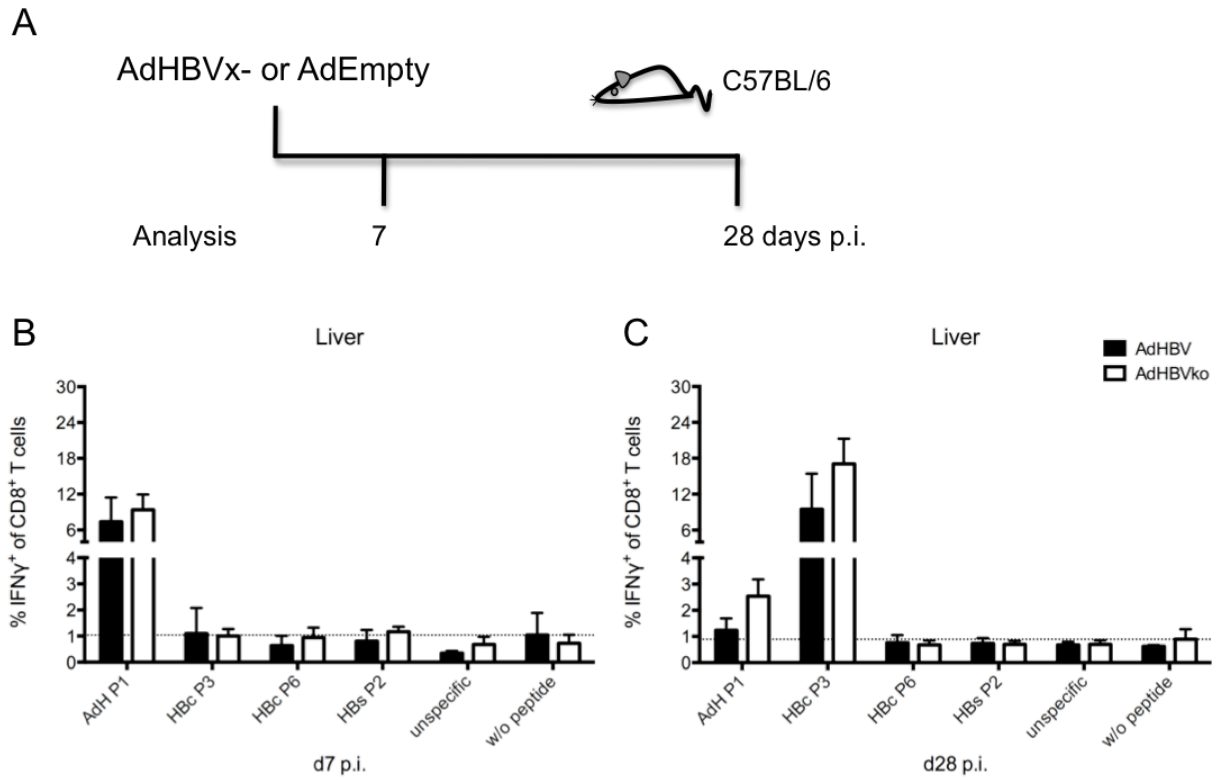

Figure 11: IEDB & netMHC predicted peptides stimulate Ad but not HBV specific CD8$^+$ T cell responses. C57BL/6 mice (n = 4) were infected intravenously with 1x10^9 IU of AdHBVx- or the control virus AdHBVko and were sacrificed on day 7 or day 28 p.i. for flow cytometric ICS analysis. (A) Experimental setup. (B) Percentages of IFNγ$^+$ CD8$^+$ T cells derived from LAL and (C) splenocytes. Data are shown as mean values with standard deviation. (ICS: intracellular cytokine staining, LAL: liver associated lymphocytes).

3.2.2 Detection of Ad specific T cell response during AdHBVx- infection

For detection of Ad specific CD8$^+$ T cell responses, C57BL/6 mice were infected with 1x10^9 IU of AdHBVx- or the control virus AdEmpty and sacrificed on day 19 or day 28 p.i. respectively for flow cytometric ICS after *ex vivo* peptide stimulation of LAL or splenocytes (Figure 12A). As shown in Figure 12B and C separation of the AdH P1 peptide pool revealed immunogenic potential of the single peptide AdH #1 on position aa470 (RNFLYSNI). AdH #1 induced a strong CD8$^+$ T cell response whereas the other two peptides AdH #2 and AdH #3 were not immunogenic. The difference in strength of the Ad specific response is due to lower Ad amounts present in AdEmpty infected compared to AdHBVx- infected mice in this experiment (Figure 12B and C). On day 19 p.i., a large number of Ad specific IFNγ$^+$ CD8$^+$ T cells were still detectable in liver and spleen (Figure 12E and F). As expected, AdH P1 and AdH #1 did not induce a CD8$^+$ T cell response in naïve mice, thus showing the identification of an immunodominant peptide that allowed monitoring of Ad5 specific CD8$^+$ T cell responses in C57BL/6 mice.

Ex vivo stimulation of AdH #1 did not only induce monofunctional IFNγ secretion of $CD8^+$ T cells but also to a lesser extent in an induction of monofunctional $IL\text{-}2^+$ $CD8^+$ T cells as well as monofunctional $TNF\alpha^+$ T cells. Furthermore, bifunctional $IFN\gamma^+$ $TNF\alpha^+$ $CD8^+$ T cells and half as much polyfunctional $IFN\gamma^+$ $IL\text{-}2^+$ $TNF\alpha^+$ $CD8^+$ T cells were detected (Figure 12G). In conclusion, *ex vivo* stimulation of lymphocytes with the single peptide AdH #1 enables the readout of Ad specific $CD8^+$ T cell responses that is useful in further studies to estimate the T cell response against the Ad5 vector in the AdHBV mouse model.

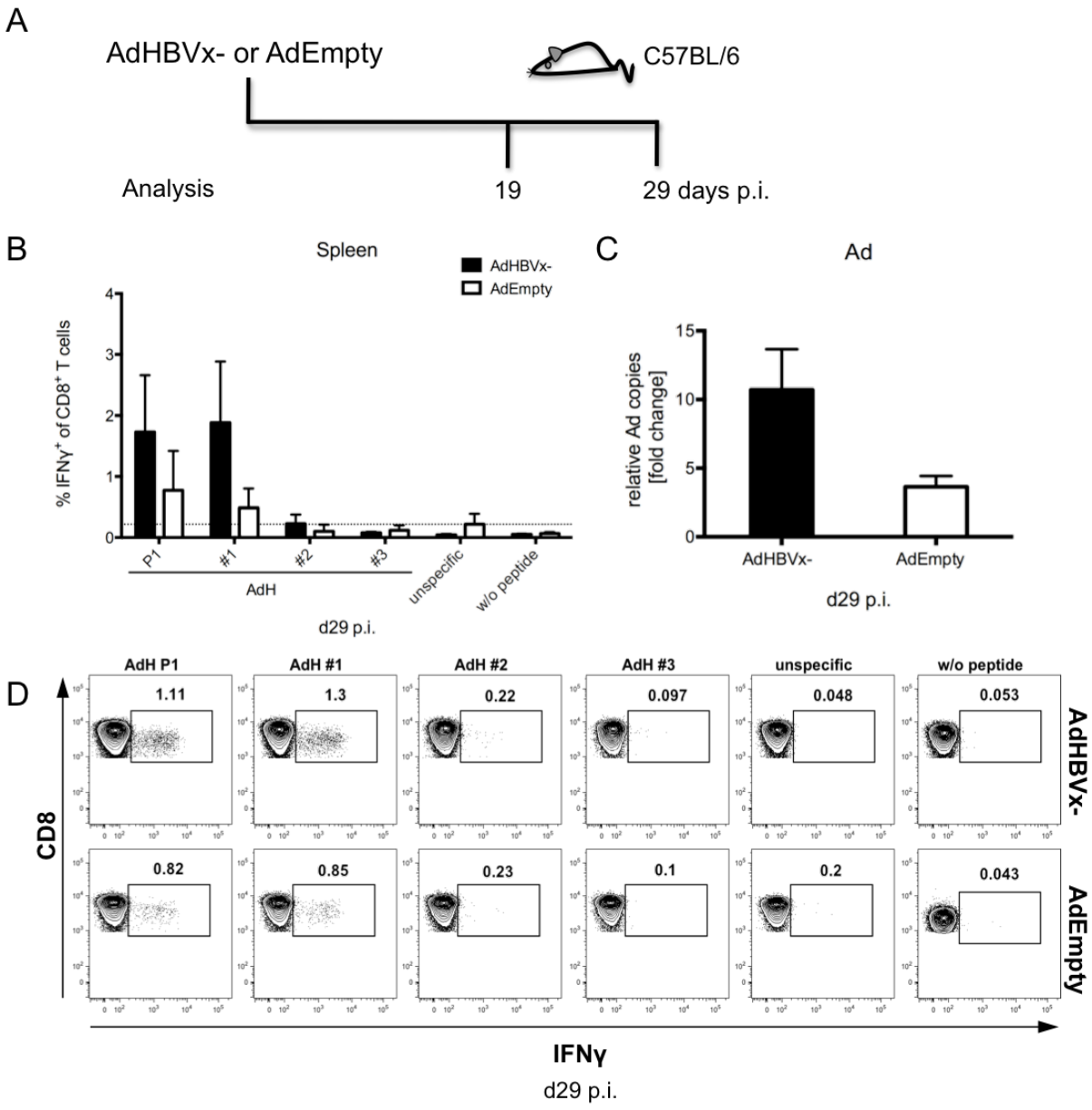

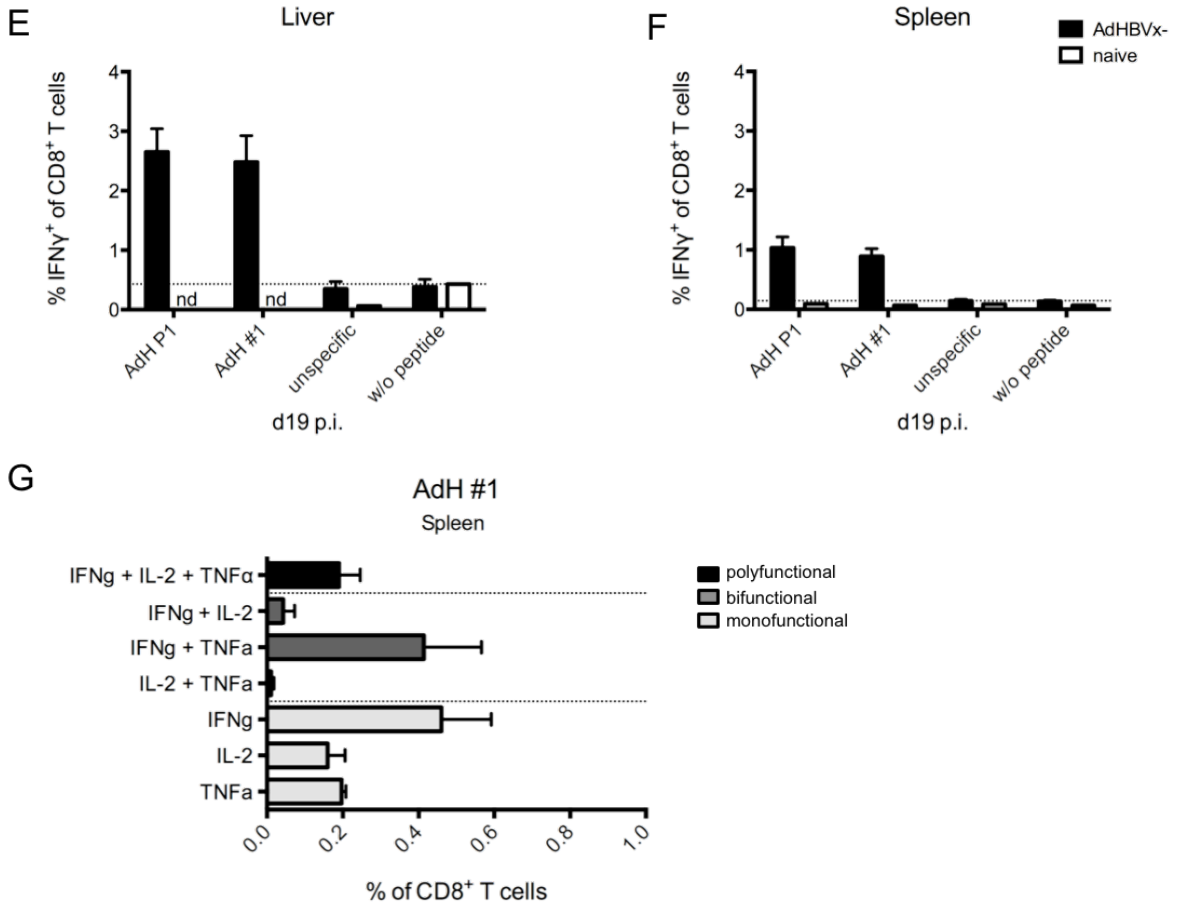

Figure 12: Strong Ad5 hexon specific CD8$^+$ T cell response induced by single peptide AdH #1. C57BL/6 mice (n=3) were infected intravenously with 1x10^9 IU of AdHBVx- or the control virus AdEmpty and were sacrificed on day 19 or day 29 p.i. for flow cytometric ICS and quantitative PCR analysis. (A) Experimental setup. (B) Percentages of IFNγ$^+$ CD8$^+$ T cells derived from splenocytes. (C) Intrahepatic Ad copy numbers relative to murine intron determined by quantitative PCR. (D) Representative flow cytometric plots of Ad hexon stimulated splenocytes on day 29 p.i.. (E) Percentages of IFNγ$^+$ CD8$^+$ T cells derived from LAL and (F) splenocytes on day 19 post AdHBVx- infection or of naïve mice. (G) Percentages of cytokine producing CD8$^+$ T cell in the spleen after AdH #1 stimulation on day 19 post AdHBVx- infection. Data are shown as mean values with standard deviation for n=3, otherwise as mean values only. (ICS: intracellular cytokine staining, LAL: liver associated lymphocytes, nd: not determined).

3.2.3 Detection of HBV specific T cell response during AdHBVx- infection

For detection of HBV specific CD8$^+$ T cell responses, C57BL/6 mice were infected with 1x10^9 IU of AdHBVx- or the control virus AdEmpty and sacrificed on day 29 p.i. for flow cytometric ICS after *ex vivo* peptide stimulation of LAL or splenocytes with another HBcAg peptide pool (HBc P7). HBc P7 consisted of 18 18-mer peptides (HBc #1 to #18) overlapping by 11 aa and was spanning the HBcAg sequence except for the potentially cross-reactive carboxyl-terminal 47 aa. As shown in Figure 13A, a slight response of IFNγ$^+$ CD8$^+$ T cells (0.5 %) against HBc P7 was detected in the liver of AdHBVx- infected mice, whereas the

percentages of IFNγ$^+$ CD8$^+$ T cells of AdEmpty infected mice were at background level. In the spleen no IFNγ$^+$ CD8$^+$ T cell response (0.2 %) above background level was detected (Figure 13B). AdH P1 and HBc P3 served as positive controls and stimulated apparent CD8$^+$ T cell responses in liver and spleen as described earlier (compare Figure 10).

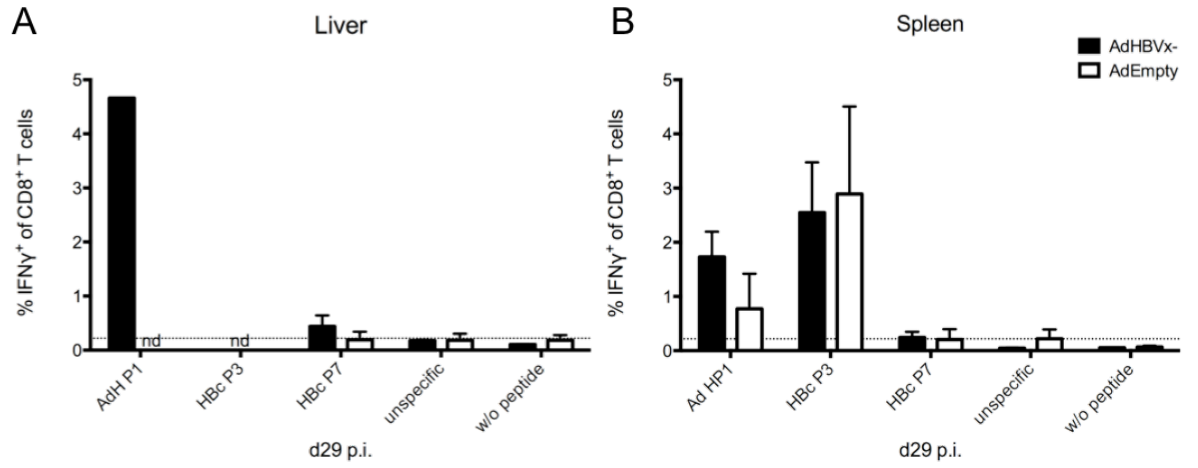

Figure 13: Weak HBV specific CD8$^+$ T cell response detected by peptide pool HBc P7 on day 29 p.i.. C57BL/6 mice (n=4) were infected intravenously with 1x10^9 IU AdHBVx- or the control virus AdEmpty and were sacrificed on 29 p.i. for flow cytometric ICS analysis. (A) Percentages of IFNγ$^+$ CD8$^+$ T cells derived from LAL and (B) splenocytes. Data are shown as mean values with standard deviation for n≥3, otherwise as mean values only. (ICS: intracellular cytokine staining, LAL: liver associated lymphocytes, nd: not determined).

Since CD8$^+$ T cell responses against Ad HP1 and HBc P3 were clearly detectable on day 29 p.i., the possibility of an earlier HBV specific T cell response during infection was investigated in a new infection experiment. C57BL/6 mice were injected with 1x10^9 IU of AdHBVx- or AdEmpty and the day of analysis was preponed to day 19 p.i. for flow cytometric ICS analysis of CD8$^+$ T cells in the spleen (Figure 14A). The CD8$^+$ T cell response against HBc P7 in AdHBVx- infected mice on day 19 p.i. in the spleen was 3-fold higher than on day 28 p.i., whereas HBc P7 stimulated splenocytes from AdEmpty infected mice induced no CD8$^+$ T cell response above background level (Figure 14C). Similarly no CD8$^+$ T cell response was detected in HBc P7 stimulated LAL or splenocytes of naïve mice as shown in Figure 15B and C.

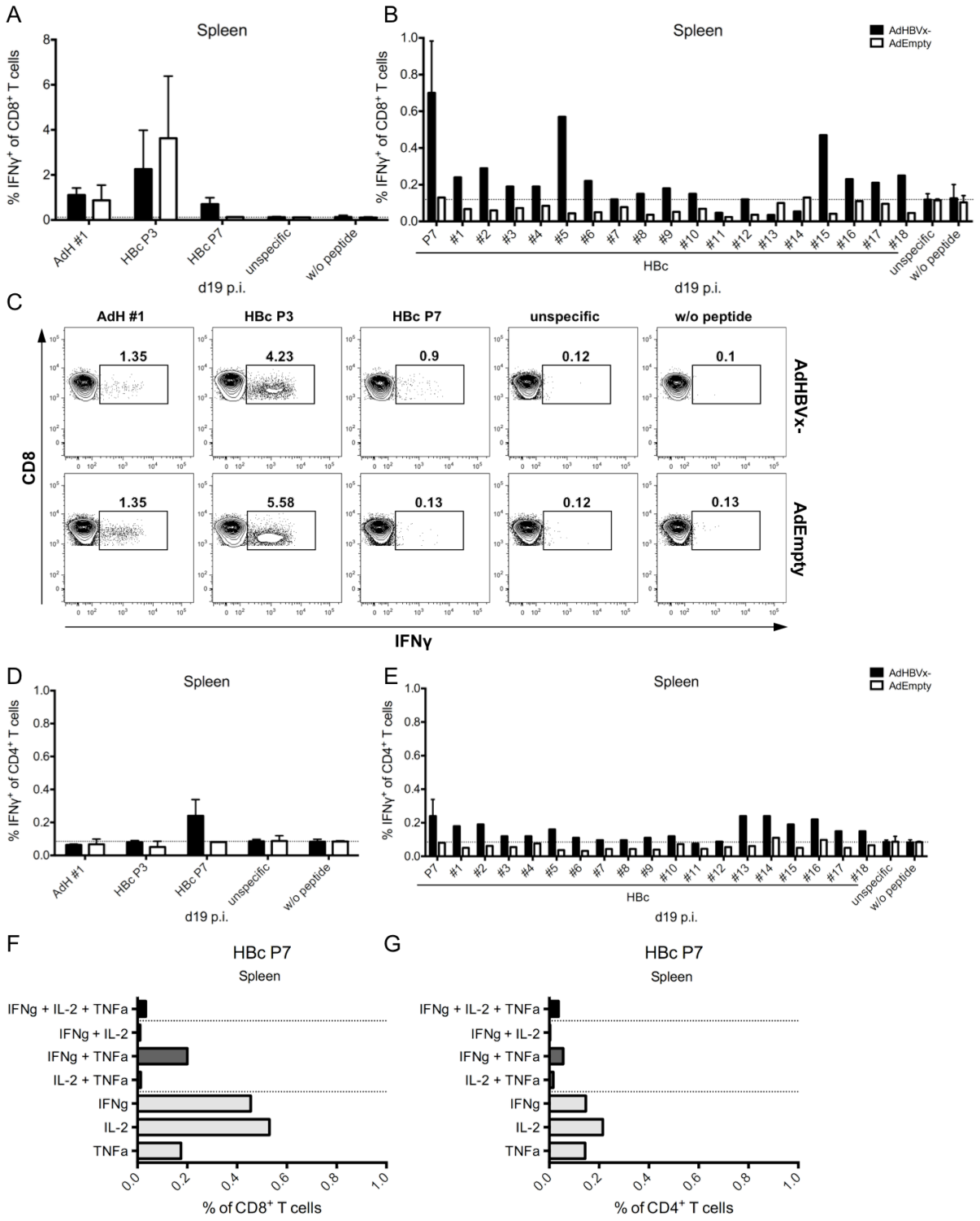

Figure 14: HBV specific CD8$^+$ T cell responses induced by peptide pool HBc P7 and corresponding single peptides on day 19 p.i.. CD45.1 mice were infected intravenously with 1x10^9 IU of AdHBVx- (n=3) or the control virus AdEmpty (n=2) and were sacrificed on day 19 p.i. for flow cytometric ICS analysis of splenocytes. (A) Percentages of IFNγ$^+$ CD8$^+$ T cells after *ex vivo* stimulation with peptide pool HBc P7 and (B) corresponding HBcAg single peptides. (C) Representative flow cytometric plots of HBc P7 stimulated splenocytes. (D) Percentages of IFNγ$^+$ CD4$^+$ T cells after *ex vivo* stimulation with peptide pool HBc P7 and (E) corresponding HBcAg single peptides. (F) Percentages of cytokine producing CD8$^+$ T cell or (G) CD4$^+$ T cell response after HBc P7 stimulation in the spleen on

day 19 post AdHBVx- infection. Data are shown as mean values with standard deviation for n=3, otherwise as mean values only. (ICS: intracellular cytokine staining, nd: not determined).

Peptides from peptide pool HBc P7 were also tested separately for *ex vivo* stimulation of splenocytes isolated from AdHBVx- or AdEmpty infected mice in order to identify immunogenic regions (Figure 14B). *Ex vivo* stimulation with the single peptides HBc #1-10 and HBc #15-18 induced a $CD8^+$ T cell response above background levels in AdHBVx-infected mice but not in AdEmpty infected mice. The $CD8^+$ T cell responses against HBc #5 (0.57 %) and HBc #15 (0.47 %) were the strongest and were almost as high as the $CD8^+$ T cell response against the HBc P7 peptide pool (Figure 14A). Stimulation with HBc #11-14 did not result in any $CD8^+$ response above background level. Moreover *ex vivo* splenocyte stimulation with HBc P7 resulted also in a moderate $IFN\gamma^+$ production by $CD4^+$ T cells (0.24 %) (Figure 14D). The HBc single peptides HBc #13-16 covered the immunogenic region for $CD4^+$ T cell response of pool HBc P7 (Figure 14 E).

HBc P7 stimulation resulted in the detection of $IFN\gamma^+$ $CD8^+$ T cells, and furthermore, also in the detection of similar amounts of monofunctional IL-2^+ $CD8^+$ T cells as well as to a lesser extent of monofunctional $TNF\alpha^+$ $CD8^+$ T cells, bifunctional $IFN\gamma^+$ $TNF\alpha^+$ $CD8^+$ T cells and polyfunctional $IFN\gamma^+$ IL-2^+ $TNF\alpha^+$ $CD8^+$ T cells (Figure 14F). Likewise, $CD4^+$ T cell responses against the HBc P7 peptide pool mainly consisted of monofunctional $CD4^+$ T cells, but also to a lesser extent of bifunctional $IFN\gamma^+$ $TNF\alpha^+$ $CD4^+$ T cells and polyfunctional $IFN\gamma^+$ IL-2^+ $TNF\alpha^+$ $CD4^+$ T cells (Figure 14G). In conclusion, stimulation with the HBc P7 peptide pool or single peptides derived from this pool enable the detection of a functional and HBV specific $CD4^+$ T cell and $CD8^+$ T cell response in C57BL/6 mice after AdHBVx-infection.

In order to explain the low percentages of HBV specific $CD8^+$ T cells compared to Ad specific $CD8^+$ T cells (see Figure 14A), it was addressed whether HBV specific T cells were escaping detection in the ICS analysis due to their potential lack of functionality. Thus peptide-MHC multimer staining was used to determine HBV specific $CD8^+$ T cells irrespective of their functionality. C57BL/6 mice were infected with $1x10^9$ IU of AdHBVx- or AdEmpty and sacrificed on day 19 p.i. for flow cytometric peptide-MHC multimer staining of splenocytes. Only minimally increased percentages of $multimer^+$ $CD8^+$ T cells against HBV_C18, HBV_S20, HBV_C93, HBV_S172 and HBV_S190 were detected above background level (Figure 15A). This minute response against HBV_C93, HBV_S172 and

HBV_S190 was also detected in *ex vivo* peptide stimulated splenocytes of AdHBVx- infected mice on day 19 p.i. as shown in Figure 15B. Even more, splenocyte stimulation with whole capsids showed a moderate $CD8^+$ T cell response (0.26 %) that was not detectable on day 28 p.i. (compare Figure 10B). On the other hand, the preponed day of analysis did not result in detection of $IFN\gamma^+$ $CD8^+$ T cells directed against the before tested peptide pools HBc P6 and HBs P2 (compare Figure 11B and C) confirming that the predicted HBc epitopes were not immunogenic in our experimental setup. The fact that proportions of $CD8^+$ T cells binding to the peptide-MHC complex reflected the HBV specific $IFN\gamma^+$ $CD8^+$ T cell responses, confirms that only low levels of HBV specific $CD8^+$ T cells are detectable in AdHBVx- infected mice on day 19 p.i..

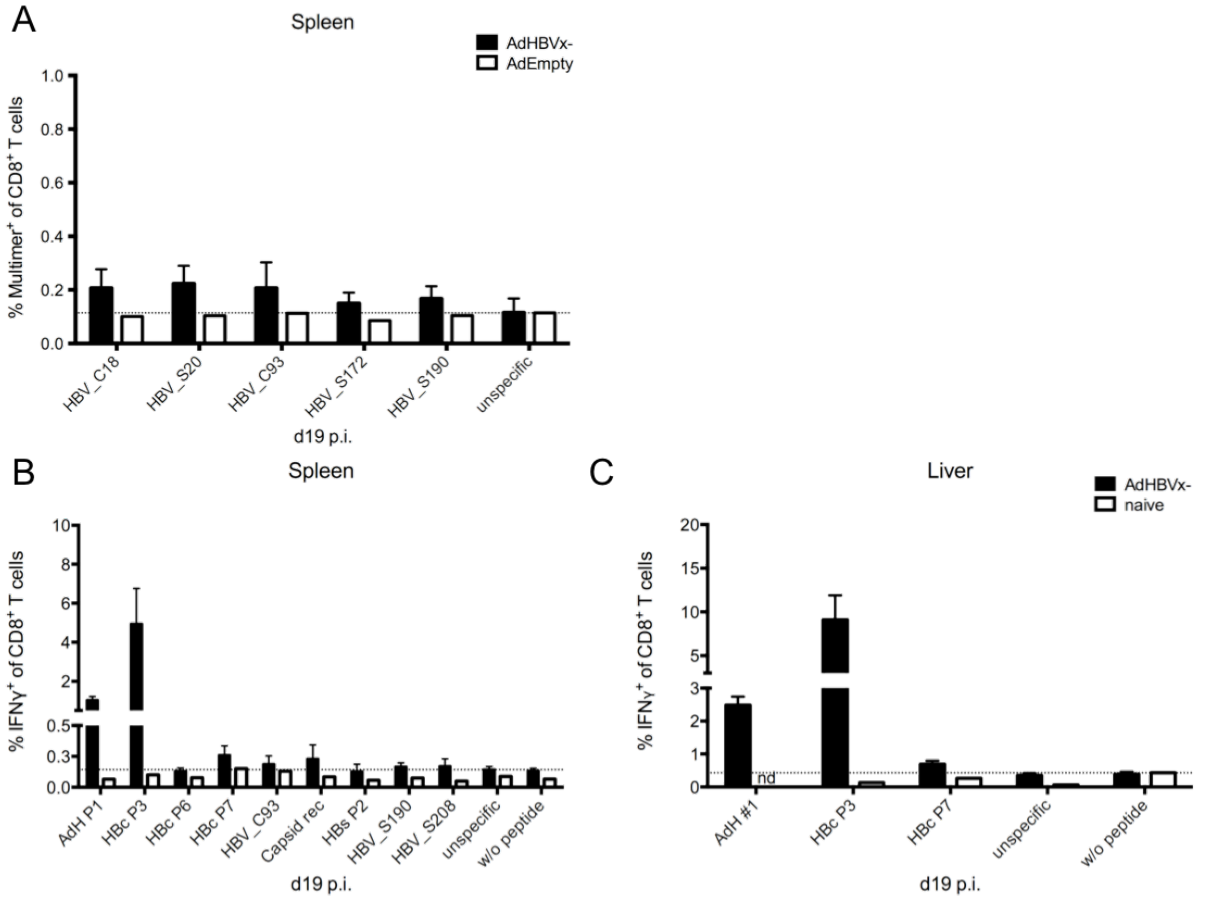

Figure 15: Low HBV multimer$^+$ CD8$^+$ T cell percentages and corresponding CD8$^+$ T cell responses. CD45.1 mice were infected intravenously with $1x10^9$ IU of AdHBVx- (n=3) or the control virus AdEmpty (n=2) and were sacrificed on day 19 p.i. for flow cytometric peptide-MHC multimer and ICS analysis. (A) Percentages of HBV peptide-MHC multimer$^+$ $CD8^+$ T cells in splenocytes. (B) Percentages of $IFN\gamma^+$ $CD8^+$ T cells in splenocytes and (C) LAL after *ex vivo* stimulation with HBV peptides. Data are shown as mean values with standard deviation for n=3, otherwise as mean values only. (ICS: intracellular cytokine staining, LAL: liver associated lymphocytes, nd: not determined).

Following infection parameters of AdHBVx- infected mice, HBsAg and HBeAg levels were highest on day 7 p.i. and declined afterwards in the AdHBVx- infected mice faster for HBsAg than for HBeAg (Figure 16B and C). Anti-HBsAg antibodies could only be detected on day 29 p.i. in one out of three AdHBVx- infected mice (Figure 16D), whereas anti-HBeAg antibodies were not detectable on day 29 p.i. (data not shown). The decline of HBV markers correlated with alanine aminotransferase (ALT) levels that were strongly increased on day 7 p.i. (1100 U/l in AdHBVx- infected mice) and declined during the course of infection (Figure 16A). In AdEmpty infected mice only a minor increase of ALT values was detected that peaked on day 19 p.i. (290 U/l). ALT background level of naïve mice was around 50 U/l. As expected, AdEmpty infected mice were negative for HBV markers and the respective antibodies. Taken together, the decline of ALT as well as HBV marker reflects the decreasing amount of HBV specific $CD8^+$ T cell responses during the course of AdHBVx- infection.

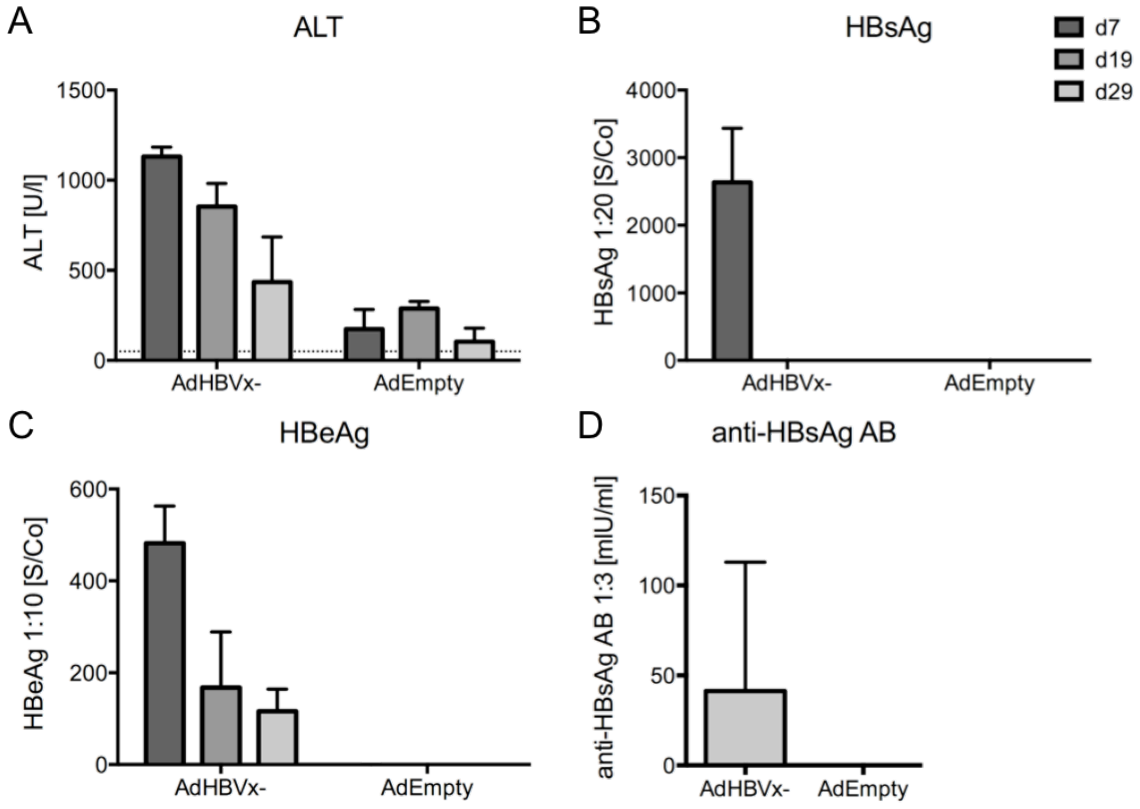

Figure 16: Decline of liver damage and HBV markers during course of AdHBVx-infection. Serological parameters of AdHBVx- or AdEmpty infected mice (n=3) on day 7, 19 and 29 p.i.. (A) ALT was measured from serum. Dotted line at 50 U/l shows ALT value of naïve mice. (B) HBsAg, (C) HBeAg and (D) anti-HBsAg antibodies were measured from serum. Data was shown as mean values with standard deviation. (ALT: alanine aminotransferase).

In summary, these results show that functional Ad and HBV specific $CD8^+$ T cell responses are detectable in the AdHBV mouse model although at low levels. An H2-kb specific immunogenic Ad5 hexon 8-mer epitope could be identified but no HBcAg or HBsAg 8-mer epitopes. HBV specific $CD8^+$ T cell responses were only observed after stimulation with 18-mer peptides. The difference in ALT activities between AdHBVx- and AdEmpty infected mice indicated that an HBV specific immune response is operative, which could not be monitored by ICS.

3.3 Role of Tregs and IL-10 production during AdHBVx- infection

In recent years, Tregs and IL-10 became increasingly important in context of immune regulation and immune tolerance. However, IL-10 is difficult to detect due to insufficient assay techniques to identify the IL-10 secreting cells from the mixture of cell populations being present in leukocytes. These technical limitations can be circumvented by using the reporter system provided by the ITIB IL-10 reporter mouse, which encodes IL-10 linked to the Bla reporter enzyme enabling flow cytometry detection of the Bla activity reflecting the IL-10 production levels. In this part of the thesis, IL-10 reporter mice were used to examine the regulatory role of Tregs in the establishment of the anti-HBV immune response by detection of the IL-10 production by Tregs and by other cells of the innate and adaptive response.

3.3.1 Kinetics of IL-10 production during AdHBVx- infection

In order to investigate the IL-10 production by different cells of the innate and adaptive immune system during the course of an acute AdHBVx- infection, mice were i.v. infected with $1x10^9$ IU of AdHBVx- or the control virus AdEmpty and sacrificed on day 3, 5, 7, 14 and 21 p.i. (Figure 17A). During the course of AdHBVx- and AdEmpty infection, liver damage reflected by ALT release and serological markers of HBV infection were investigated and are shown in Figure 17 B to D. ALT levels increased on day 5 p.i. (1000 IU/l) and remained constantly elevated until day 21 p.i. (1400 IU/l), indicating moderate to strong liver damage in AdHBVx- infected mice. Infection with the control vector AdEmpty, however, induced only a 3-fold increase of ALT levels compared to naïve (uninfected) ITIB, mice between the day 3 and day 5 p.i.. As expected, the HBV markers HBsAg and HBeAg were only detectable in AdHBVx- infected mice and not in the control group of AdEmpty infected mice. HBeAg and HBsAg were highest on day 3 p.i. (850 S/Co HBeAg, 37000 IU/ml HBsAg all in 1:10 diluted serum) and declined progressively to low levels (190 S/Co HBeAg, 2 IU/ml HBsAg, all in 1:10 diluted serum) on day 21 p.i.. The more rapid decline of HBsAg than of HBeAg pointed to the induction of anti-HBsAg antibody production, resulting in complex formation of anti-HBsAg with HBsAg. Anti-HBsAg antibodies were only detectable on day 29 p.i. after seroconversion occurred (Figure 16D). Presence of HBV markers correlated with the detection of intrahepatic HBV copies (Figure 17E) indicating maximal HBV replication in hepatocytes on day 3 p.i., but persistent HBV replication until day 21 p.i.. These data illustrate the course of an acute HBV infection.

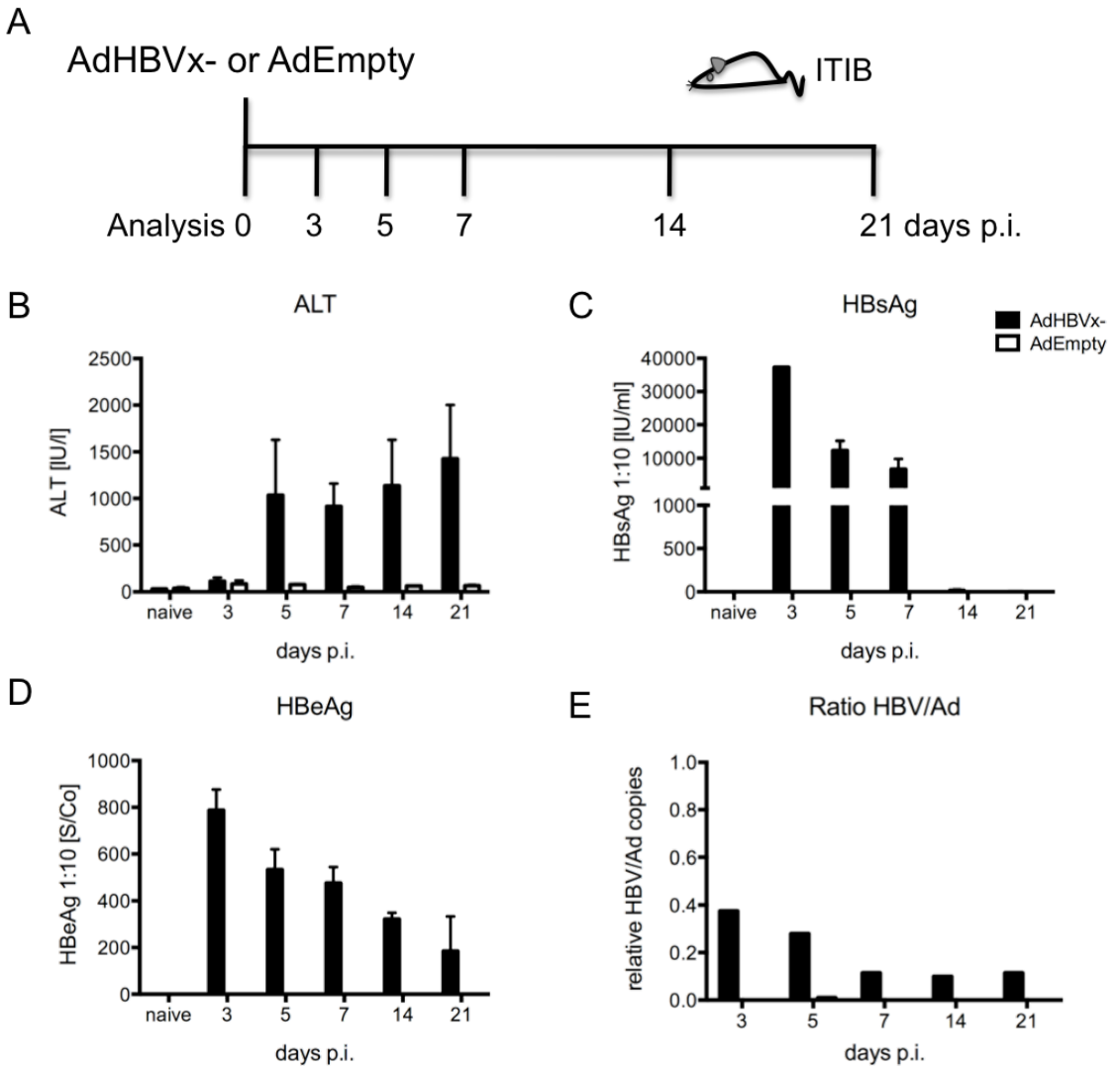

Figure 17: Increase of liver damage and decline of HBV markers during course of AdHBVx- infection. ITIB mice were infected intravenously with $1x10^9$ IU of AdHBVx- (n=3) or the control virus AdEmpty (n=2) and sacrificed on the indicated days p.i. for analysis of serum and liver parameters. (A) Experimental setup. (A) ALT, (B) HBsAg and (C) HBeAg were determined from serum. (D) Ratio of intrahepatic HBV to Ad copy numbers relative to murine intron were determined by quantitative PCR from liver DNA. Data are shown as mean values with standard deviation for n ≥ 3, otherwise as mean values only. (ALT: alanine aminotransferase).

As shown in Figure 18A and B, quantitative PCR data of intrahepatic IFNγ and IL-10 levels confirmed a peak of pro-inflammatory IFNγ (90-fold) on day 5 p.i. and a subsequent peak of anti-inflammatory IL-10 expression (8-fold) on day 7 p.i. in AdHBVx- infected mice. This indicated an immune regulating role of IL-10 during AdHBVx- infection, but without revealing the source of IL-10 production.

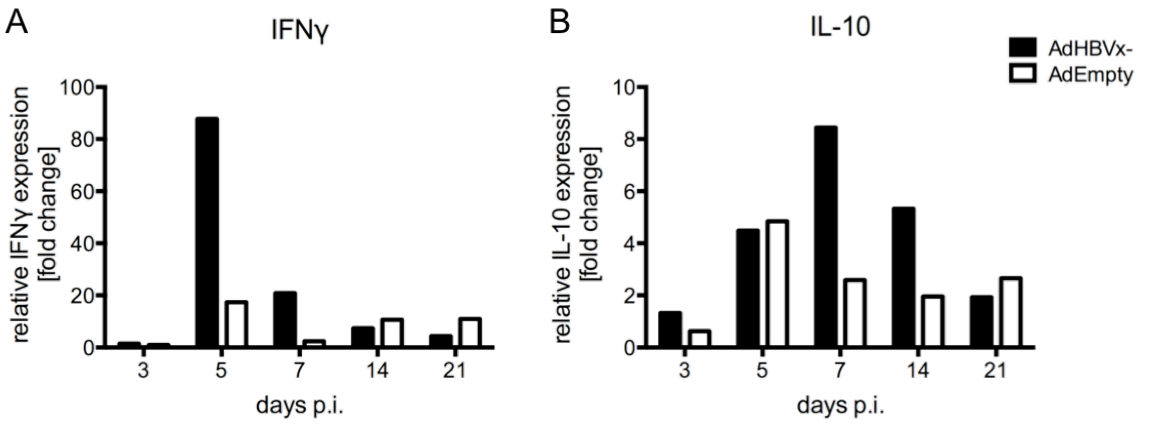

Figure 18: AdHBVx- infection induced pro- and anti-inflammatory cytokine expression. ITIB mice were infected intravenously with $1x10^9$ IU of AdHBVx- (n=2) or the control virus AdEmpty (n=2) and sacrificed on the indicated days p.i. for quantitative PCR analysis. (A) Isolated liver RNA was reversely transcribed to cDNA and used for quantitative PCR analysis of IFNγ or (B) IL-10 expression levels each relative to GAPDH and HPRT and normalized to naïve mice. Data are shown as mean values.

3.3.1.1 Kinetics of leukocyte counts during AdHBVx- infection

In order to reveal the source of IL-10 production during AdHBVx- infection, counts of leukocytes, which combine cells of the innate and adaptive immune response, and in a next step counts of several leukocyte populations as well as counts of $IL\text{-}10^+$ leukocyte populations were examined over time. AdHBVx- infection induced a 52-fold increase of total leukocyte counts (compared to naïve mice) with a maximum of $2.7x10^7$ cells in the liver on day 5 p.i.. Infection with the AdEmpty control virus induced an 11-fold increase of total leukocyte counts compared to naïve mice with a maximum of total leukocyte counts of $5.7x10^6$ cells in the liver on day 5 p.i. (Figure 19A).

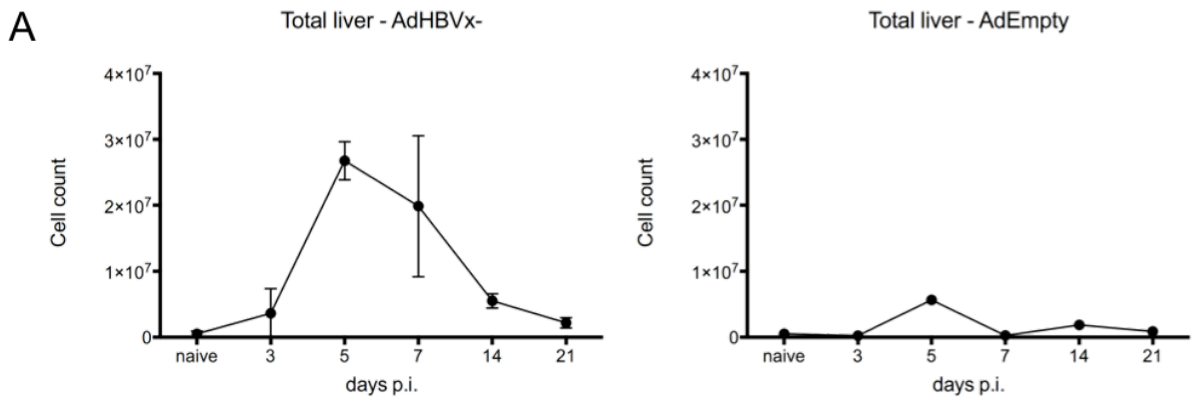

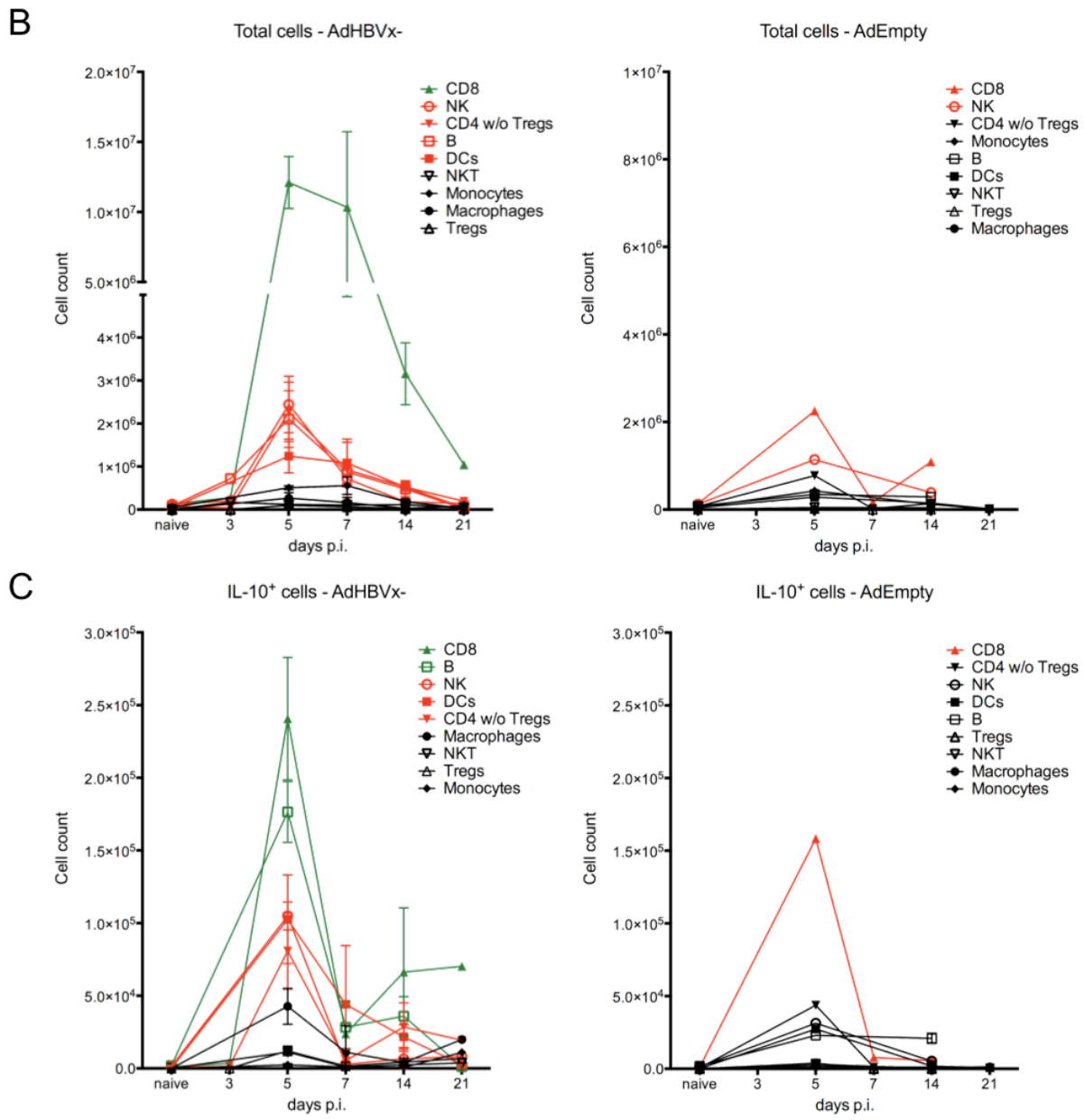

Figure 19: CD8$^+$ T cells are the main IL-10 producing population in the liver. ITIB mice were infected intravenously with 1x10^9 IU of AdHBVx- (n=3) or the control virus AdEmpty (n=2) and sacrificed on day 3, 5, 6, 14 and 21 p.i. for flow cytometric analysis of leukocytes of the liver. Cell counts of AdHBVx- infected (left) and AdEmpty infected (right) mice are shown. (A) Total leukocyte counts. (B) Counts of single leukocyte populations. Legend from top to bottom and color code are oriented on cell counts on day 5 p.i: green > 5.0x10^6 cells, red 1.1x10^6 to 5.0x10^6 cells, black: ≤ 1.0x10^6 cells. (C) Counts of single IL-10 producing leukocyte populations stained with ITIB reporter reaction. Legend from top to bottom and color code are oriented on cell counts on day 5 p.i: green > 1.5x10^5, red 5.1x10^4 to 1.5x10^5, black ≤ 5x10^4 cells Data are shown as mean values with standard deviation for n ≥ 3, otherwise as mean values only.

Separation of total leukocyte counts into the counts of single leukocyte populations revealed that the majority of leukocytes isolated from livers of AdHBVx- infected mice on day 5 p.i. were CD8$^+$ T cells (1.2x10^7 cells), followed by NK cells (2.4x10^6 cells), CD4$^+$ Foxp3$^-$ T cells

($2.3x10^6$ cells) and B cells ($2.1x10^6$ cells) with an respective 90-fold, 20-fold, 30-fold and 25-fold increase compared to naïve mice (Figure 19B). $CD8^+$ T cell counts were 5-fold higher in AdHBVx- infected mice than in the control group on day 5 p.i., while otherwise leukocyte compositions in both, AdHBVx- and AdEmpty infected mice were similar in proportion.

Cell counts of IL-10 expressing cells in the liver are depicted in Figure 19C. At the point in time of maximal leukocyte counts on day 5 p.i., $CD8^+$ T cells were the main producer of IL-10 in both, AdHBVx- ($2.4x10^5$ IL-10^+ $CD8^+$ T cells) and AdEmpty ($1.6x10^5$ IL-10^+ $CD8^+$ T cells) infected mice, however, with a slightly different composition of IL-10 expressing cells. In AdHBVx- infected mice populations with the highest IL-10 expression besides $CD8^+$ T cells were B cells ($1.8x10^5$ cells), NK cells ($1.1x10^5$ cells) and DC ($1.0x10^5$ cells), whereas in AdEmpty infected mice $CD4^+$ $Foxp3^-$ T cells ($4.4x10^4$ cells) followed $CD8^+$ T cells as the main IL-10 producing cells.

As in the liver, also in the spleen maximal counts of leukocytes were detected on day 5 p.i. with an 7-fold increase for AdHBVx- infected mice ($2.0x10^8$ cells) and an 3-fold increase for AdEmpty infected mice ($7.8x10^7$ cells) compared to naïve mice (Figure 20A). Comparison of total counts on day 5 p.i. showed a 7-fold and a 14-fold higher number of leukocytes in the spleen for AdHBVx- and AdEmpty infected mice respectively, underlining the importance of the spleen as location for priming of immune cells.

The majority of leukocytes found in spleens were B cells ($1.4x10^7$ cells; Figure 20B). Similar counts were detected in both AdHBVx- and AdEmpty infected mice on day 5 p.i. (3-fold increase compared to naïve mice). Other dominant leukocyte populations in spleens of AdHBVx- infected mice on day 5 p.i. were $CD8^+$ T cells ($2.1x10^7$ cells) and $CD4^+$ $Foxp3^-$ T cells ($1.4x10^7$ cells). In contrast to AdEmpty infected mice, in AdHBVx-infected mice the $CD8^+$ T cell population ($3.7x10^7$ cells) peaked on day 7 p.i.. Main producers of IL-10 in the spleen were B cells ($8.8x10^6$ cells). This population was 3-fold higher in AdHBVx- infected mice compared to the AdEmpty control group.

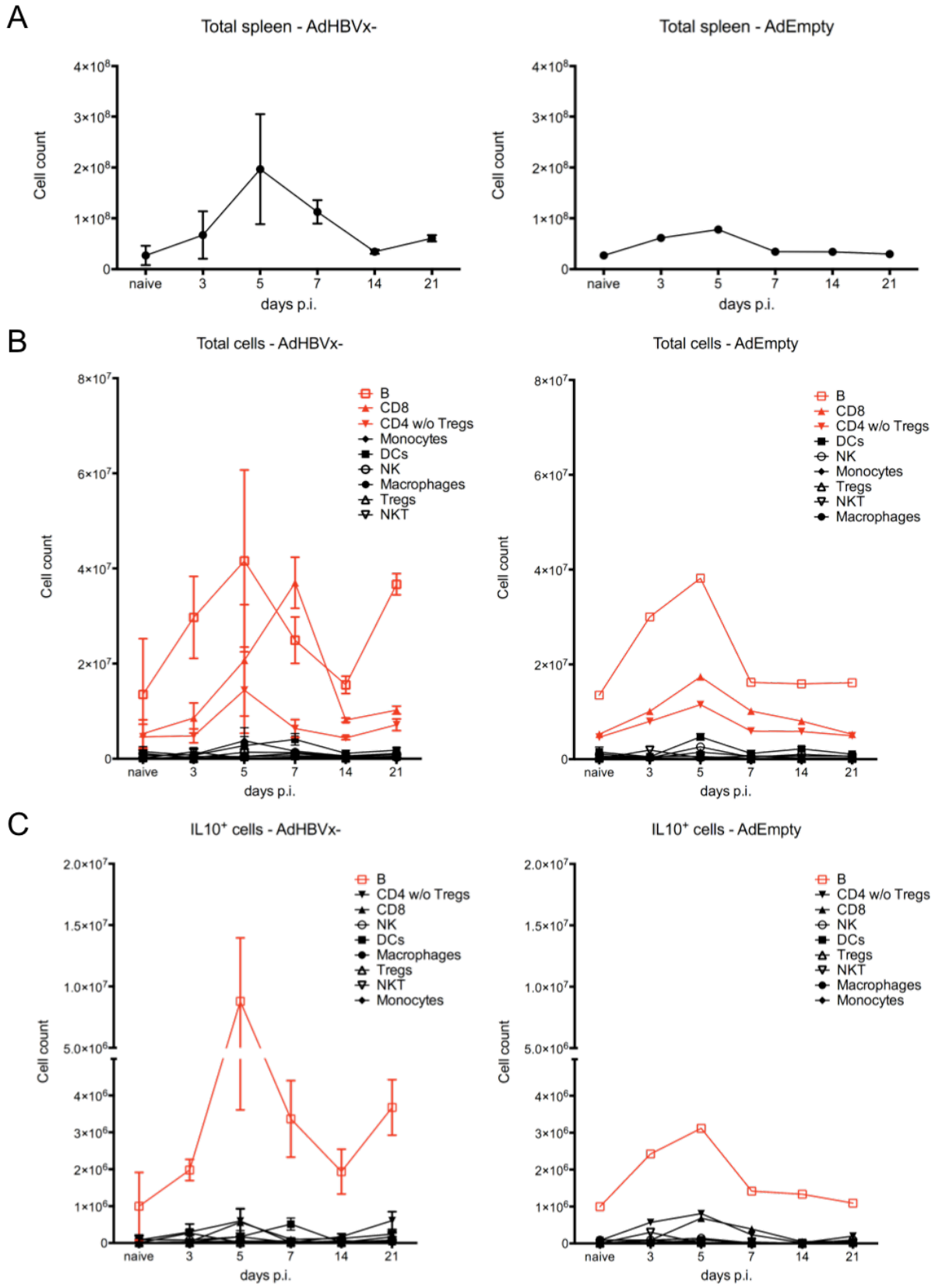

Figure 20: B cells are the main IL-10 producing population in the spleen upon Ad infection. ITIB mice were infected intravenously with 1x10^9 IU of AdHBVx- (n=3) or the control virus AdEmpty (n=2) and were sacrificed on day 3, 5, 6, 14 and 21 p.i. for flow cytometric analysis of leukocytes of the spleen. (A) Total leukocyte counts. (B) Counts of

single leukocyte populations. Legend from top to bottom and color code are oriented on cell counts on day 5 p.i: red > $1.0x10^7$ cells, black ≤ $1.0x10^6$ cells. (C) Counts of single IL-10 producing leukocyte populations stained with ITIB reporter reaction. Legend from top to bottom and color code are oriented on cell counts on day 5 p.i: red > $1.0x10^6$ cells, black ≤ $1.0x10^6$ cells. Data are shown as mean values with standard deviation for n ≥ 3, otherwise as mean values only.

In conclusion, a 3-fold decline of HBV copies until day 21 p.i. (Figure 17E) is accompanied by an increasing number of leukocytes in the liver (Figure 19A) and the spleen (Figure 20A) indicating a marked proliferation of mainly B cells and T cells. This was accompanied by a recruitment of NK cells and DC to the liver of infected mice. A variety of immune cells expressed the anti-inflammatory cytokine IL-10. Hereby, $CD8^+$ T cells and B cells were identified as the main IL-10 producing cell populations in the liver and the spleen respectively with maximal activity on day 5 post AdHBVx- or AdEmpty infection.

3.3.1.2 Kinetics of IL-10^+ leukocyte populations during AdHBVx- infection

In a next step, percentages of IL-10 producing cells of the innate and adaptive immune system in the liver and spleen were determined and are shown in Figure 21. On day 3 p.i., high percentages of IL-10^+ Tregs were observed upon AdHBVx- infection in spleens (14 %) and on day 21 p.i. in livers and spleens (50 % and 30 % respectively; Figure 21G). Further analysis of IL-10^+ Tregs is described in 3.3.2. Percentages of splenic IL-10^+ B cells in AdHBVx- infected mice were the highest on day 5 p.i. (20 %) that declined until day 21 p.i. to 10 %. From day 5 until day 21 p.i., lower percentages of IL-10^+ B cells (~8 %) in AdEmpty infected mice were detected (Figure 21C). This confirms the prominent IL-10 production by B cell in spleens upon AdHBVx- infection (shown before in Figure 20C). Early after infection (day 3 p.i.), peaks of IL-10 production were detected in NK (~30 %) and NKT (~20 %) cell populations in spleens of AdHBVx- and AdEmpty infected mice (Figure 21A and B).

IL-10 production by monocytes and macrophages was generally higher in livers than in spleens. Percentages of IL-10^+ macrophages in livers were highest on day 5 p.i. and day 21 p.i (~20 %), whereas the highest IL-10 production levels in livers of AdEmpty infected mice were detected on day 5 p.i. (28 %; Figure 21D). Monocytes of AdHBVx- infected mice showed higher IL-10 percentages than the control group on day 5 and 14 p.i. (4- and 2-fold) in the liver as well as on day 7 and 14 p.i. in the spleen (2- and 3-fold; Figure 21E). Similar low percentages of IL-10 production were observed in DC in livers and spleens (~10 %). However, AdHBVx- infected mice showed higher IL-10 production by DC in the spleen on day 5 and 7 p.i (3- and 21-fold) and on day 14 p.i. in the liver (3-fold) compared to naïve mice

(Figure 21F). Percentages of IL-10$^+$ CD4$^+$ Foxp3$^-$ T cells and IL-10$^+$ CD8$^+$ T cells (~5 % respectively) were low in liver and spleens during the course of AdHBVx- or AdEmpty infection (Figure 21H and I).

Taken together, the percentages of IL-10$^+$ cells of the innate and adaptive immune response illustrate the course of IL-10 production during HBV infection dependent of the cell type indicating that its regulation is complex. Percentages of IL-10$^+$ B cells reflected the results obtained from analysis of IL-10$^+$ B cell counts as main producer of IL-10$^+$ on day 5 p.i. in the spleen. Furthermore, this illustration of the data revealed increasing IL-10$^+$ production of Tregs after day 7 p.i. suggesting a role for Treg derived IL-10 in mitigation of the adoptive immune response during AdHBVx- infection.

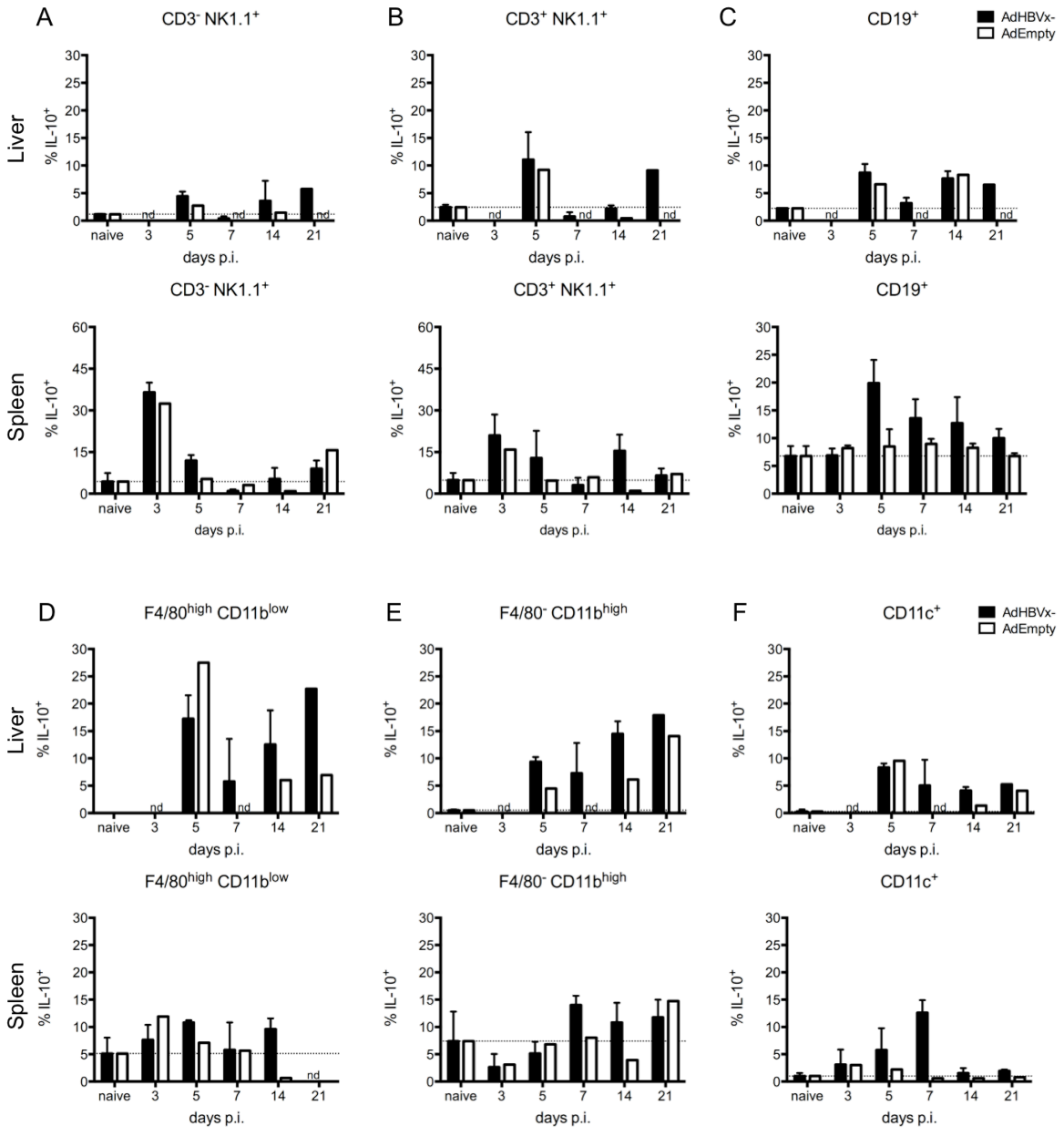

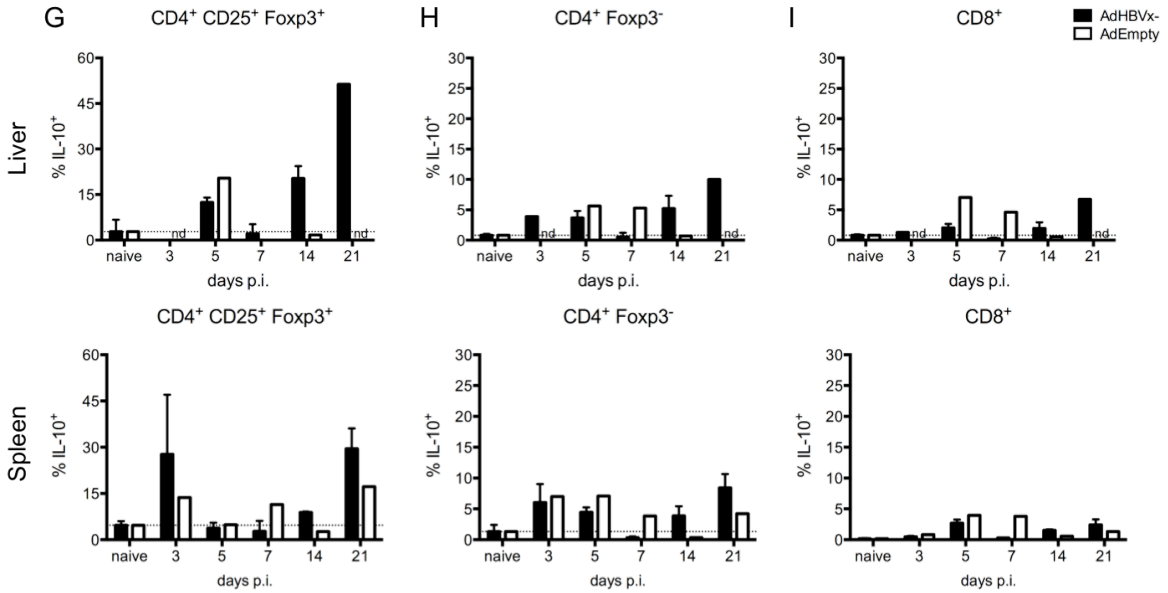

Figure 21: Course of IL-10 production in liver and spleen. Leukocyte populations of AdHBVx- or AdEmpty infected ITIB mice were stained for flow cytometric analysis of IL-10 production in the liver (1st, 3rd and 5th row) and spleen (2nd, 4th and 6th row) on indicated days p.i.. Percentages of IL-10$^+$ (A) NK cells, (B) NKT cells, (C) B cells, (D) macrophages, (E) monocytes, (F) DC, (G) Tregs, (H) CD4$^+$ Foxp3$^-$ T cells and (I) CD8$^+$ T cells are shown. The dimension of IL-10 production was estimated by β-lactamase reporter reaction. The dotted line indicates percentages IL-10$^+$ cells of naïve mice. Data was shown as mean values with standard deviation for n ≥ 3, otherwise as mean values only. (NK cells: CD3$^-$ NK1.1$^+$ cells, NKT cells: CD3$^+$ NK1.1$^+$ cells, macrophages: F4/80^{high} CD11b^{low}, monocytes: F4/80$^-$ CD11b^{high}, DC: CD11c$^+$, B cells: CD19$^+$, CD8$^+$ T cells: CD8$^+$, CD4$^+$ Foxp3$^-$ T cells: CD4$^+$ Foxp3$^-$, Tregs: CD4$^+$ CD25$^+$ Foxp3$^+$).

3.3.1.3 Kinetics of IL-10 production on single cell level

The ITIB reporter mouse not only allows for detection of IL-10 producing cells in general, but also for detection of IL-10 production levels as fold change of the β-lactamase$^+$ population of a reporter mouse to β-lactamase$^-$ population of a non-reporter mouse. For NK cells, elevated IL-10 production was detected on day 7 p.i. for AdHBVx- and on day 14 p.i. for AdEmpty infected mice in the liver and for both groups on day 21 p.i. in the spleen. Macrophages showed elevated levels only on day 21 p.i. (Figure 22D), whereas for monocytes and DC similar IL-10 production levels compared to naïve mice were observed with the exception of elevated IL-10 production levels on day 7 p.i. and also on day 21 p.i. for monocytes (Figure 22E and F). For B cells increased IL-10 production levels were observed in liver and spleen until day 7 p.i. (Figure 22C). Tregs showed elevated IL-10 production levels on day 14 p.i. only for AdEmpty infected mice (Figure 22G). CD4$^+$ Foxp3$^-$ T cells and especially CD8$^+$ T cells showed elevated IL-10 production levels on all days p.i. except on day 7 p.i. (Figure 22H and I).

In the spleen, reduced IL-10 production by NK and NKT cells was observed on day 3 and 5 p.i. (Figure 22A and B). Moreover reduced IL-10 production was observed on day 14 p.i. not only for NK cells, but also for NKT cells, B cells, macrophages and DC in liver and spleen of AdHBVx- infected mice. Macrophages showed reduced IL-10 production levels from day 3 p.i. to day 14 p.i. in liver and spleen (Figure 22D). B cells were reduced on day 14 and day 21 p.i. in the liver and even more in the spleen (Figure 22C). Tregs showed slightly reduced IL-10 production in liver and spleen compared to naïve mice (Figure 22G). Taken together, differences of IL-10 production levels between AdHBVx- and AdEmpty infected mice are not detectable on day 3 p.i. and day 5 p.i., but on day 7 p.i., indicating that increased IL-10 production levels are due to the HBV specific immune response adding to the Ad specific immune response of the first days post infection.

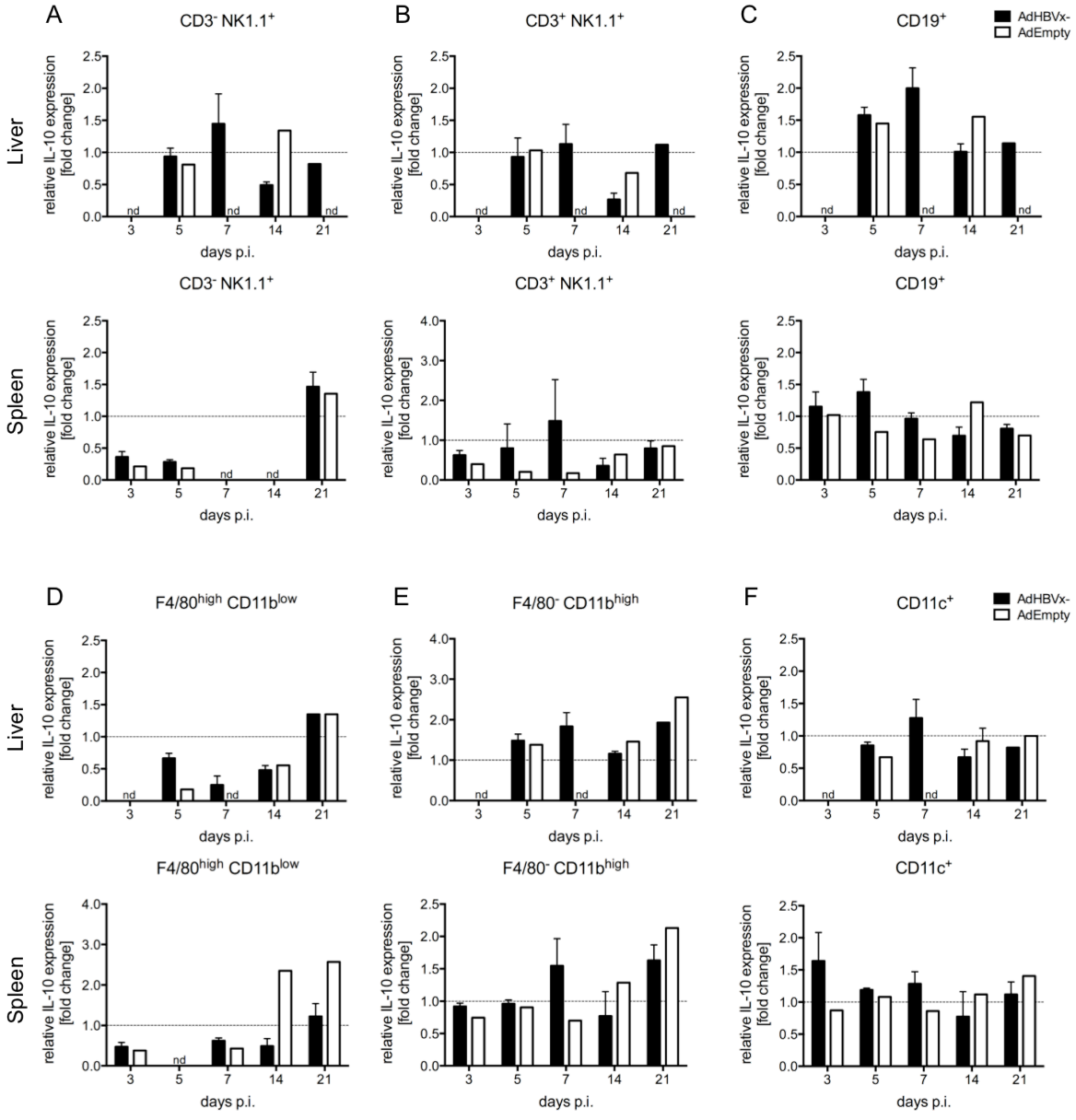

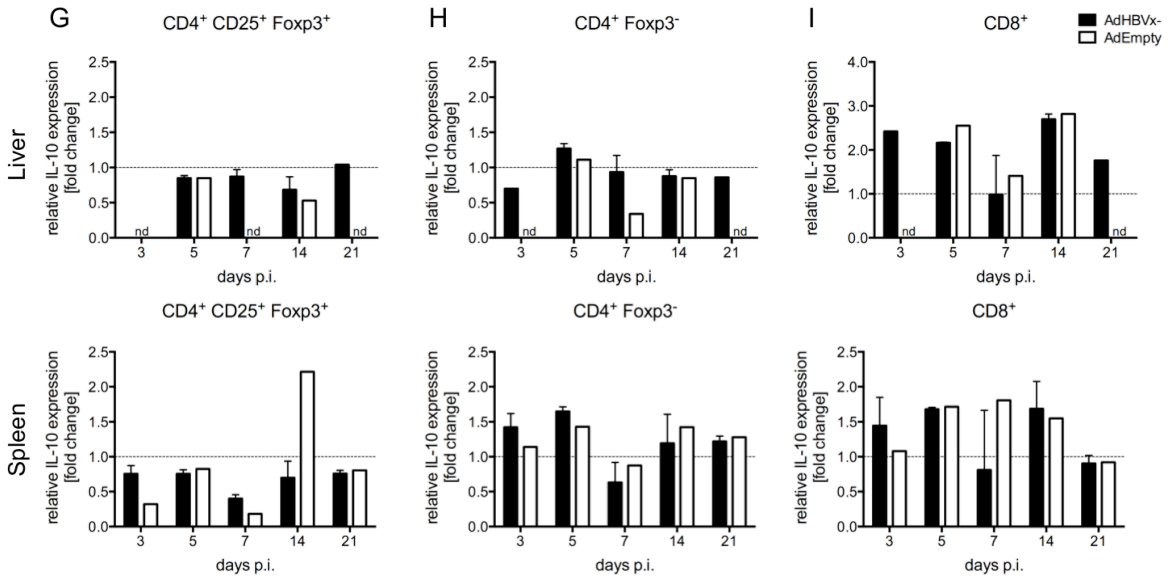

Figure 22: Course of relative IL-10 production per cell in liver and spleen. Leukocyte populations of AdHBVx- or AdEmpty infected ITIB mice were stained for flow cytometric analysis of IL-10 production in the liver (1st, 3rd and 5th row) and spleen (2nd, 4th and 6th row) on indicated days p.i.. Relative IL-10 production by (A) NK cells, (B) NKT cells, (C) B cells, (D) macrophages, (E) monocytes, (F) DC, (G) Tregs, (H) $CD4^+$ $Foxp3^-$ T cells and (I) $CD8^+$ T cells was normalized to naïve mice (dotted line) and is depicted as fold change. Data are shown as mean values with standard deviation for n ≥ 3, otherwise as mean values only. (NK cells: $CD3^-$ $NK1.1^+$ cells, NKT cells: $CD3^+$ $NK1.1^+$ cells, macrophages: $F4/80^{high}$ $CD11b^{low}$, monocytes: $F4/80^-$ $CD11b^{high}$, DC: $CD11c^+$, B cells: $CD19^+$, $CD8^+$ T cells: $CD8^+$, $CD4^+$ $Foxp3^-$ T cells: $CD4^+$ $Foxp3^-$, Tregs: $CD4^+$ $CD25^+$ $Foxp3^+$).

The results of chapter 3.3.1 indicate that all examined leukocyte populations, especially $CD8^+$ T cells and B cells, express IL-10 with varying intensity during the course of infection. Highest IL-10 production was detected on day 5 p.i. correlating with the increased ALT levels. Differences between AdHBVx- and AdEmpty infected mice were mainly observed after day 7 with increased IL-10 production in AdHBVx- infected mice. This observation indicates the activation, but also concurrent mitigation of the adaptive immune response after day 7 post Ad infection.

3.3.2 Adoptive Treg transfer in DEREG/ITIB mice

Previous Treg depletion experiments in AdHBV infected mice, showed a crucial role of Tregs in prolonging HBV clearance by alleviating liver damage, suppressing the anti-HBV immune response and delaying the antiviral $CD8^+$ T cell response. However, the mechanisms of Treg regulation still remained elusive. Hence, the regulatory role of Tregs in the establishment of the anti-HBV immune response was further investigated in the next step during an acute AdHBVx- infection. Since Tregs were known to secrete the anti-inflammatory cytokine

IL-10, the question arose, whether Tregs are required for the induction of IL-10 production by other cells of the innate and adaptive immune response.

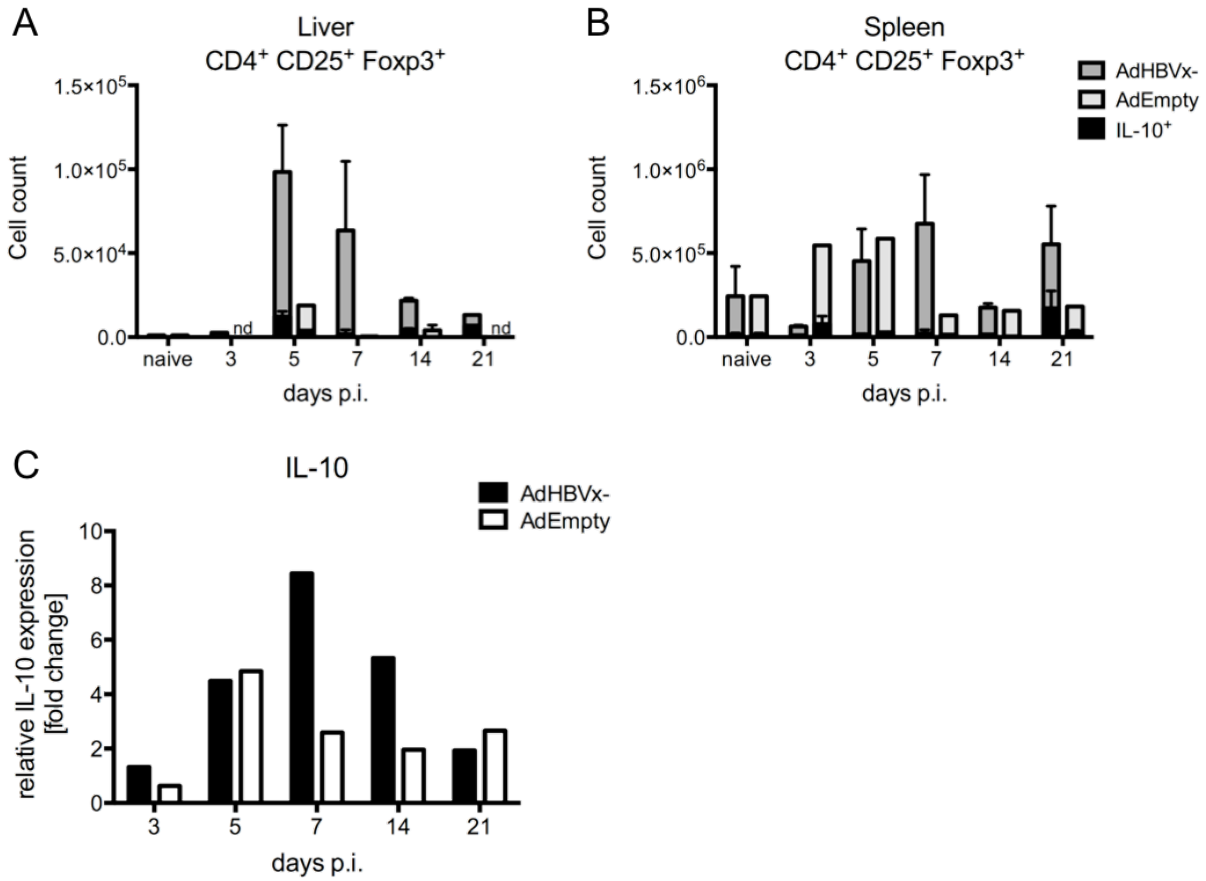

Figure 23: Treg counts peaked in the liver on day 5 p.i.. ITIB mice were infected intravenously with 1x10^9 IU of AdHBVx- (n=3) or the control virus AdEmpty (n=2) and were sacrificed on day 3, 5, 7, 14 and 21 p.i. for flow cytometric analysis of leukocytes of liver and spleen. (A) Cell counts of Tregs and IL-10$^+$ Tregs in liver and (B) spleen. (C) Isolated liver RNA was reversely transcribed to cDNA and used for quantitative PCR analysis of IL-10 expression levels, which are relative to GAPDH and HPRT and normalized to naïve mice (same as shown in Figure 18). Data are shown as mean values with standard deviation for n ≥ 3, otherwise as mean values only.

The kinetics of IL-10 production during AdHBVx- infection shown in the previous chapter revealed that CD8$^+$ T cells and B cells were the main producers of IL-10, and that overall Treg counts in the liver were lowest of all the examined leukocyte populations (compare Figure 19). During AdHBVx- infection maximal Treg counts of 9.8x10^4 cells were observed in the liver on day 5 p.i. (100-fold increased compared to naïve mice) and maximal Treg counts of 6.7x10^5 cells were detected on day 7 p.i. in the spleen (3-fold increased compared to naïve mice) (Figure 23), meanwhile percentages of IL-10$^+$ Tregs were comparatively low. Increased IL-10 production was detected in liver and spleen on day 14 and day 21 p.i. of AdHBVx- infected mice (compare Figure 21G). Furthermore, Figure 22G

shows that IL-10 production levels of the single cells varied only little during the course or infection. The peak of Tregs is detected prior to the peak of total hepatic IL-10 (Figure 23C), suggesting that an initial stimulus of Tregs at the very onset of the AdHBVx- infection is required for the induction of IL-10 production by other leukocytes e.g. by B cells and T cells in order to mitigate the anti-HBV immune response.

3.3.2.1 Adoptive Treg transfer in Treg depleted DEREG/ITIB mice

The next question assessed, was whether Tregs were initially required for the induction of IL-10 production by various leukocyte populations. A mouse model was required that allows both: Treg depletion upon diphtheria toxin (DT) administration and detection of IL-10. For this purpose DEREG mice were crossbred with ITIB mice to combine two features: 1) *in vivo* depletion of Tregs via administration of DT on three subsequent days and 2) *ex vivo* detection of IL-10 on single cell levels (Figure 24). The newly obtained mouse strain was named DEREG/ITIB.

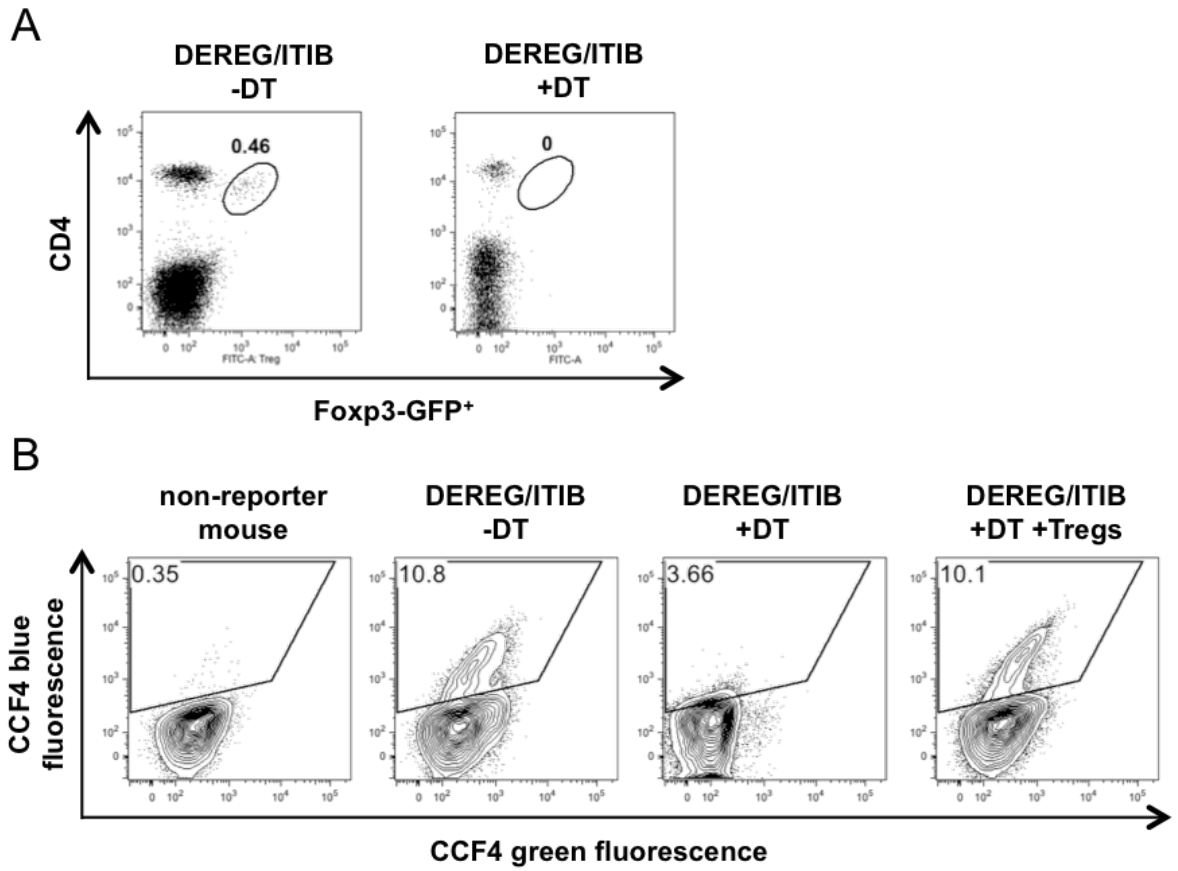

Figure 24: Features of DEREG/ITIB mice. Crossbreeding of DEREG and ITIB mice resulted in DEREG/ITIB mice that can be depleted for Tregs *in vivo* and stained for intracellular IL-10 production. (A) Representative flow cytometry plot of DEREG/ITIB mice before (left) and after administration of DT on three subsequent days for Treg depletion

(right). (B) Representative flow cytometric plot of hepatic $CD4^+$ T cells stained for IL-10 production via the β-lactamase reporter reaction on day 7 p.i.. From left to right: non-reporter mouse, DEREG/ITIB without DT, DEREG/ITIB with DT and DEREG/ITIB with DT and adoptively transferred Tregs. Dot plots show Foxp3-GFP^+ or IL-10 $reporter^+$ cells respectively with numbers as percentage of total living leukocytes. (DT: diphtheria toxin).

With the new DEREG/ITIB mice the question, whether Tregs were initially required for the induction of IL-10 production by various leukocyte populations, could be assessed. Therefore, FACS sorted Tregs ($CD4^+$ $CD25^{high}$ T cells) from splenocytes of naïve C57BL/6 donor mice were adoptively transferred into Treg depleted DEREG/ITIB mice directly after i.v. injection of AdHBVx- (Treg resubstituted mice) (Figure 25A). Flow cytometric staining of the sorted cells showed that 30 % of the transferred cells were $Foxp3^+$ Tregs (Figure 25B). On day 7 p.i., the mice were sacrificed and analysed for IL-10 production by leukocytes as well as for HBV markers in the serum. AdHBVx- infected mice, which were either non-depleted or Treg depleted served as control groups.

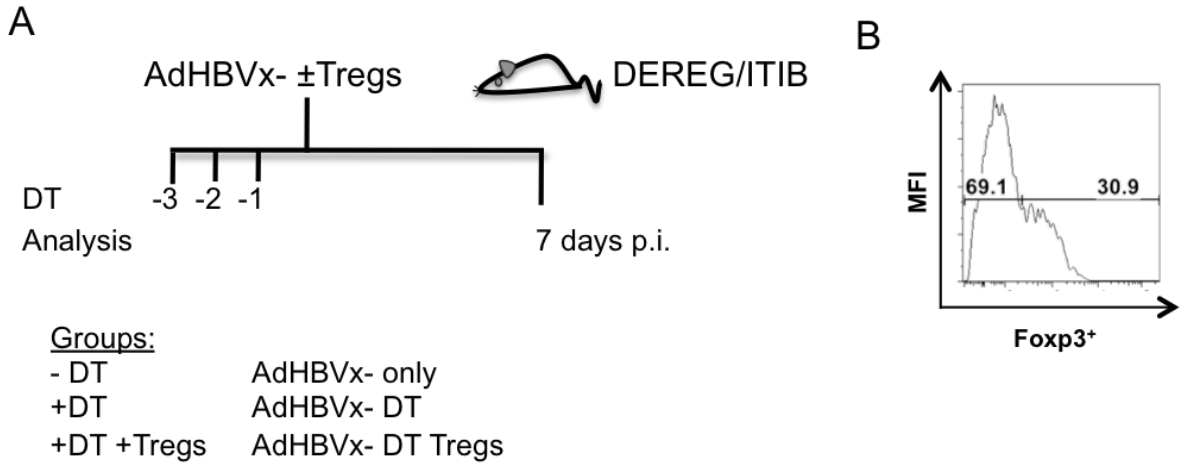

Figure 25: Experimental setup of adoptive Treg transfer. DEREG/ITIB mice were Treg depleted via DT administration on three subsequent days prior to intravenous injection of $1x10^9$ IU AdHBVx- and intraperitoneal injection of CD4+ $CD25^{high}$ T cells isolated from splenocytes of CD45.1 mice. Treg resubstituted mice (+DT +Tregs; n=6) received $1.5x10^4$ $CD4^+$ $CD25^{high}$ T cells per DEREG/ITIB mouse. Control groups were either non-depleted (-DT; n=5) or Treg depleted (+DT; n=5) prior to intravenous injection of $1x10^9$ IU of AdHBVx-. Mice were sacrificed on day 7 p.i. for flow cytometric ICS and quantitative PCR analysis. (A) Experimental setup. (B) Flow cytometric plot of FACS sorted $CD4^+$ $CD25^{high}$ T cells stained for $Foxp3^+$ Tregs. (DT: diphtheria toxin, ICS: intracellular cytokine staining).

3.3.2.2 IL-10 percentages and counts after adoptive Treg transfer

In order to examine the initial role of Tregs at the beginning of AdHBVx- infection for the induction of IL-10 production by various leukocyte populations, the percentages of $IL\text{-}10^+$ leukocyte populations were examined in presence and absence of Tregs. As shown in

Figure 26, IL-10^{+} Tregs (44 % in Treg non-depleted mice) were efficiently depleted in liver and spleen (0 % in Treg depleted mice).

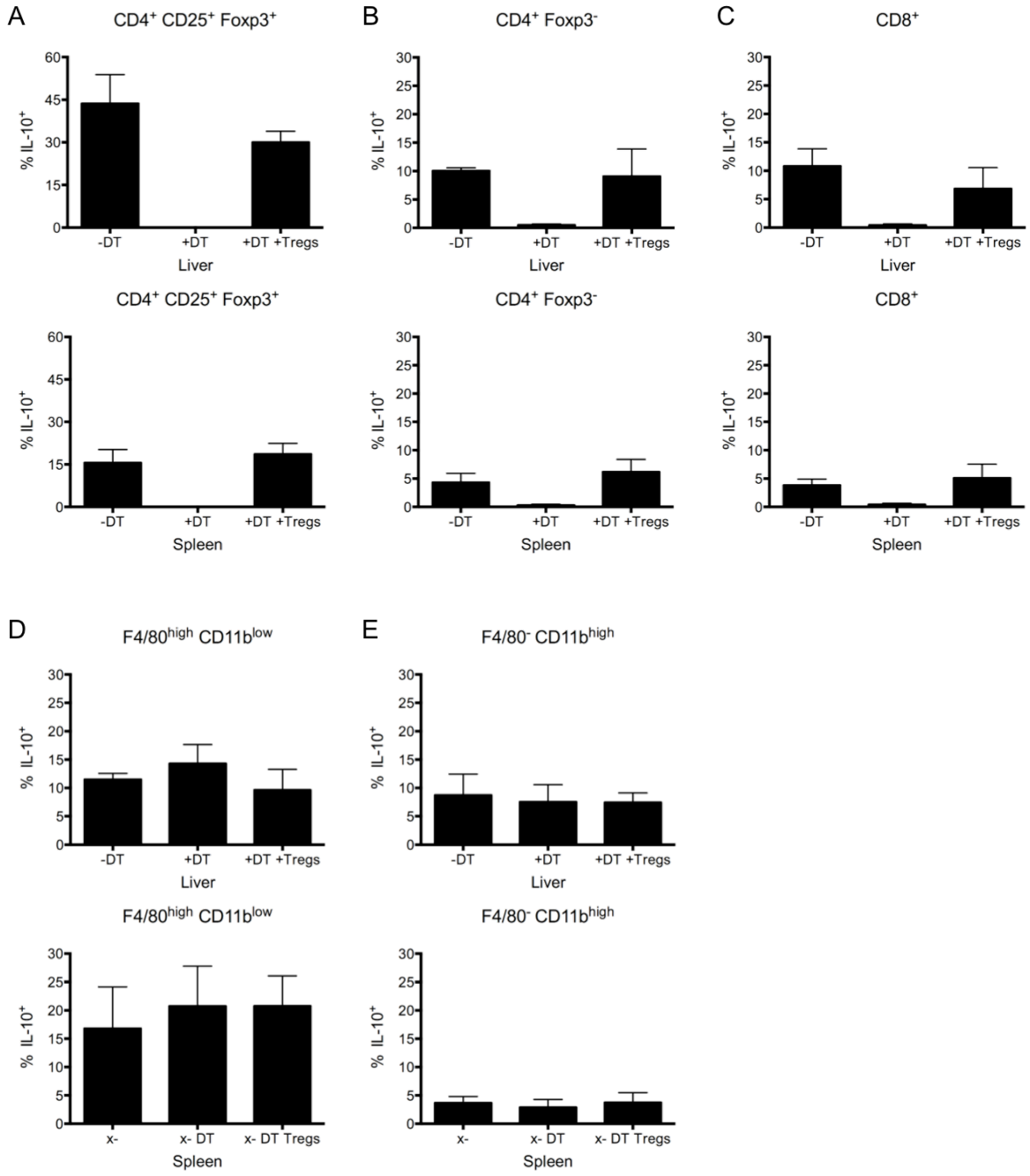

Figure 26: Tregs mediate IL-10 production by CD4^{+} and CD8^{+} T cells but not of macrophages or monocytes. Leukocyte populations of AdHBVx- infected mice resubstituted with Tregs (+DT +Treg) as well as control groups of either non-depleted (-DT) or Treg depleted mice (+DT) were sacrificed on day 7 p.i. for flow cytometric analysis of IL-10 production in the liver (top and 3rd row) and the spleen (2nd and bottom row) and quantitative PCR analysis. Percentages of IL-10^{+} (A) Tregs, (B) CD4^{+} Foxp3^{-} T cells, (C) CD8^{+} T cells, (D) macrophages and (E) monocytes were measured via β-lactamase reporter reaction. Data are shown as mean values with standard deviation.

(DT: diphtheria toxin, macrophages: F4/80^{high} CD11b^{low}, monocytes: F4/80^{-} CD11b^{high}, CD8^{+} T cells: CD8^{+}, CD4^{+} Foxp3^{-} T cells: CD4^{+} Foxp3^{-}, Tregs: CD4^{+} CD25^{+} Foxp3^{+}).

As expected, IL-10 production by Tregs in the liver recovered after adoptive transfer of Tregs (30 %; Figure 26A). Importantly, the proportion of IL-10^{+} CD4^{+} Foxp3^{-} T cells and of IL-10^{+} CD8^{+} T cells also significantly increased in mice resubstituted with Tregs (9 % and 7 % respectively, Figure 26B and C). On the contrary, no change in IL-10^{+} macrophages or monocytes was observed (Figure 26D and E). All trends described for leukocytes in the liver were observed also in the spleen (Fig 10). In mice with resubstituted Tregs, the percentages of IL-10^{+} Tregs (19 %), CD4^{+} Foxp3^{-} T cells (6 %) and CD8^{+} T cells (5 %) were higher than for to non-depleted mice (13 %, 4 % and 4 % respectively) in spleens. Hence, the presence of Tregs at the time of infection seemed in fact to be important for IL-10 production by CD4^{+} Foxp3^{-} T cells and CD8^{+} T cells, but not for IL-10 production by monocytes and macrophages.

In addition, the cell count of Tregs in the liver was reduced drastically to 370 cells in Treg depleted mice as expected (Figure 27A). Surprisingly, in Treg resubstituted mice total Treg counts increased to $1.1x10^5$ cells were observed, whereas in non-depleted control mice lower total Treg counts of $0.6x10^5$ cells were detected. This was accompanied by strongly decreasing cell counts of IL-10^{+} CD4^{+} Foxp3^{-} T cells ($1.7x10^3$ cells) and IL-10^{+} CD8^{+} T cells ($1.1x10^4$ cells) in Treg depleted mice. A 2-fold reduction in total cell count numbers of CD4^{+} Foxp3^{-} T cells ($6.3x10^5$ cells) and CD8^{+} T cells ($3.9x10^6$ cells) in Treg depleted mice was observed compared to cell counts in non-depleted control mice ($1.2x10^6$ CD4^{+} Foxp3^{-} T cells, $8.5x10^6$ CD8^{+} T cells) (Figure 27B and C). This decline in cell counts was also detected in macrophages ($2.5x10^5$ cells compared to $3.7x10^6$ cells in non-depleted control mice) and monocytes in Treg depleted mice ($7.6x10^5$ cells compared to $4.3x10^6$ cells in non-depleted control mice) (Figure 27D and E). At the same time, cell counts of the CD8^{+} T cells ($1.5x10^7$ cells), macrophages ($6.3x10^6$ cells) and monocytes ($9.7x10^6$ cells) in Treg resubstituted mice were 2-fold increased compared to the non-depleted control mice, whereas the cell count of CD4^{+} Foxp3^{-} T cells ($5.2x10^6$ cells) was even 4-fold higher. Similar to the results shown in Figure 20, higher cell counts were detected overall in the spleen compared to the liver (Figure 27F). Treg depleted mice showed a 4-fold lower leukocyte count in the liver ($6.0x10^6$ cells) and a 7-fold lower leukocyte count in the spleen ($1.5x10^7$ cells) along with a smaller ratio between spleen and liver leukocytes compared to non-depleted control mice (cells counts in the liver of $2.3x10^7$ cells and in the spleen of

$1.0x10^8$ cells). However, for Treg resubstituted mice higher cell counts of total leukocytes in the liver ($6.1x10^7$ cells) and spleen ($1.2x10^8$ cells) were detected compared to non-depleted control mice (in the liver 3-fold increase and in the spleen 1.2-fold increase). Furthermore, Treg resubstituted mice showed an even smaller ratio between spleen and liver leukocytes than Treg depleted mice. These results suggest that Tregs were important for regulation of IL-10 production by $CD4^+$ T cells and $CD8^+$ T cells.

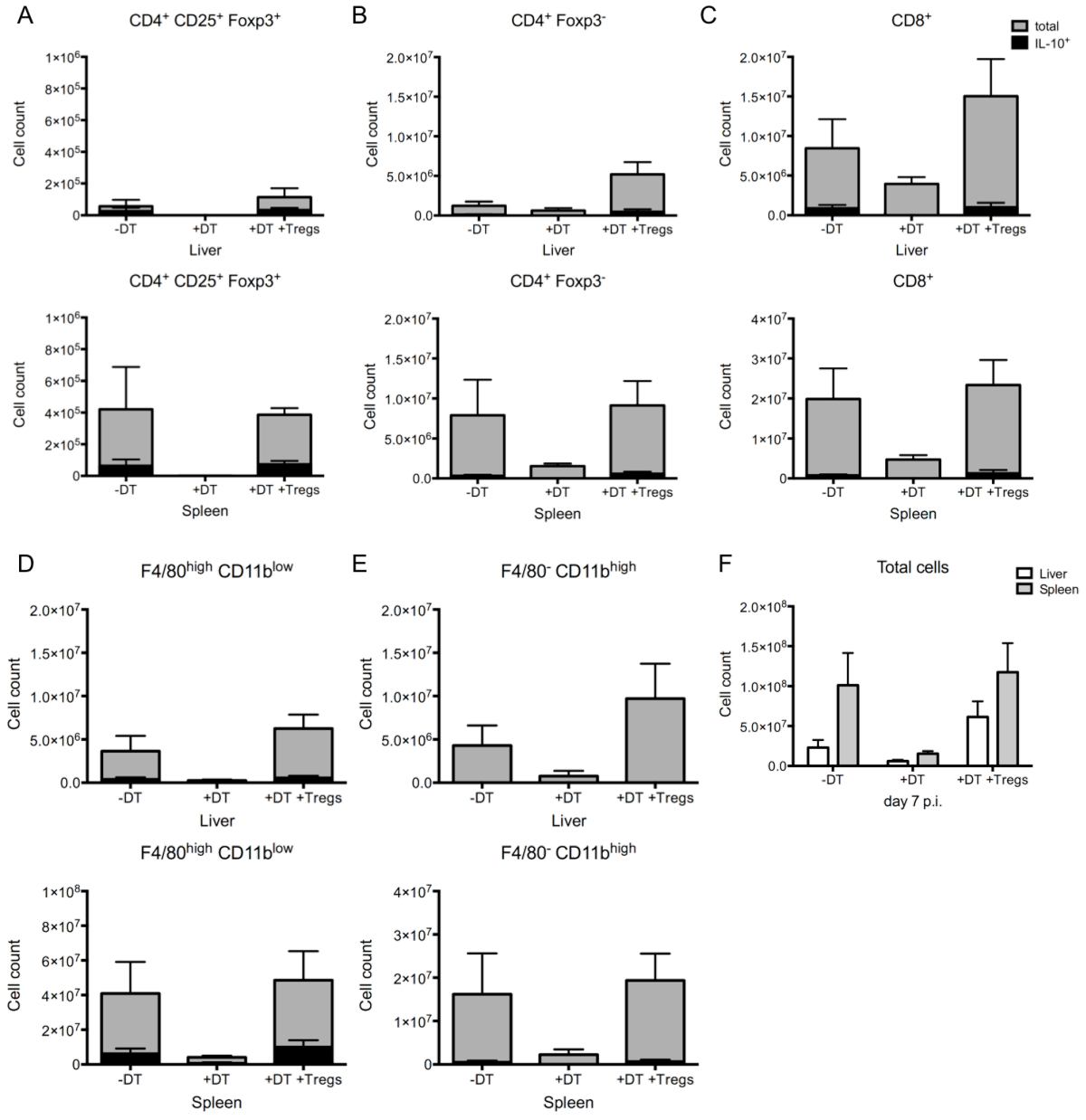

Figure 27: Tregs are responsible for homing of innate and adaptive immune cells into liver and spleen. Leukocyte populations of AdHBVx- infected mice depleted for Tregs and with adoptively transferred Tregs (+DT +Tregs). Control groups are either non-depleted for Tregs (-DT) or depleted for Tregs (+DT). Flow cytometric analysis of leukocytes of liver (top and 3rd row) and spleen (2nd and bottom row) on day 7 p.i.. Counts of (A) Tregs,

(B) $CD4^+$ $Foxp3^-$ T cells , (C) $CD8^+$ T cells, (D) macrophages, (E) monocytes and (F) total cells. Data are shown as mean values with standard deviation. (DT: diphtheria toxin).

Taken together, these results suggest that there is an association between initial presence of Tregs during the very onset of AdHBVx- infection and the infiltration or expansion of T cells as well as macrophages and monocytes into the liver and spleen. Furthermore, these results suggest that Tregs were responsible for the induction of IL-10 production by $CD4^+$ T cells and $CD8^+$ T cells.

3.3.2.3 Serology and cytokine expression after adoptive Treg transfer

In a next step, the influence of the presence and absence of Tregs and Treg derived IL-10 on serological markers and cytokine expression was examined in AdHBVx- infected mice. Increased ALT levels were detected in Treg depleted mice compared to non-depleted control mice as was described earlier. In contrast to the supposed rescue of IL-10 production, Treg resubstituted mice did not decrease the liver damage to levels of the non-depleted control mice (Figure 28A). HBeAg and HBsAg levels in Treg depleted and Treg resubstituted mice were slightly elevated compared to the non-depleted control mice (Figure 28B and C). This increase in HBV antigens relates to slightly increased HBV copies in Treg depleted and Treg resubstituted mice (Figure 28F). Moreover a 6-fold rise of total hepatic IFNγ expression level was detected in Treg depleted mice compared to non-depleted control mice (Figure 28D). In Treg resubstituted mice, IFNγ levels were only 4-fold higher than in non-depleted control mice, indicating only a partially rescued suppression mediated by the presence of Tregs. On the other hand, hepatic total IL-10 expression levels increased slightly (1.2-fold) in Treg depleted mice and further increased in Treg resubstituted mice (1.6 fold) compared to the non-depleted control mice (Figure 28E).

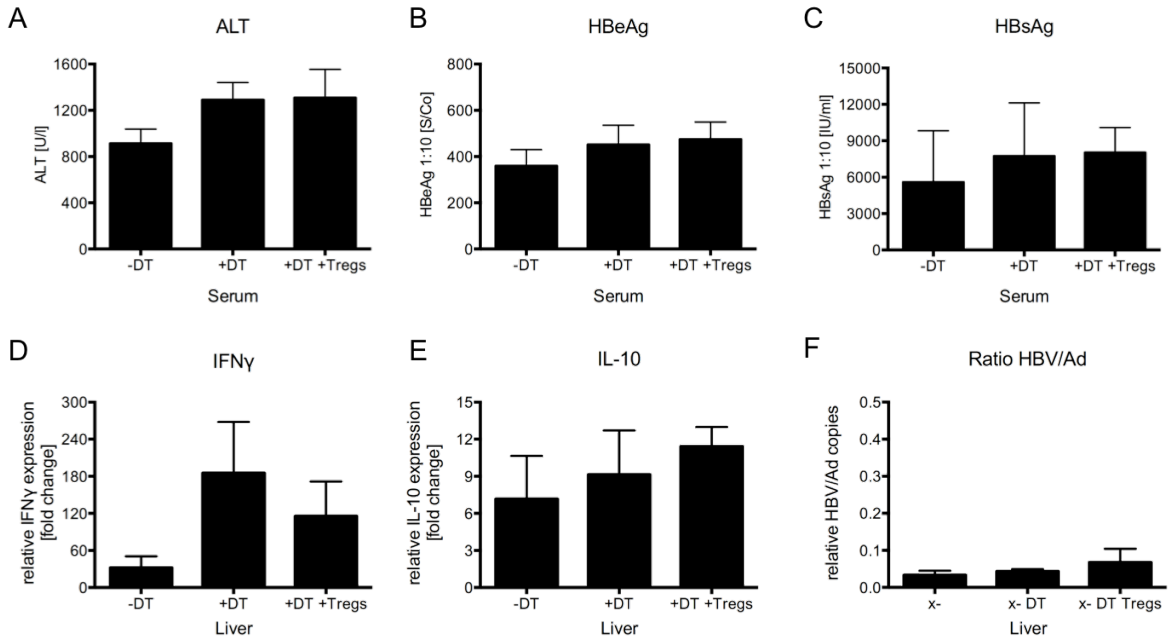

Figure 28: Adoptively transferred Tregs rescue IFNγ expression levels but not liver damage and IL-10 expression. AdHBVx- infected mice depleted for Tregs and with adoptively transferred Tregs (+DT +Treg) as well as of control groups either non-depleted for Tregs (-DT) or depleted for Tregs (+DT) were sacrificed on day 7 p.i. for serological parameters and quantitative PCR analysis. (A) ALT, (B) HBsAg and (C) HBeAg were determined from serum. (D) Isolated liver RNA was reversely transcribed to cDNA and used for quantitative PCR analysis of IFNγ and (E) IL-10 expression levels each relative to GAPDH and HPRT and normalized to naïve mice. (F) Ratio of intrahepatic HBV to Ad copy numbers relative to murine intron were determined by quantitative PCR from liver DNA. Data are shown as mean values with standard deviation. (DT: diphtheria toxin).

Taken together, Tregs suppress overall pro-inflammatory IFNγ expression, but not overall anti-inflammatory IL-10 expression or liver damage. Since the adoptively transferred Tregs were able to restore T cell homing, but did not mitigate liver damage or restore IL-10 production levels, the transferred Tregs might not have been fully functional or simply not localized correctly.

4 Discussion

4.1 T cell priming by *in vitro* HBcAg stimulated APC

Previous studies have shown that non-enveloped HBV capsids are released if apoptosis is induced and that ablation of the CD95 pathway of apoptosis prevents the induction of an anti-HBV immune response (Arzberger 2009, Arzberger *et al.* 2010). Furthermore, HBV capsids are shown to directly stimulate B cells more efficiently than macrophages or DC (Milich *et al.* 1997). These findings led to the hypothesis that HBV capsids can be taken up and presented by B cells, which subsequently prime HBcAg specific T cells. This hypothesis was tested by an *in vitro* co-culture study of T cells, which were equipped with an HBcAg specific TCR, with capsid stimulated B cells, macrophages and DC.

APC are known to play a crucial role in antigen processing and cross-presentation of epitopes via the MHC class I molecule resulting in priming of $CD8^+$ T cells (Germain 1994, Jung *et al.* 2002). The observation of an increase in activation markers on HBcAg specific $CD8^+$ T cells and the subsequent IFNγ secretion upon capsid or HBcAg derived peptide stimulation of DC proved the functionality of the here performed *in vitro* assay (Figure 8, 9). The functionality of the used B and T cells was further demonstrated by activation of pp65 specific T cells upon co-culture with B cells that were stimulated with the whole protein of carbamylated-pp65 or the HCMV peptide pool. These results agree with findings of another study, in which the ability of B cells to prime $CD4^+$ T cells was shown (Constant *et al.* 1995). However, co-culture of T cells with capsid stimulated B cells did not result in $CD8^+$ T cell activation in the applied experimental settings. Therefore, this result argues against a potential role of capsid stimulated B cells in the priming of HBcAg specific $CD8^+$ T cells. Nevertheless, this finding is consistent with observations of a previously described study, in which capsid stimulated B cells did also not lead to B cell activation and antigen uptake unless CpG adjuvant was present (Jäger 2015). Synthetic oligonucleotides containing unmethylated CpG motifs boost the B cell and CTL immune response to protein antigen and therefore are used as adjuvant to improve the activity of vaccines (Bode *et al.* 2011, Lipford *et al.* 1997). However, CpG cannot be implemented in order to elucidate the role of B cells during T cell priming in a natural HBV infection.

Contrary to the results obtained with B cells, priming of T cells was achieved by co-culture of T cells with recombinant capsids stimulated DC. Furthermore, T cell activation was achieved

to a lesser extent by co-culture with DC, which were stimulated with capsids that originated from envelope denatured virions of an HBV producing cell line (Figure 8). A reason for this difference in antigenicity might come from the in-house preparation of the envelope denatured capsids with potential unfavorable buffer conditions in contrast to the production of the recombinant capsid in an industrial and strongly quality-controlled environment. Since no priming of T cells with specificity for HBsAg occurred, it can be said that the denaturation procedure successfully removed the enveloped derived antigens from the self-made capsids. HBcAg specific $CD8^+$ T cells were further primed by HBV_C18 stimulated DC, although to a lesser extent than by recombinant capsid stimulated DC. This finding is contradictory to the previously reported observation that vaccinations with peptides induce stronger $CD8^+$ T cell responses than vaccinations with whole protein (Rosalia *et al.* 2013), thus suggesting that the minimal epitope, in form of the HBV_C18 peptide, for TCR_core develops a higher binding affinity to TCR_core and therefore induces a stronger T cell response than longer peptides do. For $CD4^+$ T cells higher activation was observed when co-cultured with capsid stimulated DC in contrast to HBV_C18 stimulated DC, thus being consistent with the finding that whole protein stimulation primarily activates $CD4^+$ T cells (Zhang *et al.* 2009). This result may be explained by the fact that DC use different trafficking routes after antigen internalization. During antigen processing, peptides are shown to localize in the endosome as well as in the cytosol, whereas whole proteins are only found in endosomal compartments (Rosalia *et al.* 2013, Zhang *et al.* 2009). The *in vitro* study showed that macrophages were only able to prime HBcAg specific T cells, when stimulated with HBV_C18 peptide, but not when stimulated with whole protein capsids. A similar result was obtained for pp65 specific T cells, which were primed by macrophages upon stimulation with the HCMV peptide pool, but not with the whole protein of carbamylated-pp65 (Figure 8). These results of the different abilities by DC or macrophages in activation of T cells support the previously reported idea of APC type dependent differences in antigen delivery and presentation (Stier *et al.* 2005). Furthermore, they support the notion of a dominant role of DC in priming naïve T cells upon viral infection (Barker *et al.* 2002, Busche *et al.* 2013).

Observed events of unspecific T cell priming during this *in vitro* study can be explained by an incomplete transduction of T cells with the respective TCRs and the presence of naturally occurring TCRs on the transduced cells, which can lead to T cell activation upon binding to peptide-MHC complexes that fit their specificities. In order to prevent the occurrence of these

unspecific T cell responses, simultaneous staining of activation markers and the transduced TCR could be performed.

Furthermore, unspecific priming of T cells after co-culture with capsid or pp65 stimulated APC might be explained by sequence similarity between the two proteins pp65 and HBcAg (see 6.4). The protein sequence of pp65 contains a region from position aa 245–253 that shows 3 identical aa and 6 aa with similar characteristics of their side-chains compared to HBV_C18, which could enable the recognition by T cells containing TCR_core (Berg *et al.* 2003). Furthermore, alignment of the protein sequences of pp65 and HBcAg showed sequence similarities of 122 aa out of 183 aa of HBcAg sharing similar characteristics of their side-chains or even the identical aa at the same position (14 times) in the region from aa 324–507 of pp65, which also contains the epitope recognized by TCCl_pp65 in position aa 495–503 enabling recognition of HBcAg derived antigens on B cells and DC. In accordance with the present results, an association between pp65 and HBcAg induced T cell responses was previously described, showing an enhanced pp65 specific $CD8^+$ T cell response that is dependent on an HBcAg specific $CD4^+$ T cell response (Reiser *et al.* 2011). The abilities of T cells for cross-reactive immune responses are further discussed in chapter 4.2.4.

Taken together, the results obtained by this *in vitro* study, that was carried out without adjuvants, did not confirm the ability of HBcAg stimulated B cells to prime T cells. However, the results support the notion of the dominant role of DC in T cell priming during HBV infection.

4.2 Detection of Ad and HBV specific T cell responses

The AdHBV mouse model was shown to be a good model in order to establish an acute hepatitis B during which liver damage, HBV replication, secretion of the HBV markers HBeAg and HBsAg as well as the corresponding antibodies were detected in the course of a self-limiting AdHBV infection (Sprinzl *et al.* 2001, von Freyend *et al.* 2011). However, detection of HBV specific $CD8^+$ T cell or $CD4^+$ T cell responses have not been successful in this model until now, due to a lack of immunogenic epitopes in AdHBVx- infected mice. Determination of immunodominant Ad and HBV specific epitopes was performed by screening epitope predicted peptides from HBcAg, HBsAg or the Ad hexon protein as well as testing of peptide pools.

The reason why HBV derived $CD8^+$ T cell epitopes, that are described to be immunogenic in protein-primed HBV transgenic mice (Backes *et al.* submitted), did not elicit a $CD8^+$ T cell response in AdHBVx- infected mice, although having the same H-2kb background, remains elusive (Figure 10). Differences in HBV antigen presentation in these two mouse models might be influenced by the exogenous or endogenous source of the antigen like reported previously for two HBV epitopes (Riedl *et al.* 2014). In vaccinated mice, HBV proteins derive from an exogenous source, whereas in AdHBVx- infected hepatocytes endogenously expressed HBV proteins are present. The inability to mount a strong T cell response in mice with the HBV_C18 or HBV_S20 peptides, that are identified epitopes in HBV-infected humans, can be explained by known genetic differences of the murine and human MHC molecules, species-restricted interactions between $CD8^+$ T cells and MHC class I molecules and the restriction of epitopes to a certain MHC molecule (Irwin *et al.* 1989, Kuhober *et al.* 1996, Murphy 2011). Due to the finding that the HBcAg derived peptide pool HBc P3 induced a mixed T cell response against Ad and HBV (Figure 10) instead of an HBV specific T cell response that was reported earlier (Stross *et al.* 2012), HBc P3 can only be used henceforth as a positive control for the functionality of the ICS, but not for the detection of an HBV specific T cell response. This result highlights the need for the identification of new Ad and HBV epitopes, which prove to be a valid method for detection of specific T cell responses against the Ad vector and the HBV transgene in AdHBVx- infected mice.

4.2.1 Identification of a new Ad hexon epitope by epitope prediction

Identification of Ad and HBV specific epitopes in AdHBVx- infected mice was performed by screening high score peptides that were predicted by epitope prediction software. In contrast to the HBV derived peptides, one of the tested epitope predicted Ad hexon peptides resulted in strong *ex vivo* stimulation of lymphocytes and elicited a polyfunctional T cell response (Figure 12), thus enabling estimation of the specific T cell response against the Ad5 vector in the AdHBVx- infected mice. The Ad hexon peptide AdH #1 (RNFLYSNI) on position aa 470–477 is a newly identified immunodominant epitope, which binds to the H-2kb molecule of C57BL/6 mice.

Output comparison of the binding prediction databases showed concordant results for AdH #1 as the highest affinity binder and the strongest binder predicted by IEDB and netMHC respectively (Table 24), succeeding in the prediction of an immunogenic epitope of the Ad hexon protein. In the epitope prediction by the SYFPEITHI database, AdH #1 obtained only the second best score, whereas the predicted epitope with the best score (AdH #2) showed no immunogenic potential when tested in AdHBVx- infected mice. This aberration confirms the notion that the SYFPEITHI database is outcompeted by newer methods like netMHC (Lundegaard *et al.* 2010). Nonetheless, the performed binding predictions did not succeed in the identification of immunogenic 8-mer peptides derived from the HBcAg or HBsAg proteins, although the same binding affinity was predicted for HBV_S81 as for the immunodominant AdH #1 (Figure 11). This finding pronounces the statement that epitope prediction results are no guarantor of success, but a way to focus the experimental work on peptides with the highest potential (Lundegaard *et al.* 2010).

4.2.2 Identification of a new HBcAg epitope

Eliciting of an HBV specific T cell response in AdHBVx- infected mice was only obtained by *ex vivo* stimulation of lymphocytes with pooled (HBc P7) or single 18-mer peptides (HBc #1-10 and HBc #15-18) derived from HBcAg, but not with epitope predicted 8-mer epitopes of HBcAg (Figure 11, 13, 14). Shortening of the immunogenic HBc #33 peptide (15-mer) to a predicted 8-mer epitope abolished the immunogenic potential of this epitope (Figure 10). A similar loss of the immunogenic potential was observed upon shortening of the hepatitis C virus (HCV) core derived C18 peptide, which consists of 14 aa (Wolfertstetter 2014). It can therefore be assumed that shortening of the immunogenic

HBcAg derived 18-mer peptides also results in abolishment of the immunogenic potential of these peptides.

Peptides of different lengths are reported to be accommodated by the MHC class I (8- to 14-mer) and MHC class II (12-, 13-, 15- and 20-mer) molecules. The longer the peptide, which is binding to the MHC class I molecule, the more the peptide bulges out of the binding groove due to its closed ends. Otherwise, the ends of the MHC class II binding groove are open so that longer peptides can be accommodated without bulging of the peptide (Sewell 2012). Furthermore, formation of peptide-MHC class I and II complexes with 18-mer peptides have been previously described (Billeskov *et al.* 2007, Knapp *et al.* 2009). This suggests that the identified immunogenic HBcAg 18-mer peptides could be fitted into the binding groove of the MHC class I molecule by formation of a bulge, which would enable recognition by HBcAg epitope specific $CD8^+$ T cells (Figure 14). With regard to the results obtained by peptide stimulated $CD4^+$ T cells, 4 immunogenic 18-mer peptides (HBc #13-16) were identified, which could be fitted in the binding groove of the MHC class II molecule, and additionally were able to elicit an HBcAg specific $CD4^+$ T cell response (Figure 14). However, these identified epitopes elicited only weak T cell responses in comparison to the predicted AdH #1 peptide, which might be explained due to their lower binding affinity to the MHC class I molecule and therefore in a lower position in the previously described epitope hierarchy (Bertoletti *et al.* 2006, Riedl *et al.* 2014) (Figure 12). Examination of the binding affinities of the identified peptides could be performed by an isothermal titration calorimetry or surface plasmon resonance like reported previously (Willcox *et al.* 1999).

The two HBcAg 18-mer peptides of HBc P7, which induced the strongest $CD8^+$ T cell responses, were HBc #5 (SDFFPSVRDLLDTASALY) on position aa 21–38 and HBc #15 (TNMGLKFRQLLWFHISCL) on position aa 91–108 (Figure 14). HBc #15 contains the before-mentioned HBV_C93 epitope, which induced only slight $CD8^+$ T cell response above background level on day 19 p.i. but not on day 28 p.i. in AdHBVx- infected mice (Figure 13, 14). HBc #5 does not contain any previously described HBcAg epitopes and is therefore a completely new identified immunodominant HBcAg epitope, which binds to the H-2kb molecule. With these HBV specific T cell epitopes, it is henceforth possible to determine also the cellular immune response via ICS in the AdHBVx- mouse model.

More research using overlapping peptide pools covering the overall HBV sequence or covering only the HBV proteins HBsAg and polymerase, for which T cell epitopes

are described in the human system (Boni *et al.* 2007, Desmond *et al.* 2008, Rehermann *et al.* 1995), is needed in order to identify epitopes that elicit stronger HBV specific $CD8^+$ T cell responses in AdHBVx- infected mice. In a different approach other than epitope predictions, naturally processed and loaded peptides could be eluted from their MHC class I molecules and subsequently identified by mass spectrometry (Flyer *et al.* 2002). Moreover, T cell epitopes can be optimized in order to improve antigen affinity for the MHC molecule or the TCR (Pentier *et al.* 2013). However, these methods are cost intensive and at the same time do not guarantee the identification of immunogenic epitopes, so that it is necessary to weigh the cost-value ratio for identifying an optimized epitope that is used for the readout of T cell activation in a mouse model and not for a vaccine or immunotherapy, which aim to help patients directly.

4.2.3 Low percentages of $IFN\gamma^+$ $CD8^+$ T cells

Percentages of HBc P7 specific $IFN\gamma^+$ $CD8^+$ T cells were low on day 19 p.i. and further declined until day 29 p.i. (Figure 13, 14) or in case of HBV_C93 specific $IFN\gamma^+$ $CD8^+$ T cells were no longer detectable on day 28 p.i. (Figure 15). The replication marker HBeAg was still detectable on day 29 p.i., so that HBV antigen processing and presentation still occurs in AdHBVx- transduced hepatocytes or in APC after the uptake of secreted HBV antigen (Figure 16). By use of peptide-MHC multimer staining (Figure 15), the notion that the HBV specific $CD8^+$ T cells might loose their ability to bind to the peptide-MHC class I complex, like described previously (Maini *et al.* 1999), was counteracted. Low numbers of $multimer^+$ $CD8^+$ T cells coincide with low numbers of HBV-specific $IFN\gamma^+$ $CD8^+$ T cells, thus suggesting that the detected $CD8^+$ T cells are functionally active. Furthermore, the observation of low percentages of $IFN\gamma^+$ $CD8^+$ T cells agrees with findings of other studies, in which in general only low numbers of HBV antigen specific T cells are detected. Moreover, antiviral T cells are shown to be susceptible to NK cell mediated deletion or antigen-induced cell death (Knolle *et al.* 2014, Lenardo *et al.* 1999, Maini *et al.* 1999, Peppa *et al.* 2013), which could further explain the low HBV specific $CD8^+$ T cell numbers during AdHBVx-infection. Additional explanations for low HBV specific $CD8^+$ T cells could come from the observation that activated T cells down-regulate their TCR, which is thought to prevent severe organ damage (Sandalova *et al.* 2012, Valitutti *et al.* 1997). Moreover, Tregs are reported to mediate mitigation of T cell function and numbers as well as T cell migration into non-lymphoid organs, where the T cells reside as memory T cells (Busca *et al.* 2014, Welsh *et*

al. 2002). The here observed decline of Ad specific IFNγ$^+$ CD8$^+$ T cells during AdHBVx-infection from day 7 p.i. to day 28 p.i. (Figure 11) could be influenced by clearance of circulating Ad particles from the host by APC, which would result in a reduced activation of Ad specific T cells (Kafri *et al.* 1998).

Further work needs to be done to establish, whether higher numbers of HBV specific CD8$^+$ T cells could be detected by bringing forward the day of analysis for example to the period between days 7 to 14 p.i., at which high CD8$^+$ T cell counts have been detected in the liver (Figure 19). This consideration of a preponed day of analysis is further supported by findings of the highest numbers of HBV specific CD8$^+$ T cells coinciding with the clinically acute phase of the hepatitis in HBV infected patients (Maini *et al.* 1999). A further improvement of the readout of HBV specific CD8$^+$ T cells could be achieved by *ex vivo* stimulation of the isolated lymphocytes with several peptides in parallel or with a peptide pool, which would enable the detection of the described multispecific T cell response during HBV infection (Chisari *et al.* 1995). Taking into account that an immunodominance hierarchy was described for CD8$^+$ T cell responses against HBV antigens and that immunodominant epitopes are able to suppress subdominant epitopes independently from their number (Reiser *et al.* 2011, Riedl *et al.* 2014), peptides pools with an identified immunogenic potential should also be tested without the immunodominant epitope in order to enable identification of unsuppressed subdominant epitopes.

4.2.4 Cross-reactivity between HBV and Ad

In contrast to prior observation, percentages of CD8$^+$ T cells stimulated with HBc P3 increased during the AdHBVx- and AdEmpty infection from day 7 p.i. to day 28 p.i. (Figure 11). This increase could be explained by the recruitment of non-virus specific T cells or rather of cross-reactive memory T cells, which was previously described by other groups (Haanen *et al.* 1999, Maini *et al.* 2000). T cell cross-reactivity is reported to be caused by TCR binding degeneracy, which is essential to cope with the vast number of potential foreign peptide-MHC complexes (Sewell 2012). Thereby, T cells have the capacity to recognize viral variants or closely related antigens of heterologous virus (Haanen *et al.* 1999, Selin *et al.* 1998). The here observed increasing numbers of HBc P3 stimulated CD8$^+$ T cells is consistent with studies from other groups, which have shown that cross-reactive T cells may outnumber strain specific T cells and further that cross-reactive T cells are easier to stimulate than naïve T cells (Haanen *et al.* 1999, Selin *et al.* 1998).

Cross-reactive $CD8^+$ T cells in AdHBVx- as well as in AdEmpty infected mice were detected after *ex vivo* stimulation with the peptide pool HBc P3 (Figure 10), which covers the carboxyl-terminal last 62 aa of the HBcAg. Silke Arzberger revealed sequence similarity of HBcAg and the Ad protein V in their ARD, whereof HBcAg contains 4 and Ad protein V contains 5 ARD. These findings agree with findings of other studies reporting that in case of a concordant sequence motif for the presenting MHC molecule, unrelated peptides with little amino acid homology can be bound by the same TCR and hence elicit a cross-reactive T cell response (Falk *et al.* 1991, Selin *et al.* 1994, Welsh *et al.* 2002). Examples of epitopes that induce $CD8^+$ T cell cross-reactivity are described for various subtypes of influenza A (Altenburg *et al.* 2015), for Varicella Zoster virus, Herpes Simplex virus and Epstein Barr virus (EBV) (Chiu *et al.* 2014) and for the influenza A and EBV (Clute *et al.* 2005). Although cross-reactivity is used in a targeted manner to break tolerance in HBsAg transgenic mice (Schirmbeck *et al.* 2003b), the usage of cross-reactive peptides or peptide pools like HBc P3 is extremely unfavorable during the readout of antigen specific T cell responses and hence should be avoided.

4.2.5 Obstacles with Ad vectors

Technical problems with Ad vectors encountered during one experiment resulting in different amounts of Ad vectors in infected mice (Figure 12), might be due to varied vitality of HEK 293A cells that were used for titration of Ad stocks. This finding agrees with the previously described occurrence of cell line dependent variations in determined viral titers (Thomas *et al.* 2007). In order to avoid varied results, titration of the Ad vectors used in the same experiment should be performed simultaneously with cells from the same cell passage. Upon infection of mice with the same amounts of Ad vectors, no difference between the amounts of intrahepatic Ad DNA of different Ad vectors should be detectable.

With the AdHBVx- mouse model characteristic features of an acute HBV infection like the induction of liver damage, secretion of the HBV markers as well as antibody production were observed (Figure 16, 17). Recruitment of cells of the innate and adaptive immune system to the site of infection (Figure 19), cytokine expression (Figure 18, 19) and the induction of an HBV specific T cell responses (Figure 14) were detected in this easy-to-handle small animal model. Furthermore, this model has previously been used to examine immune modulators, which determine the acute or persistent outcome of HBV infection (Stross *et al.* 2012, von Freyend *et al.* 2011). However, every model has its limitations, which in case of the AdHBV

mouse model are described to be the lack of a gradual transduction of hepatocytes like during the natural course of HBV infection and the induction of an Ad vector specific immune response (Sprinzl *et al.* 2001, von Freyend *et al.* 2011). Although the E1 and E3 regions, which are responsible for interactions of the adenovirus with the host immune system, were deleted from the Ad genome, the presence of high amounts of Ad antigens upon AdHBV injection was inevitable and resulted in the induction of an innate and adaptive immune response as shown by increased cell counts of leukocytes and cytokine expression after AdEmpty infection (Figure 12, 18, 19). In the literature, an Ad induced immune response influencing HBV replication and the HBV specific immune response is described a number of times (Cavanaugh *et al.* 1998, Kafri *et al.* 1998, Lieber *et al.* 1997, Muruve *et al.* 2008, Yang *et al.* 1994) and needs to be avoided. Circumvention or at least a reduction of an Ad induced immune response can be obtained by future usage of gutless, high-capacity, Ad vectors that are deleted for their entire Ad genome in order to prevent the induction of the immune response by residual expression from Ad genes (Alba *et al.* 2005). Packaging of gutless Ad vectors is implemented by coinfection of the virus-producing cell with the gutless Ad vector encoding the transgene and a helper virus encoding the Ad structural proteins (Morral *et al.* 1998, Muruve *et al.* 2004, Parks *et al.* 1996). As long as the hexon protein of the gutless Ad vector is derived from Ad5 as in the first-generation AdHBV or AdEmpty vectors, the identified AdH #1 peptide could be used for the readout of Ad specific $CD8^+$ T cell responses induced by the Ad vector shortly after injection. At a later date, no Ad specific $CD8^+$ T cell responses should be detectable in the gutless AdHBV infected mice.

Taken together, greater efforts are needed to improve the AdHBV mouse model by reducing the Ad induced immune response, in order to obtain genuine results of the HBV-host interactions. As a first step in this process, the AdHBV mouse model was successfully improved by means of the newly identified epitopes that allow for the separate analysis of the Ad and HBV specific immune response.

4.3 Role of Tregs and IL-10 production during AdHBVx- infection

The immunosuppressive environment of the liver prevents massive tissue damage during HBV infection and thereby maintains organ function (Protzer *et al.* 2012). Tregs and the cytokine IL-10 are hypothesized to play a regulatory role in the establishment of the anti-HBV immune response by exerting their anti-inflammatory potential (Rouse *et al.* 2010, Stross *et al.* 2012), which is why the IL-10 production by Tregs and other cells of the innate and adaptive immune response was examined during the course of an acute AdHBVx- infection.

4.3.1 Course of an acute AdHBVx- infection

The observed course of AdHBVx- infection resembles the course of an acute AdHBV infection described earlier in this thesis, which shows the reproducibility of results that were obtained by using this mouse model (Stross *et al.* 2012, von Freyend *et al.* 2011). Previous studies mostly focused on liver-infiltrating HBV specific T cells but not on other cells (Isogawa *et al.* 2005a). Upon AdHBVx- infection a strong infiltration of leukocytes in the liver and the spleen was detected, which reflects the recruitment of immune cells to the site of infection and the periphery (Figure 19, 20). In this study, beside T cells and Tregs, also NK cells, NKT cells, monocytes, macrophages, DC and B cells, which are shown to contribute to the establishment of an acute viral hepatitis (Sitia *et al.* 2004), were monitored simultaneously during the first 21 days of an acute AdHBVx- infection.

The establishment of liver damage occurred on day 5 p.i. and correlated with the large infiltrate of non-antigen specific mononuclear cells (Figure 17, 19). Furthermore, elevated ALT levels and moreover the expression of large amounts of IFNγ reflected the activity of NK cell and $CD8^+$ T cell mediated killing of infected cells, thus resulting instantly in the reduction of HBV markers in the blood and intrahepatic DNA (Figure 17, 18). These results match previously described observations obtained from HBV infected patients (Bertoletti *et al.* 2013, Bertoletti *et al.* 2007, Chen *et al.* 2005). Reduced recruitment of non-antigen specific mononuclear cells to the liver on day 7 p.i., suggests that the liver damage at a later date is initiated by antigen specific T cells that are primed within the liver or in secondary lymphoid organs like the spleen, whereby the primed T cells migrate to the site of infection like described previously (Bertolino *et al.* 2001, Sitia *et al.* 2004). Elevated ALT levels persisted for the duration of the kinetic and declined subsequently as was shown at a

later date (Figure 16, 17). These findings are consistent with the clinical course of an acute hepatitis caused by HBV (Liaw *et al.* 2009). The usual lag-phase of the immune response, that is common in HBV infected humans (Busca *et al.* 2014), was not observed in this mouse model, due to the holistic infection of hepatocytes after Ad gene of transfer the HBV genome.

In AdHBVx- infected mice, the liver-infiltrating cells consisted primarily of $CD8^+$ T cells, NK cells and $CD4^+$ T cells on day 5 p.i., which accounted for the large amount of expressed IFNγ counteracting the HBV infection (Figure 18, 19). Strong hepatic IFNγ expression and high amounts of T cells are shown to be favorable for HBV clearance and further prevent a chronic course of HBV infection (Hodgson *et al.* 2001). Minor amounts of liver-infiltrating cells like DC, NKT cells, monocytes and macrophages support the notion that HBV uses strategies to impair the innate immune response in order to favor its own replication (Busca *et al.* 2014). Tregs are reported to constitute 2 to 4 % of peripheral $CD4^+$ T cells (Baecher-Allan *et al.* 2004), so that the low Treg numbers upon AdHBVx- infection were in the expected range (Figure 23).

The increase in leukocyte numbers in the spleen on day 5 p.i. was primarily caused by B cells, $CD8^+$ T cells and $CD4^+$ T cells, whereby the $CD8^+$ T cells peaked delayed on day 7 p.i. (Figure 20). As expected, B cell numbers were high, since the spleen was reported to be the place for B cell maturation and priming (Loder *et al.* 1999). Furthermore, the spleen is shown to contribute to priming of an anti-HBV immune response, after which the primed T cells home to the site of antigen synthesis in the liver in order to exert their effector functions (Isogawa *et al.* 2005a, Zheng *et al.* 2013).

The influence of the Ad vector on the induction of liver damage and an immune response were clearly visible in AdEmpty infected mice (Figures 18 to 22) and are a known side effect of using first-generation Ad vectors, which were already discussed in chapter 4.2.4. The lack of HBV encoding genes in AdEmpty infected mice suggests that the elicited immune response originates from an HBV transgene independent immune response, but that it rather dependents on the Ad vector. However, differences between AdHBVx- and AdEmpty infected mice were apparent by means of a weaker infiltration of immune cells into liver and spleen of AdEmpty infected mice. Moreover, AdHBVx- infected mice showed a higher amount of T cells in the spleen on day 7 p.i. (Figure 20), thus suggesting this to be an HBV specific effect, since no equivalent was detected in the control. In order to examine the role of IL-10 expression upon HBV infection, the main focus of the following discussion is directed

to events that are more pronounced in AdHBVx- infected mice than in AdEmpty infected mice.

Notwithstanding the mentioned limitations, in general it seems that the results obtained with the AdHBVx- mouse model are in line with previously collected data from other HBV infection models or even HBV infected patients. Therefore, it is a valuable model, which can be used for monitoring the cells of the innate and adaptive immune response in order to further elucidate the virus-host interaction during an acute HBV infection.

4.3.2 Kinetic of IL-10 production during AdHBVx- infection

The anti-inflammatory cytokine IL-10 is expressed by many different cells, with the major source of IL-10 varying according to the tissue or the state of infection. Furthermore, IL-10 functions as potent regulator of the innate and adaptive immune response, which needs to be controlled intensively to balance pathogen control and the severity of immune pathology (Couper *et al.* 2008, Pils *et al.* 2010). In order to enable this subtle IL-10 mediated regulation, IL-10 gene expression is complex and multi-layered comprising changes in chromatin structure, various cell type specific transcription factors and post-transcriptional mechanisms (Saraiva *et al.* 2010). Due to a reported link between early elevation of IL-10 and a better control of HBV infection (Keating *et al.* 2014) as well as the previously described expression of vast amounts of IL-10 early during AdHBVx- infection (von Freyend *et al.* 2011), it was hypothesized that IL-10 also plays a role in the anti-HBV immune response. This peak of IL-10 early during AdHBVx- infection was confirmed in this study (Figure 18). In order to monitor the kinetics of IL-10 production by cells of the innate and adaptive immune response during AdHBVx- infection, an ITIB IL-10 reporter mouse was used that enabled the detection of IL-10 expression of various cells of the immune system.

During AdHBVx- infection, staining of IL-10$^+$ leukocytes revealed that especially CD8$^+$ T cells and B cells were the main producers of IL-10 in hepatic and splenic leukocytes respectively (Figure 19, 20). Although IL-10 was expressed constantly during the time measured, the largest amount of IL-10 was detectable simultaneously with increased liver damage on day 5 p.i., suggesting that the produced IL-10 counteracts immune pathology. In accordance with present results, previous studies have described a dominant role for IL-10 production by B cell and T cell populations of naïve mice and mice infected with the murine cytomegalovirus (MCMV) (Madan *et al.* 2009). In contrast to earlier findings

(Stross 2011), no evidence of macrophages as the major source of IL-10 was detected. The discrepancy of maximal cell counts of IL-10$^+$ cells on day 5 p.i. (Figure 19) and the detection of maximal hepatic IL-10 expression levels detected on day 7 p.i. (Figure 18), where cell counts of IL-10$^+$ cells were already reduced, suggests that not all IL-10 producing cells are included in this analysis. Therefore, future studies should also examine the IL-10 production by hepatocytes, eosinophils and neutrophils during AdHBVx- infection (Madan *et al.* 2009). The notion of IL-10 production being induced by the presence of secretory HBV proteins in order to modulate the inflammatory liver environment (Bertoletti *et al.* 2013) is in line with the findings on day 3 p.i., where increased HBeAg and HBsAg levels as well as IL-10 production were observed (Figure 17, 18).

Differences between AdHBVx- and AdEmpty infected mice were mainly observed after day 7 p.i. with increased IL-10 production in AdHBVx- infected mice (Figure 21), which indicates the activation of an HBV specific adaptive immune response after day 7. Though, high percentages of B cells, CD4$^+$ T cells and Tregs produced IL-10 on days 14 and 21 p.i. in AdHBVx- infected mice, cells of the innate immune response (NK and NKT cells, macrophages, monocytes and DC) were still contributing to IL-10 production (Figure 21), which is necessary for counteracting the immune pathology. Although only ~2 % of total hepatic CD8$^+$ T cells produced IL-10, CD8$^+$ T cells were the main producer of IL-10 in the liver, due to the vast numbers of liver-infiltrating CD8$^+$ T cells, that were dominant over the other cell populations (Figure 19). In contrast to the common understanding of CD8$^+$ T cells, which act as effector cells in favor of the inflammation, IL-10 producing CD8$^+$ regulatory T cells were detected, which are reported to suppress IFNγ secretion and antigen specific proliferation of CD8$^+$ effector T cells in order to prevent immune pathology during HCV infection (Abel *et al.* 2006, Accapezzato *et al.* 2004). Whether the IL-10 producing CD8$^+$ T cells detected in this study belong to the previously described regulatory T cells (Endharti *et al.* 2005), should be examined by staining of CD8$^+$ CD122$^+$ T cells. CD4$^+$ T cell derived IL-10 is shown to have an inhibitory effect on DC and macrophages in order to prevent immune pathology (Saraiva *et al.* 2010). Similar to IL-10 mediated inhibition of CD8$^+$ T cells effector functions, also CD4$^+$ T cell proliferation, differentiation as well as effector functions are directly impaired by IL-10 (Couper *et al.* 2008). The observed IL-10 production by CD4$^+$ T cells without Foxp3$^+$ Tregs (Figure 21) might be mediated by IL-10 secreting T regulatory type 1 (Tr1) cells, which are described to be induced by antigen

stimulation via an IL-10 dependent process (Roncarolo *et al.* 2006). IL-10 production by $CD4^+$ $Foxp3^+$ Tregs is discussed further below.

The observed dominance of IL-10^+ B cells in the spleen during the phase of an acute hepatitis (Figure 20) was surprising, due to earlier reports that myeloid cells are the main producers of IL-10 in liver and spleen of naïve mice and mice infected with *Yersinia enterocolitica* (Bouabe *et al.* 2011). Nevertheless, the here obtained results agree with findings of other studies, in which IL-10 production by B cells in MCMV infected mice are dominant in lymphoid tissues and are further responsible for the decrease of the virus specific $CD8^+$ T cell response (Madan *et al.* 2009). As IL-10 is known to function at different stages of an immune response and at different anatomical locations, these conflicting observations might not be based on the usage of different IL-10 reporter mice but on the different life cycles of the pathogens used in the reported experiments, which resulted in a different induction of the immune response and hence IL-10 production (Bouabe *et al.* 2011, Saraiva *et al.* 2010). Further support for the role of IL-10 producing B cells that counteract cytotoxic T cell responses comes from observations of patients with chronic HBV, that showed enriched amounts of IL-10^+ B cells in temporal correlation with liver damage (Das *et al.* 2012) correlating also with observations during the IL-10 kinetics in AdHBVx- infected mice. In order to determine the counter-regulative role of IL-10 producing B cells, $CD19^+$ $CD24^{high}$ $CD38^{high}$ regulatory B cells (Bregs) should be stained at the peak of liver damage.

IL-10 production by myeloid cells like monocytes and macrophages is shown to be dominant in blood and liver of MCMV infected mice (Madan *et al*. 2009), which was not confirmed in AdHBVx- infected mice (Figure 19). However, observation of increased hepatic IL-10 production by macrophages, monocytes and DC are thought to influence directly the impairment of CTL and NK cell responses. Previously, this impairment was described to be mediated by limiting the production of pro-inflammatory cytokines and chemokines by APC as well as by inducing a tolerogenic state of the APC (Couper *et al*. 2008, Steinbrink *et al*. 1997). The regulation of innate effector functions is achieved upon autocrine IL-10 signaling or by IL-10 that is secreted by T_H1, T_H2 or Tregs (Saraiva *et al*. 2010). Otherwise, macrophage derived IL-10 is also shown to be required for Treg maintenance and moreover in the mitigation of NK cell derived IFNγ (Murai *et al*. 2009, Tu *et al*. 2008).

As first line of defense, NK cells are activated early during HBV infection. IL-10 production by NK cells is associated with enhanced NK cell proliferation and production of IFNγ

(Grant *et al.* 2008), which is in line with the observed IL-10 production on day 3 p.i. before liver damage occurs (Figure 17, 18, 21). But, in a different role, NK cell derived IL-10 can control the magnitude of the $CD8^+$ T cell response during infection (Lee *et al.* 2009). Moreover, similar to $CD8^+$ T cells, the ability of NK cells to produce the pro-inflammatory cytokine IFNγ is described to be dampened by IL-10 signaling of macrophages and DC (Lassen *et al.* 2010). In order to examine the previously described correlation between IL-10 levels and NK cell mediated IFNγ production (Dunn *et al.* 2009), simultaneous staining of $IFN\gamma^+$ NK cells and $IL\text{-}10^+$ NK cells should be performed during the first 7 days of AdHBVx-infection.

Treg numbers were generally low compared to other cells of the immune response during AdHBVx- infection. Nonetheless, increasing numbers of Tregs, which peaked on day 5 p.i., were observed in the livers of AdHBVx- infected mice. Although Treg numbers were declining in the continuing course of the disease, the percentages of IL-10 producing cells of the whole Treg population increased during the course of infection to more than 50 % on day 21 p.i. (Figure 21, 23). An increase of Tregs during disease progression was previously linked to the immunosuppressive state induced by HBV that results in a decrease of HBV specific T cells in number and function (Busca *et al.* 2014). Another study found that increased Treg levels are restored to normal levels upon resolution of the HBV infection (Xu *et al.* 2006). IL-10 is shown to enhance the differentiation of Tregs, which again produce IL-10 and thereby contribute to their own induction (Barrat *et al.* 2002).

In conclusion, the IL-10 reporter mouse has proven to be a useful tool to gain first insights into the diversity of IL-10 signaling during AdHBVx- infection. Localization and timing of IL-10 production by multiple sources form a coordinated response, which is involved in regulation of the innate and adaptive immune response in order to reduce immune pathology (Saraiva *et al.* 2010).

4.3.3 Adoptive transfer of Tregs in AdHBVx- infected DEREG/ITIB mice

Previous Treg depletion studies have shown a crucial role of Tregs in prolonging HBV clearance by alleviating liver damage, suppressing the anti-HBV immune response and delaying the antiviral $CD8^+$ T cell response (Stross *et al.* 2012). Taking this into account, in order to elucidate further the regulatory role of Tregs in the establishment of the anti-HBV immune response during an HBV infection, a study with focus on Tregs and production of the

anti-inflammatory cytokine IL-10 by cells of the innate and adaptive immune response is needed.

For this purpose, a new DEREG/ITIB mouse was created via crossbreeding of DEREG and ITIB mice. DEREG/ITIB mice have a C57BL/6 background, which allows the analysis of $CD8^+$ T cell responses by exploiting the previously identified immunodominant epitopes of the Ad hexon protein and HBcAg (see 4.2.1 and 4.2.2). This DEREG/ITIB mouse combines the features of *in vivo* depletion of GFP^+ $Foxp3^+$ Tregs upon administration of DT and *ex vivo* detection on single cell levels due to an IL-10 reporter reaction (Figure 24), that have been described previously by the original mouse strains (Bouabe *et al.* 2011, Lahl *et al.* 2007). By using AdHBVx- infected DEREG/ITIB mice, that underwent DT mediated Treg depletion or DT mediated Treg depletion followed by an adoptive Treg transfer, the hypothesized regulatory role of Tregs in the establishment of the anti-HBV immune response via induction of IL-10 production by cells of the innate and adaptive immune response was examined. The day of analysis was set to day 7 p.i., where the adaptive immune response against HBV was expected to be established as observed earlier (compare 4.3.2).

Treg depletion resulted in strongly diminished recruitment of leukocytes to liver and spleen compared to mice without Treg depletion. After the adoptive Treg transfer, the number of leukocytes in liver and spleen were rescued (Figure 27), which shows that the adoptive transfer was successful. This further suggests that Tregs are needed at the very onset of the infection, thus being important for recruitment of leukocytes to the site of infection. This suggestion agrees with findings of another study, in which mice with a mucosal herpes simplex virus infection showed an impaired immune cell trafficking to the infected tissue upon Treg depletion (Lund *et al.* 2008). The reduced counts of leukocytes at the site of infection and in the periphery in Treg depleted mice are unlikely to be related to toxic side effects of DT, since the cell counts were rescued in Treg resubstituted mice. Here, complete Treg depletion was achieved by DT administration on three subsequent days, with the last day of DT administration being the day of AdHBVx- infection (Figure 27). Upon initial Treg depletion before AdHBVx- infection, Tregs did not repopulate the liver and spleen within seven days, unlike described for DEREG mice that were Treg depleted in the first three days of infection (Stross 2011). With the latter depletion strategy, Tregs that were not affected by the first round of DT administration on the day of infection are supposed to be sufficient to exert their function and recruit leukocytes to liver and spleen. Therefore, the chronology adopted in this study of Treg depletion and AdHBVx- infection in DEREG/ITIB mice

provides a good model to examine the initial effect of Tregs on the establishment of the adaptive immune response.

Apart from lower cell counts of T cells, monocytes and macrophages, hepatic IL-10 production by $CD4^+$ T cells and $CD8^+$ T cells, but not of monocytes and macrophages, was strongly reduced after Treg depletion. However, this reduced IL-10 production by $CD4^+$ T cells and $CD8^+$ T cells was rescued after the adoptive transfer of Tregs (Figure 26), suggesting that the initial presence of Tregs rather affects cells of the adaptive than cells of the innate immune response. This finding is further supported by the observation that the overall hepatic expression of IL-10 increased after Treg depletion. As IL-10 production by macrophages was increased after Treg depletion, the lack of IL-10 derived from Tregs, $CD8^+$ T cells or $CD4^+$ T is likely to be compensated by other cells. Further studies are needed in order to monitor IL-10 production by other IL-10 producing cells like B cells, NK cells, hepatocytes, eosinophils and neutrophils in Treg depleted mice in order to prove the assumption of occurring compensation. Especially B cells are of interest, since they were shown to be a main producer of IL-10 early during AdHBVx- infection (compare 4.3.2). Thus, the investigation of the influence of Treg depletion and adoptive Treg transfer on regulatory $CD8^+$ T cells and Bregs would be highly insightful (Das *et al.* 2012, Endharti *et al.* 2005).

As expected, Treg depletion resulted in increased hepatic IFNγ expression (Figure 28), which supports the notion that the presence of Tregs suppresses the anti-HBV immune response mediated by $CD8^+$ effector T cells (Stross *et al.* 2012, Xu *et al.* 2006). The adaptive transfer of Tregs partially rescued the IFNγ expression to a lower level and thus further illustrates the anti-inflammatory affect of Tregs. A further study performed by an ICS of $IFN\gamma^+$ cells on day 7 p.i. should confirm the Treg mediated mitigation of IFNγ production by $CD8^+$ T cells as well as NK and NKT cells, which have been described as source of IFNγ (Busca *et al.* 2014, Nakagawa *et al.* 2001).

Furthermore, as expected Treg depletion and the adoptive Treg transfer did not interfere with HBV replication or secretion of HBV markers HBeAg and HBsAg. An increase in liver damage after Treg depletion was also expected, since Tregs have previously been shown to alleviate liver damage (Stross *et al.* 2012). Unexpectedly, the liver damage was not rescued upon adoptive Treg transfer. A similar finding was made after an adoptive transfer of Tregs in AdHBV infected $IL\text{-}10^{flx/flx}CD4Cre^+$ mice, whose $CD4^+$ T cells are deficient in IL-10

production. Hereby, also increased ALT and hepatic IL-10 levels were observed after adoptive Treg depletion (data not shown) indicating that this effect is mediated by the transferred Tregs and not by the administration of DT. The transferred Tregs in the experiment with the IL-$10^{flx/flx}$CD4Cre^{+} mice were sorted via the CD4 surface marker and GFP expression of the $Foxp3^{+}$ Tregs of DEREG mice (data not shown). In order to prevent a possible depletion of DEREG derived Tregs, which harbor the DT promoter, in DT mediated Tregs depleted DEREG/ITIB mice, the adoptively transferred Tregs originated from mice that did not harbor the DT promoter containing transgene. In the case of this second Treg sort, only surface markers CD4 and CD25, but not the intracellular marker of Foxp3, could be used in order to prevent loss of viability due to permeabilization of the Tregs. Foxp3 staining of a small aliquot of sorted cells revealed that only 30 % of the adoptively transferred cells were $Foxp3^{+}$ (Figure 25), which indicates that the remaining 70 % are naïve $CD4^{+}$ T cells. An effect on increased ALT levels by these $CD4^{+}$ T cells is rather unlikely, since the same kind of cells should be present in the DEREG/ITIB mice with only AdHBVx- infection. An influencing effect on ALT levels and increased cell counts by the transferred Tregs can therefore only be connected to the number of transferred cells or that the adoptive Treg transfer impaired Tregs functions. The numbers of transferred cells with $1.5x10^{4}$ $CD4^{+}$ $CD25^{high}$ cells do not account for the increase in leukocyte numbers after the adoptive transfer. As more Tregs were present in the liver on the day of analysis, the transferred number of Tregs should be titrated in order to find the optimal amount for transferred Tregs that will result in steady cell counts and ideally also in rescued ALT levels compared to mice with AdHBVx- infection only. Though, cell counts of hepatic $CD4^{+}$ T cells and $CD8^{+}$ T cells were also higher in mice after adoptive Treg transfer (Figure 27), which is unlikely a result of transferred cells but of recruitment. Analysis of a potential impairment dependent on the sort and adoptive transfer of the Treg function should be performed by tracking the fate of the adoptively transferred cells.

In order to determine the fate of the transferred Tregs in future experiments, staining of the congenic marker CD45.1 should be used, which allows for the separation of the $CD45.1^{+}$ transferred cells of the CD45.1 donor mice from the $CD45.2^{+}$ cells in liver and spleen of the recipient DEREG/ITIB mouse. Tracking of the IL-10 production by the transferred Tregs is not possible due to the missing transgene for the IL-10 reporter reaction in CD45.1 donor mice. Monitoring of the IL-10 production solely by the transferred Tregs would only be allowed by the transfer of DEREG/ITIB derived Tregs into CD45.1 recipient

mice lacking the transgene for the IL-10 reporter reaction. Moreover, histological staining of Tregs in the liver could answer the question whether the i.p. injected Tregs are actually migrating to the liver. If the transferred Tregs are not detectable in the liver shortly after adoptive transfer, the time of the adoptive transfer could be preponed so that the Tregs would have more time for distribution before i.v. injection of AdHBVx- that is directed to the liver (Shayakhmetov *et al.* 2004). The question, whether the regulatory role of Tregs is mediated by Treg derived IL-10 is responsible for the induction of IL-10 production by adaptive immune cells, needs to be addressed in a future experiment by transferring IL-10 deficient Tregs obtained from IL-$10^{flx/flx}$CD4Cre^{+} mice into Treg depleted DEREG/ITIB mice. In comparison with the here presented data, the adoptively transferred IL-10 deficient Tregs should not induce IL-10 production by $CD4^{+}$ T cells and $CD8^{+}$ T cells. A kinetic of AdHBVx-infected and Treg depleted DEREG/ITIB mice with and without adoptively transferred Tregs would allow further monitoring of the importance of Treg mediated establishment of the adaptive immune response.

In conclusion, the AdHBVx- infected DEREG/ITIB mouse proved to be a very useful tool to investigate the critical role of Tregs at the very beginning of the infection in regulating the immune response with regard to IL-10 production that balances suppressor and effector functions. The present study confirms previous findings of Treg depletion experiments and contributes additional evidence suggesting that Tregs are initially needed for the recruitment of cells of the innate and the adaptive immune response and that Tregs are further important for IL-10 production by cells of the adaptive immune response. With these findings the initially made hypothesis needs to be revised. Thus, it is hypothesized that Tregs induce the IL-10 production only of cells of the adaptive immune response, thereby mitigating the establishment of the adaptive immune response against HBV. The IL-10 production by cells of the innate immune response seems to be independent of Tregs. A more profound understanding of the mitigation of the anti-HBV immune response by Tregs provides a valuable basis for the development of novel therapeutic strategies. In order to prevent disturbances in the immune homeostasis, only well-known mechanisms of the anti-inflammatory regulation can be targeted in chronic HBV patients in order to recover the deficient HBV specific T cell response, whose lack is thought to be the reason for persistence of the virus.

5 Bibliography

Abel, M. *et al.* (2006). Intrahepatic virus-specific IL-10-producing CD8 T cells prevent liver damage during chronic hepatitis C virus infection, *Hepatology* 44 (6):1607-16

Accapezzato, D. *et al.* (2004). Hepatic expansion of a virus-specific regulatory CD8(+) T cell population in chronic hepatitis C virus infection, *J Clin Invest* 113 (7):963-72

Akira, S. *et al.* (2006). Pathogen recognition and innate immunity, *Cell* 124 (4):783-801

Alatrakchi, N., Koziel, M. (2009). Regulatory T cells and viral liver disease, *J Viral Hepat* 16 (4):223-9

Alba, R. *et al.* (2005). Gutless adenovirus: last-generation adenovirus for gene therapy, *Gene Ther* 12 Suppl 1 S18-27

Altenburg, A.F. *et al.* (2015). Virus-specific T cells as correlate of (cross-)protective immunity against influenza, *Vaccine* 33 (4):500-506

Araki, K. *et al.* (1989). Expression and replication of hepatitis B virus genome in transgenic mice, *Proc Natl Acad Sci U S A* 86 (1):207-11

Arzberger, S. (2009). Significance of Apoptosis in Hepatitis B Virus Infection, *PhD Thesis*

Arzberger, S. *et al.* (2010). Apoptosis of hepatitis B virus-infected hepatocytes prevents release of infectious virus, *J Virol* 84 (22):11994-2001

Asabe, S. *et al.* (2009). The size of the viral inoculum contributes to the outcome of hepatitis B virus infection, *J Virol* 83 (19):9652-62

Backes, S. *et al.* (submitted). Protein-prime/ modified vaccinia virus Ankara vector-boost vaccination overcomes tolerance in high-antigenemic HBV-transgenic mice,

Baecher-Allan, C. *et al.* (2004). Human CD4+CD25+ regulatory T cells, *Semin Immunol* 16 (2):89-98

Banchereau, J., Steinman, R.M. (1998). Dendritic cells and the control of immunity, *Nature* 392 (6673):245-52

Barabas, S. *et al.* (2008). Urea-mediated cross-presentation of soluble Epstein-Barr virus BZLF1 protein, *PLoS Pathog* 4 (11):e1000198

Barker, L.F. *et al.* (1973). Transmission of type B viral hepatitis to chimpanzees, *J Infect Dis* 127 (6):648-62

Barker, R.N. *et al.* (2002). Antigen presentation by macrophages is enhanced by the uptake of necrotic, but not apoptotic, cells, *Clin Exp Immunol* 127 (2):220-5

Barrat, F.J. *et al.* (2002). In vitro generation of interleukin 10-producing regulatory CD4(+) T cells is induced by immunosuppressive drugs and inhibited by T helper type 1 (Th1)- and Th2-inducing cytokines, *J Exp Med* 195 (5):603-16

Bauer, T. *et al.* (2011). Immune control of hepatitis B virus, *Dig Dis* 29 (4):423-33

Beck, J., Nassal, M. (2007). Hepatitis B virus replication, *World J Gastroenterol* 13 (1):48-64

Bendelac, A. *et al.* (2007). The biology of NKT cells, *Annu Rev Immunol* 25 297-336

Benihoud, K. *et al.* (1999). Adenovirus vectors for gene delivery, *Curr Opin Biotechnol* 10 (5):440-7

Bercovici, N. *et al.* (2000). New methods for assessing T-cell responses, *Clin Diagn Lab Immunol* 7 (6):859-64

Berg, J.M. *et al.*: Biochemie, 5. Auflage, 5th. Aufl., Berlin 2003.

Bertoletti, A., Ferrari, C. (2013). Innate and adaptive immune responses in chronic hepatitis B virus infections: towards restoration of immune control of viral infection, *Postgrad Med J* 89 (1051):294-304

Bertoletti, A., Gehring, A. (2007). Immune response and tolerance during chronic hepatitis B virus infection, *Hepatol Res* 37 Suppl 3 S331-8

Bertoletti, A., Gehring, A.J. (2006). The immune response during hepatitis B virus infection, *J Gen Virol* 87 (Pt 6):1439-49

Bertolino, P. *et al.* (2001). Antigen-specific primary activation of CD8+ T cells within the liver, *J Immunol* 166 (9):5430-8

Billerbeck, E. *et al.* (2007). Regulatory T cells in viral hepatitis, *World J Gastroenterol* 13 (36):4858-64

Billeskov, R. *et al.* (2007). Induction of CD8 T cells against a novel epitope in TB10.4: correlation with mycobacterial virulence and the presence of a functional region of difference-1, *J Immunol* 179 (6):3973-81

Blair, G.E., Blair-Zajdel, M.E. (2004). Evasion of the immune system by adenoviruses, *Curr Top Microbiol Immunol* 273 3-28

Bode, C. *et al.* (2011). CpG DNA as a vaccine adjuvant, *Expert Rev Vaccines* 10 (4):499-511

Boni, C. *et al.* (2007). Characterization of hepatitis B virus (HBV)-specific T-cell dysfunction in chronic HBV infection, *J Virol* 81 (8):4215-25

Bordner, A.J. (2013). Structure-based prediction of Major Histocompatibility Complex (MHC) epitopes, *Methods Mol Biol* 1061 323-43

Bouabe, H. (2012). Cytokine reporter mice: the special case of IL-10, *Scand J Immunol* 75 (6):553-67

Bouabe, H. *et al.* (2011). Novel highly sensitive IL-10-beta-lactamase reporter mouse reveals cells of the innate immune system as a substantial source of IL-10 in vivo, *J Immunol* 187 (6):3165-76

Bruss, V. (2007). Hepatitis B virus morphogenesis, *World J Gastroenterol* 13 (1):65-73

Bruss, V., Vieluf, K. (1995). Functions of the internal pre-S domain of the large surface protein in hepatitis B virus particle morphogenesis, *J Virol* 69 (11):6652-7

Bryceson, Y.T., Long, E.O. (2008). Line of attack: NK cell specificity and integration of signals, *Curr Opin Immunol* 20 (3):344-52

Busca, A., Kumar, A. (2014). Innate immune responses in hepatitis B virus (HBV) infection, *Virol J* 11 22

Busche, A. *et al.* (2013). Priming of CD8+ T cells against cytomegalovirus-encoded antigens is dominated by cross-presentation, *J Immunol* 190 (6):2767-77

Caridade, M. *et al.* (2013). Mechanisms Underlying CD4+ Treg Immune Regulation in the Adult: From Experiments to Models, *Front Immunol* 4 378

Cavanaugh, V.J. *et al.* (1998). Inhibition of hepatitis B virus replication during adenovirus and cytomegalovirus infections in transgenic mice, *J Virol* 72 (4):2630-7

Chen, Y. *et al.* (2005). Activation and function of hepatic NK cells in hepatitis B infection: an underinvestigated innate immune response, *J Viral Hepat* 12 (1):38-45

Chisari, F.V., Ferrari, C. (1995). Hepatitis B virus immunopathogenesis, *Annu Rev Immunol* 13 29-60

Chiu, C. *et al.* (2014). Broadly reactive human CD8 T cells that recognize an epitope conserved between VZV, HSV and EBV, *PLoS Pathog* 10 (3):e1004008

Chu, T.H. *et al.* (2014). Nucleic acid chaperone activity associated with the arginine-rich domain of human hepatitis B virus core protein, *J Virol* 88 (5):2530-43

Clute, S.C. *et al.* (2005). Cross-reactive influenza virus-specific CD8+ T cells contribute to lymphoproliferation in Epstein-Barr virus-associated infectious mononucleosis, *J Clin Invest* 115 (12):3602-12

Cohen, D. *et al.* (2010). Hepatitis B virus activates deoxynucleotide synthesis in nondividing hepatocytes by targeting the R2 gene, *Hepatology* 51 (5):1538-46

Constant, S. *et al.* (1995). B lymphocytes can be competent antigen-presenting cells for priming CD4+ T cells to protein antigens in vivo, *J Immunol* 155 (8):3734-41

Constant, S.L. (1999). B lymphocytes as antigen-presenting cells for CD4+ T cell priming in vivo, *J Immunol* 162 (10):5695-703

Couper, K.N. *et al.* (2008). IL-10: the master regulator of immunity to infection, *J Immunol* 180 (9):5771-7

Crowther, R.A. *et al.* (1994). Three-dimensional structure of hepatitis B virus core particles determined by electron cryomicroscopy, *Cell* 77 (6):943-50

Dane, D.S. *et al.* (1970). Virus-like particles in serum of patients with Australia-antigen-associated hepatitis, *Lancet* 1 (7649):695-8

Das, A. *et al.* (2012). IL-10-producing regulatory B cells in the pathogenesis of chronic hepatitis B virus infection, *J Immunol* 189 (8):3925-35

Debrick, J.E. *et al.* (1991). Macrophages as accessory cells for class I MHC-restricted immune responses, *J Immunol* 147 (9):2846-51

Dembek, C., Protzer, U. (2015). Mouse models for therapeutic vaccination against hepatitis B virus, *Med Microbiol Immunol* 204 (1):95-102

Desmond, C.P. *et al.* (2008). A systematic review of T-cell epitopes in hepatitis B virus: identification, genotypic variation and relevance to antiviral therapeutics, *Antivir Ther* 13 (2):161-75

Di, Q. *et al.* (1997). Major differences between WHV and HBV in the regulation of transcription, *Virology* 229 (1):25-35

Dunn, C. *et al.* (2009). Temporal analysis of early immune responses in patients with acute hepatitis B virus infection, *Gastroenterology* 137 (4):1289-300

Durantel, D., Zoulim, F. (2009). Innate response to hepatitis B virus infection: observations challenging the concept of a stealth virus, *Hepatology* 50 (6):1692-5

Endharti, A.T. *et al.* (2005). Cutting edge: CD8+CD122+ regulatory T cells produce IL-10 to suppress IFN-gamma production and proliferation of CD8+ T cells, *J Immunol* 175 (11):7093-7

Falk, K. *et al.* (1991). Allele-specific motifs revealed by sequencing of self-peptides eluted from MHC molecules, *Nature* 351 (6324):290-6

Feitelson, M.A. *et al.* (2014). The roles of hepatitis B virus-encoded X protein in virus replication and the pathogenesis of chronic liver disease, *Expert Opin Ther Targets* 18 (3):293-306

Fisicaro, P. *et al.* (2009). Early kinetics of innate and adaptive immune responses during hepatitis B virus infection, *Gut* 58 (7):974-82

Flyer, D.C. *et al.* (2002). Identification by mass spectrometry of CD8(+)-T-cell Mycobacterium tuberculosis epitopes within the Rv0341 gene product, *Infect Immun* 70 (6):2926-32

Franzese, O. *et al.* (2005). Modulation of the CD8+-T-cell response by CD4+ CD25+ regulatory T cells in patients with hepatitis B virus infection, *J Virol* 79 (6):3322-8

Fung, J., Yuen, M.F. (2012). This is hepatitis - it is closer than you think, *Indian J Med Res* 136 (1):3-6

Gajewski, T.F. (2000). Monitoring specific T-cell responses to melanoma vaccines: ELISPOT, tetramers, and beyond, *Clin Diagn Lab Immunol* 7 (2):141-4

Ganem, D., Prince, A.M. (2004). Hepatitis B virus infection - natural history and clinical consequences, *N Engl J Med* 350 (11):1118-29

Gao, G.F., Jakobsen, B.K. (2000). Molecular interactions of coreceptor CD8 and MHC class I: the molecular basis for functional coordination with the T-cell receptor, *Immunol Today* 21 (12):630-6

Germain, R.N. (1994). MHC-dependent antigen processing and peptide presentation: providing ligands for T lymphocyte activation, *Cell* 76 (2):287-99

Grant, L.R. *et al.* (2008). Stat4-dependent, T-bet-independent regulation of IL-10 in NK cells, *Genes Immun* 9 (4):316-27

Gregoire, C. *et al.* (2007). The trafficking of natural killer cells, *Immunol Rev* 220 169-82

Grimm, D. *et al.* (2013). Hepatitis B virus: from immunobiology to immunotherapy, *Clin Sci (Lond)* 124 (2):77-85

Guidotti, L.G. *et al.* (1996). Intracellular inactivation of the hepatitis B virus by cytotoxic T lymphocytes, *Immunity* 4 (1):25-36

Guidotti, L.G. *et al.* (1995). High-level hepatitis B virus replication in transgenic mice, *J Virol* 69 (10):6158-69

Guidotti, L.G. *et al.* (1999). Viral clearance without destruction of infected cells during acute HBV infection, *Science* 284 (5415):825-9

Gunther, S. *et al.* (1998). Analysis of hepatitis B virus populations in an interferon-alpha-treated patient reveals predominant mutations in the C-gene and changing e-antigenicity, *Virology* 244 (1):146-60

Haanen, J.B. *et al.* (1999). Selective expansion of cross-reactive CD8(+) memory T cells by viral variants, *J Exp Med* 190 (9):1319-28

Hadziyannis, S.J. (2011). Milestones and perspectives in viral hepatitis B, *Liver Int* 31 Suppl 1 129-34

Haribhai, D. *et al.* (2011). A requisite role for induced regulatory T cells in tolerance based on expanding antigen receptor diversity, *Immunity* 35 (1):109-22

Heermann, K.H. *et al.* (1984). Large surface proteins of hepatitis B virus containing the pre-s sequence, *J Virol* 52 (2):396-402

Hegenbarth, S. *et al.* (2000). Liver sinusoidal endothelial cells are not permissive for adenovirus type 5, *Hum Gene Ther* 11 (3):481-6

Heit, A. *et al.* (2004). CpG-DNA aided cross-priming by cross-presenting B cells, *J Immunol* 172 (3):1501-7

Held, P. (2007). GeneBLAzer® FRET Cell-based Assay from InvitrogenTM on SynergyTM 4, *www.biotek.com*

Hodgson, P.D., Michalak, T.I. (2001). Augmented hepatic interferon gamma expression and T-cell influx characterize acute hepatitis progressing to recovery and residual lifelong

virus persistence in experimental adult woodchuck hepatitis virus infection, *Hepatology* 34 (5):1049-59

Hsieh, C.S. *et al.* (2004). Recognition of the peripheral self by naturally arising CD25+ CD4+ T cell receptors, *Immunity* 21 (2):267-77

Huang, H.C. *et al.* (2012). Entry of hepatitis B virus into immortalized human primary hepatocytes by clathrin-dependent endocytosis, *J Virol* 86 (17):9443-53

Huang, L.R. *et al.* (2006). An immunocompetent mouse model for the tolerance of human chronic hepatitis B virus infection, *Proc Natl Acad Sci U S A* 103 (47):17862-7

Hyodo, N. *et al.* (2004). Hepatitis B core antigen stimulates interleukin-10 secretion by both T cells and monocytes from peripheral blood of patients with chronic hepatitis B virus infection, *Clin Exp Immunol* 135 (3):462-6

Irwin, M.J. *et al.* (1989). Species-restricted interactions between CD8 and the alpha 3 domain of class I influence the magnitude of the xenogeneic response, *J Exp Med* 170 (4):1091-101

Isogawa, M. *et al.* (2005a). Differential dynamics of the peripheral and intrahepatic cytotoxic T lymphocyte response to hepatitis B surface antigen, *Virology* 333 (2):293-300

Isogawa, M. *et al.* (2005b). Toll-like receptor signaling inhibits hepatitis B virus replication in vivo, *J Virol* 79 (11):7269-72

Jäger, C. (2015). Therapeutic vaccination using MVA-vectors in a murine model of chronic HBV infection, *PhD Thesis*

Joffre, O.P. *et al.* (2012). Cross-presentation by dendritic cells, *Nat Rev Immunol* 12 (8):557-69

Jung, S. *et al.* (2002). In vivo depletion of CD11c+ dendritic cells abrogates priming of CD8+ T cells by exogenous cell-associated antigens, *Immunity* 17 (2):211-20

Kafri, T. *et al.* (1998). Cellular immune response to adenoviral vector infected cells does not require de novo viral gene expression: implications for gene therapy, *Proc Natl Acad Sci U S A* 95 (19):11377-82

Kakimi, K. *et al.* (2000). Natural killer T cell activation inhibits hepatitis B virus replication in vivo, *J Exp Med* 192 (7):921-30

Karre, K. (2008). Natural killer cell recognition of missing self, *Nat Immunol* 9 (5):477-80

Keating, S.M. *et al.* (2014). Cytokine and chemokine responses in the acute phase of hepatitis B virus replication in naive and previously vaccinated blood and plasma donors, *J Infect Dis* 209 (6):845-54

Kimura, K. *et al.* (2002). Activated intrahepatic antigen-presenting cells inhibit hepatitis B virus replication in the liver of transgenic mice, *J Immunol* 169 (9):5188-95

Kinloch, R. *et al.* (1984). Adenovirus hexon. Sequence comparison of subgroup C serotypes 2 and 5, *J Biol Chem* 259 (10):6431-6

Knapp, B. *et al.* (2009). 3-Layer-based analysis of peptide-MHC interaction: in silico prediction, peptide binding affinity and T cell activation in a relevant allergen-specific model, *Mol Immunol* 46 (8-9):1839-44

Knolle, P.A., Thimme, R. (2014). Hepatic immune regulation and its involvement in viral hepatitis infection, *Gastroenterology* 146 (5):1193-207

Kondo, Y. *et al.* (2013). Hepatitis B surface antigen could contribute to the immunopathogenesis of hepatitis B virus infection, *ISRN Gastroenterol* 2013 935295

Kuhober, A. *et al.* (1996). DNA immunization induces antibody and cytotoxic T cell responses to hepatitis B core antigen in H-2b mice, *J Immunol* 156 (10):3687-95

Lahl, K. *et al.* (2007). Selective depletion of Foxp3+ regulatory T cells induces a scurfy-like disease, *J Exp Med* 204 (1):57-63

Lambotin, M. *et al.* (2010). A look behind closed doors: interaction of persistent viruses with dendritic cells, *Nat Rev Microbiol* 8 (5):350-60

Lassen, M.G. *et al.* (2010). Intrahepatic IL-10 maintains NKG2A+Ly49- liver NK cells in a functionally hyporesponsive state, *J Immunol* 184 (5):2693-701

Lavanchy, D. (2005). Worldwide epidemiology of HBV infection, disease burden and vaccine prevention, *J Clin Virol* 34 Suppl 1 S1-3

Lazdina, U. *et al.* (2003). Priming of cytotoxic T cell responses to exogenous hepatitis B virus core antigen is B cell dependent, *J Gen Virol* 84 (Pt 1):139-46

Lee, S.H. *et al.* (2009). Activating receptors promote NK cell expansion for maintenance, IL-10 production, and CD8 T cell regulation during viral infection, *J Exp Med* 206 (10):2235-51

Leistner, C.M. *et al.* (2008). Role of glycosaminoglycans for binding and infection of hepatitis B virus, *Cell Microbiol* 10 (1):122-33

Lenardo, M. *et al.* (1999). Mature T lymphocyte apoptosis--immune regulation in a dynamic and unpredictable antigenic environment, *Annu Rev Immunol* 17 221-53

Leu, C.M. *et al.* (2014). The hepatitis B virus e antigen suppresses the respiratory burst and mobility of human monocytes and neutrophils, *Immunobiology*

Li, J. *et al.* (2011). Dynamic changes of cytotoxic T lymphocytes (CTLs), natural killer (NK) cells, and natural killer T (NKT) cells in patients with acute hepatitis B infection, *Virol J* 8 199

Liaw, Y.F., Chu, C.M. (2009). Hepatitis B virus infection, *Lancet* 373 (9663):582-92

Lieber, A. *et al.* (1997). The role of Kupffer cell activation and viral gene expression in early liver toxicity after infusion of recombinant adenovirus vectors, *J Virol* 71 (11):8798-807

Limmer, A. *et al.* (2000). Efficient presentation of exogenous antigen by liver endothelial cells to CD8+ T cells results in antigen-specific T-cell tolerance, *Nat Med* 6 (12):1348-54

Lin, H.H. *et al.* (2008). Evaluation of MHC class I peptide binding prediction servers: applications for vaccine research, *BMC Immunol* 9 8

Lipford, G.B. *et al.* (1997). CpG-containing synthetic oligonucleotides promote B and cytotoxic T cell responses to protein antigen: a new class of vaccine adjuvants, *Eur J Immunol* 27 (9):2340-4

Liu, Y.M. *et al.* (2014). High expression of beta2-glycoprotein I is associated significantly with the earliest stages of hepatitis B virus infection, *J Med Virol* 86 (8):1296-306

Loder, F. *et al.* (1999). B cell development in the spleen takes place in discrete steps and is determined by the quality of B cell receptor-derived signals, *J Exp Med* 190 (1):75-89

Lund, J.M. *et al.* (2008). Coordination of early protective immunity to viral infection by regulatory T cells, *Science* 320 (5880):1220-4

Lundegaard, C. *et al.* (2008). NetMHC-3.0: accurate web accessible predictions of human, mouse and monkey MHC class I affinities for peptides of length 8-11, *Nucleic Acids Res* 36 (Web Server issue):W509-12

Lundegaard, C. *et al.* (2010). Major histocompatibility complex class I binding predictions as a tool in epitope discovery, *Immunology* 130 (3):309-18

Madan, R. *et al.* (2009). Nonredundant roles for B cell-derived IL-10 in immune counter-regulation, *J Immunol* 183 (4):2312-20

Maini, M.K. *et al.* (2000). The role of virus-specific CD8(+) cells in liver damage and viral control during persistent hepatitis B virus infection, *J Exp Med* 191 (8):1269-80

Maini, M.K. *et al.* (1999). Direct ex vivo analysis of hepatitis B virus-specific CD8(+) T cells associated with the control of infection, *Gastroenterology* 117 (6):1386-96

Maini, M.K., Schurich, A. (2010). The molecular basis of the failed immune response in chronic HBV: therapeutic implications, *J Hepatol* 52 (4):616-9

Malmstrom, M. *et al.* (2013). Unraveling the evolution of the Atlantic cod's (Gadus morhua L.) alternative immune strategy, *PLoS One* 8 (9):e74004

Manigold, T., Racanelli, V. (2007). T-cell regulation by CD4 regulatory T cells during hepatitis B and C virus infections: facts and controversies, *Lancet Infect Dis* 7 (12):804-13

Martinet, J. *et al.* (2012). Altered functions of plasmacytoid dendritic cells and reduced cytolytic activity of natural killer cells in patients with chronic HBV infection, *Gastroenterology* 143 (6):1586-1596 e8

Milich, D.R. *et al.* (1997). Role of B cells in antigen presentation of the hepatitis B core, *Proc Natl Acad Sci U S A* 94 (26):14648-53

Milich, D.R., McLachlan, A. (1986). The nucleocapsid of hepatitis B virus is both a T-cell-independent and a T-cell-dependent antigen, *Science* 234 (4782):1398-401

Moore, K.W. *et al.* (2001). Interleukin-10 and the interleukin-10 receptor, *Annu Rev Immunol* 19 683-765

Morral, N. *et al.* (1998). High doses of a helper-dependent adenoviral vector yield supraphysiological levels of alpha1-antitrypsin with negligible toxicity, *Hum Gene Ther* 9 (18):2709-16

Mosmann, T.R. *et al.* (1990). Isolation of monoclonal antibodies specific for IL-4, IL-5, IL-6, and a new Th2-specific cytokine (IL-10), cytokine synthesis inhibitory factor, by using a solid phase radioimmunoadsorbent assay, *J Immunol* 145 (9):2938-45

Murai, M. *et al.* (2009). Interleukin 10 acts on regulatory T cells to maintain expression of the transcription factor Foxp3 and suppressive function in mice with colitis, *Nat Immunol* 10 (11):1178-84

Muris, A.H. *et al.* (2012). Intracellular IL-10 detection in T cells by flowcytometry: the use of protein transport inhibitors revisited, *J Immunol Methods* 381 (1-2):59-65

Murphy, K.: Janeway's Immunobiology, 8th. Aufl., New York 2011.

Muruve, D.A. *et al.* (2004). Helper-dependent adenovirus vectors elicit intact innate but attenuated adaptive host immune responses in vivo, *J Virol* 78 (11):5966-72

Muruve, D.A. *et al.* (2008). The inflammasome recognizes cytosolic microbial and host DNA and triggers an innate immune response, *Nature* 452 (7183):103-7

Nakagawa, R. *et al.* (2001). Mechanisms of the antimetastatic effect in the liver and of the hepatocyte injury induced by alpha-galactosylceramide in mice, *J Immunol* 166 (11):6578-84

Nassal, M. (2008). Hepatitis B viruses: reverse transcription a different way, *Virus Res* 134 (1-2):235-49

Neefjes, J. *et al.* (2011). Towards a systems understanding of MHC class I and MHC class II antigen presentation, *Nat Rev Immunol* 11 (12):823-36

Oberwinkler, H. *et al.*: Transfer of HBV Genomes into Mice, Basel 2005.

Op den Brouw, M.L. *et al.* (2009). Hepatitis B virus surface antigen impairs myeloid dendritic cell function: a possible immune escape mechanism of hepatitis B virus, *Immunology* 126 (2):280-9

Ott, J.J. *et al.* (2012). Global epidemiology of hepatitis B virus infection: new estimates of age-specific HBsAg seroprevalence and endemicity, *Vaccine* 30 (12):2212-9

Pace, L. *et al.* (2012). Regulatory T cells increase the avidity of primary CD8+ T cell responses and promote memory, *Science* 338 (6106):532-6

Parks, R.J. *et al.* (1996). A helper-dependent adenovirus vector system: removal of helper virus by Cre-mediated excision of the viral packaging signal, *Proc Natl Acad Sci U S A* 93 (24):13565-70

Patient, R. *et al.* (2009). Morphogenesis of hepatitis B virus and its subviral envelope particles, *Cell Microbiol* 11 (11):1561-70

Penna, A. *et al.* (1991). Cytotoxic T lymphocytes recognize an HLA-A2-restricted epitope within the hepatitis B virus nucleocapsid antigen, *J Exp Med* 174 (6):1565-70

Pentier, J.M. *et al.* (2013). Advances in T-cell epitope engineering, *Front Immunol* 4 133

Peppa, D. *et al.* (2013). Up-regulation of a death receptor renders antiviral T cells susceptible to NK cell-mediated deletion, *J Exp Med* 210 (1):99-114

Peters, B. *et al.* (2005). The immune epitope database and analysis resource: from vision to blueprint, *PLoS Biol* 3 (3):e91

Pils, M.C. *et al.* (2010). Monocytes/macrophages and/or neutrophils are the target of IL-10 in the LPS endotoxemia model, *Eur J Immunol* 40 (2):443-8

Pollicino, T. *et al.* (2014). Hepatitis B virus PreS/S gene variants: pathobiology and clinical implications, *J Hepatol* 61 (2):408-17

Pourkarim, M.R. *et al.* (2014). Molecular identification of hepatitis B virus genotypes/subgenotypes: revised classification hurdles and updated resolutions, *World J Gastroenterol* 20 (23):7152-68

Pozzi, L.A. *et al.* (2005). Both dendritic cells and macrophages can stimulate naive CD8 T cells in vivo to proliferate, develop effector function and differentiate into memory cells, *J Immunol* 175 (4):2071-81

Protzer, U. *et al.* (2012). Living in the liver: hepatic infections, *Nat Rev Immunol* 12 (3):201-13

Quasdorff, M. *et al.* (2008). A concerted action of HNF4alpha and HNF1alpha links hepatitis B virus replication to hepatocyte differentiation, *Cell Microbiol* 10 (7):1478-90

Rammensee, H. *et al.* (1999). SYFPEITHI: database for MHC ligands and peptide motifs, *Immunogenetics* 50 (3-4):213-9

Rehermann, B. *et al.* (1995). The cytotoxic T lymphocyte response to multiple hepatitis B virus polymerase epitopes during and after acute viral hepatitis, *J Exp Med* 181 (3):1047-58

Rehermann, B., Nascimbeni, M. (2005). Immunology of hepatitis B virus and hepatitis C virus infection, *Nat Rev Immunol* 5 (3):215-29

Reiser, M. *et al.* (2011). The immunodominant CD8 T cell response to the human cytomegalovirus tegument phosphoprotein pp65(495-503) epitope critically depends on CD4 T cell help in vaccinated HLA-A*0201 transgenic mice, *J Immunol* 187 (5):2172-80

Riedl, P. *et al.* (2014). Differential presentation of endogenous and exogenous hepatitis B surface antigens influences priming of CD8(+) T cells in an epitope-specific manner, *Eur J Immunol* 44 (7):1981-91

Roggendorf, M., Tolle, T.K. (1995). The woodchuck: an animal model for hepatitis B virus infection in man, *Intervirology* 38 (1-2):100-12

Roncarolo, M.G. *et al.* (2006). Interleukin-10-secreting type 1 regulatory T cells in rodents and humans, *Immunol Rev* 212 28-50

Roomp, K. *et al.* (2010). Predicting MHC class I epitopes in large datasets, *BMC Bioinformatics* 11 90

Roose, K. *et al.* (2013). Hepatitis B core-based virus-like particles to present heterologous epitopes, *Expert Rev Vaccines* 12 (2):183-98

Rosalia, R.A. *et al.* (2013). Dendritic cells process synthetic long peptides better than whole protein, improving antigen presentation and T-cell activation, *Eur J Immunol* 43 (10):2554-65

Rouse, B.T., Sehrawat, S. (2010). Immunity and immunopathology to viruses: what decides the outcome?, *Nat Rev Immunol* 10 (7):514-26

Sag, D. *et al.* (2014). IL-10-producing NKT10 cells are a distinct regulatory invariant NKT cell subset, *J Clin Invest* 124 (9):3725-40

Sakaguchi, S. (2004). Naturally arising CD4+ regulatory t cells for immunologic self-tolerance and negative control of immune responses, *Annu Rev Immunol* 22 531-62

Sakaguchi, S. (2005). Naturally arising Foxp3-expressing CD25+CD4+ regulatory T cells in immunological tolerance to self and non-self, *Nat Immunol* 6 (4):345-52

Sandalova, E. *et al.* (2012). Increased levels of arginase in patients with acute hepatitis B suppress antiviral T cells, *Gastroenterology* 143 (1):78-87 e3

Saraiva, M., O'Garra, A. (2010). The regulation of IL-10 production by immune cells, *Nat Rev Immunol* 10 (3):170-81

Schaefer, S. (2007). Hepatitis B virus taxonomy and hepatitis B virus genotypes, *World J Gastroenterol* 13 (1):14-21

Schieck, A. *et al.* (2013). Hepatitis B virus hepatotropism is mediated by specific receptor recognition in the liver and not restricted to susceptible hosts, *Hepatology* 58 (1):43-53

Schirmbeck, R. *et al.* (2003a). Different immunogenicity of H-2 Kb-restricted epitopes in natural variants of the hepatitis B surface antigen, *Eur J Immunol* 33 (9):2429-38

Schirmbeck, R. *et al.* (2003b). Breaking tolerance in hepatitis B surface antigen (HBsAg) transgenic mice by vaccination with cross-reactive, natural HBsAg variants, *Eur J Immunol* 33 (12):3342-52

Schulze, A. *et al.* (2007). Hepatitis B virus infection initiates with a large surface protein-dependent binding to heparan sulfate proteoglycans, *Hepatology* 46 (6):1759-68

Selin, L.K. *et al.* (1994). Cross-reactivities in memory cytotoxic T lymphocyte recognition of heterologous viruses, *J Exp Med* 179 (6):1933-43

Selin, L.K. *et al.* (1998). Protective heterologous antiviral immunity and enhanced immunopathogenesis mediated by memory T cell populations, *J Exp Med* 188 (9):1705-15

Sellon, R.K. *et al.* (1998). Resident enteric bacteria are necessary for development of spontaneous colitis and immune system activation in interleukin-10-deficient mice, *Infect Immun* 66 (11):5224-31

Sewell, A.K. (2012). Why must T cells be cross-reactive?, *Nat Rev Immunol* 12 (9):669-77

Shayakhmetov, D.M. *et al.* (2004). Analysis of adenovirus sequestration in the liver, transduction of hepatic cells, and innate toxicity after injection of fiber-modified vectors, *J Virol* 78 (10):5368-81

Shepard, C.W. *et al.* (2006). Hepatitis B virus infection: epidemiology and vaccination, *Epidemiol Rev* 28 112-25

Shimizu, Y. (2012). T cell immunopathogenesis and immunotherapeutic strategies for chronic hepatitis B virus infection, *World J Gastroenterol* 18 (20):2443-51

Shouval, D.S. *et al.* (2014). Interleukin-10 receptor signaling in innate immune cells regulates mucosal immune tolerance and anti-inflammatory macrophage function, *Immunity* 40 (5):706-19

Sitia, G. *et al.* (2004). MMPs are required for recruitment of antigen-nonspecific mononuclear cells into the liver by CTLs, *J Clin Invest* 113 (8):1158-67

Sprinzl, M.F. *et al.* (2001). Transfer of hepatitis B virus genome by adenovirus vectors into cultured cells and mice: crossing the species barrier, *J Virol* 75 (11):5108-18

Steinbrink, K. *et al.* (1997). Induction of tolerance by IL-10-treated dendritic cells, *J Immunol* 159 (10):4772-80

Stier, E.M. *et al.* (2005). Differential cytosolic delivery and presentation of antigen by listeriolysin O-liposomes to macrophages and dendritic cells, *Mol Pharm* 2 (1):74-82

Stoop, J.N. *et al.* (2005). Regulatory T cells contribute to the impaired immune response in patients with chronic hepatitis B virus infection, *Hepatology* 41 (4):771-8

Stross, L. (2011). The influence of regulatory T cells and other immunoregulators on the course of Hepatitis B virus infection, *PhD Thesis*

Stross, L. *et al.* (2012). Foxp3+ regulatory T cells protect the liver from immune damage and compromise virus control during acute experimental hepatitis B virus infection in mice, *Hepatology* 56 (3):873-83

Summers, J. (1981). Three recently described animal virus models for human hepatitis B virus, *Hepatology* 1 (2):179-83

Tan, Z. *et al.* (2015). The interface between hepatitis B virus capsid proteins affects self-assembly, pregenomic RNA packaging, and reverse transcription, *J Virol* 89 (6):3275-84

Taraban, V.Y. *et al.* (2002). Expression and costimulatory effects of the TNF receptor superfamily members CD134 (OX40) and CD137 (4-1BB), and their role in the generation of anti-tumor immune responses, *Eur J Immunol* 32 (12):3617-27

Thomas, M.A. *et al.* (2007). A real-time PCR method to rapidly titer adenovirus stocks, *Methods Mol Med* 130 185-92

Tian, Z. *et al.* (2013). Natural killer cells in liver disease, *Hepatology* 57 (4):1654-62

Trobonjaca, Z. *et al.* (2002). Activating immunity in the liver. II. IFN-beta attenuates NK cell-dependent liver injury triggered by liver NKT cell activation, *J Immunol* 168 (8):3763-70

Tu, Z. *et al.* (2008). TLR-dependent cross talk between human Kupffer cells and NK cells, *J Exp Med* 205 (1):233-44

Untergasser, A. *et al.* (2008a). Production of Adenoviral Vectors, *Untergasser's Lab*

Untergasser, A. *et al.* (2008b). Production of Adenoviral Vectors for aplication in test animals, *Untergasser's Lab*

Untergasser, A. *et al.* (2008c). Titration of Adenoviral Vectors, *Untergasser's Lab*

Untergasser, A. *et al.* (2006). Dendritic cells take up viral antigens but do not support the early steps of hepatitis B virus infection, *Hepatology* 43 (3):539-47

Urban, S. *et al.* (2010). The replication cycle of hepatitis B virus, *J Hepatol* 52 (2):282-4

Valitutti, S. *et al.* (1997). Degradation of T cell receptor (TCR)-CD3-zeta complexes after antigenic stimulation, *J Exp Med* 185 (10):1859-64

Veiga-Parga, T. *et al.* (2013). Role of regulatory T cells during virus infection, *Immunol Rev* 255 (1):182-96

von Freyend, M.J. *et al.* (2011). Sequential control of hepatitis B virus in a mouse model of acute, self-resolving hepatitis B, *J Viral Hepat* 18 (3):216-26

Walter, E. *et al.* (1996). Hepatitis B virus infection of tupaia hepatocytes in vitro and in vivo, *Hepatology* 24 (1):1-5

Warrington, K.H., Jr., Herzog, R.W. (2006). Treatment of human disease by adeno-associated viral gene transfer, *Hum Genet* 119 (6):571-603

Watts, C. (2012). The endosome-lysosome pathway and information generation in the immune system, *Biochim Biophys Acta* 1824 (1):14-21

Webster, G.J. *et al.* (2000). Incubation phase of acute hepatitis B in man: dynamic of cellular immune mechanisms, *Hepatology* 32 (5):1117-24

Welsh, R.M., Selin, L.K. (2002). No one is naive: the significance of heterologous T-cell immunity, *Nat Rev Immunol* 2 (6):417-26

Werle-Lapostolle, B. *et al.* (2004). Persistence of cccDNA during the natural history of chronic hepatitis B and decline during adefovir dipivoxil therapy, *Gastroenterology* 126 (7):1750-8

Whitacre, D.C. *et al.* (2009). Use of hepadnavirus core proteins as vaccine platforms, *Expert Rev Vaccines* 8 (11):1565-73

Whitmire, J.K. (2011). Induction and function of virus-specific CD4+ T cell responses, *Virology* 411 (2):216-28

WHO (2009). Hepatitis B vaccines, *Weekly Epidemiological Record* 84, 405-420

WHO: Hepatitis B Factsheet No. 204. Revised July 2004, Erscheinungsort: http://www.who.int/mediacentre/factsheets/fs204/en/#

Wieland, S.F., Chisari, F.V. (2005). Stealth and cunning: hepatitis B and hepatitis C viruses, *J Virol* 79 (15):9369-80

Willcox, B.E. *et al.* (1999). TCR binding to peptide-MHC stabilizes a flexible recognition interface, *Immunity* 10 (3):357-65

Willerford, D.M. *et al.* (1995). Interleukin-2 receptor alpha chain regulates the size and content of the peripheral lymphoid compartment, *Immunity* 3 (4):521-30

Windheim, M. *et al.* (2004). Immune evasion by adenovirus E3 proteins: exploitation of intracellular trafficking pathways, *Curr Top Microbiol Immunol* 273 29-85

Wolfertstetter, F. (2014). Immunological characterization of cross-reactive hepatitis C virus specific T cells, *Master thesis*

Wu, J. *et al.* (2009). Hepatitis B virus suppresses toll-like receptor-mediated innate immune responses in murine parenchymal and nonparenchymal liver cells, *Hepatology* 49 (4):1132-40

Wu, J.F. *et al.* (2014). The impact of hepatitis B virus precore/core gene carboxyl terminal mutations on viral biosynthesis and the host immune response, *J Infect Dis* 209 (9):1374-81

Xu, D. *et al.* (2006). Circulating and liver resident CD4+CD25+ regulatory T cells actively influence the antiviral immune response and disease progression in patients with hepatitis B, *J Immunol* 177 (1):739-47

Xu, L. *et al.* (2014). Kupffer cell-derived IL-10 plays a key role in maintaining humoral immune tolerance in hepatitis B virus-persistent mice, *Hepatology* 59 (2):443-52

Yan, H. *et al.* (2013). Molecular determinants of hepatitis B and D virus entry restriction in mouse sodium taurocholate cotransporting polypeptide, *J Virol* 87 (14):7977-91

Yan, H. *et al.* (2012). Sodium taurocholate cotransporting polypeptide is a functional receptor for human hepatitis B and D virus, *Elife* 1 e00049

Yang, G. *et al.* (2007). Association of CD4+CD25+Foxp3+ regulatory T cells with chronic activity and viral clearance in patients with hepatitis B, *Int Immunol* 19 (2):133-40

Yang, P.L. *et al.* (2002). Hydrodynamic injection of viral DNA: a mouse model of acute hepatitis B virus infection, *Proc Natl Acad Sci U S A* 99 (21):13825-30

Yang, Y. *et al.* (1994). MHC class I-restricted cytotoxic T lymphocytes to viral antigens destroy hepatocytes in mice infected with E1-deleted recombinant adenoviruses, *Immunity* 1 (5):433-42

Yu, X. *et al.* (2013). 3.5A cryoEM structure of hepatitis B virus core assembled from full-length core protein, *PLoS One* 8 (9):e69729

Zeissig, S. *et al.* (2012). Hepatitis B virus-induced lipid alterations contribute to natural killer T cell-dependent protective immunity, *Nat Med* 18 (7):1060-8

Zhang, H. *et al.* (2009). Comparing pooled peptides with intact protein for accessing cross-presentation pathways for protective CD8+ and CD4+ T cells, *J Biol Chem* 284 (14):9184-91

Zhang, W.W. (1999). Development and application of adenoviral vectors for gene therapy of cancer, *Cancer Gene Ther* 6 (2):113-38

Zheng, M. *et al.* (2013). Characterization of the liver-draining lymph nodes in mice and their role in mounting regional immunity to HBV, *Cell Mol Immunol* 10 (2):143-50

Zlotnick, A. *et al.* (1999). A theoretical model successfully identifies features of hepatitis B virus capsid assembly, *Biochemistry* 38 (44):14644-52

6 Appendix

6.1 Peptides of HBc P1, HBc P2, HBc P3

Table 25: Peptide pools HBc P1, HBc P2, HBc P3 with peptide sequences. The sequence is based on the HBcAg, genotype D, sequence of (Gunther *et al.* 1998).

Peptide pool	Peptide number	Sequence
HBc P1	1	MDIDPYKEFGATVQL
	2	PYKEFGATVQLLSFL
	3	FGATVQLLSFLPHDF
	4	VQLLSFLPHDFFPSV
	5	SFLPHDFFPSVRDLL
	6	HDFFPSVRDLLDTAS
	7	PSVRDLLDTASALFR
	8	DLLDTASALFRDALE
	9	TASALFRDALESPEH
	10	LFRDALESPEHCSPH
	11	ALESPEHCSPHHTAL
	12	PEHCSPHHTALRQAI
	13	SPHHTALRQAILCWG
	14	TALRQAILCWGELMT
	15	QAILCWGELMTLATW
HBc P2	16	CWGELMTLATWVGAN
	17	LMTLATWVGANLQDP
	18	ATWVGANLQDPASRE
	19	GANLQDPASRELVVT
	20	QDPASRELVVTYVNI
	21	SRELVVTYVNINMGL
	22	VVTYVNINMGLKFRQ
	23	VNINMGLKFRQLLWF
	24	MGLKFRQLLWFHISC
	25	FRQLLWFHISCLTFG
	26	LWFHISCLTFGRETV
	27	ISCLTFGRETVIEYL
	28	TFGRETVIEYLVSFG
	29	ETVIEYLVSFGVWIR
	30	EYLVSFGVWIRTPQA
HBc P3	31	SFGVWIRTPQAYRPP
	32	WIRTPQAYRPPNAPI
	33	PQAYRPPNAPILSTL
	34	RPPNAPILSTLPETT
	35	APILSTLPETTVVRR
	36	STLPETTVVRRRGRS
	37	ETTVVRRRGRSPRRR
	38	VRRRGRSPRRRTPSP
	39	GRSPRRRTPSPRRRR
	40	RRRTPSPRRRRSQSP
	41	PSPRRRRSQSPRRRR
	42	RRRSQSPRRRRSQSR
	43	QSPRRRRSQSRESQC

6.2 Epitope prediction results of HBc P5

Table 26: SYFPEITHI scores of peptides after epitope prediction performed by Silke Arzberger. Peptides were combined to form peptide pool HBc P5.

Peptide Pool	Position (aa)	Sequence	SYFPEITHI Score
HBc P5	136-143	NAPILSTL	14
	133-140	RPPNAPIL	12
	140-147	LSTLPETT	4
	137-144	APILSTLP	3
	20-27	PTDFFPSV	16
	86-93	VNYVNTNM	15

6.3 Sequences used for epitope prediction

The sequences used for epitope prediction of Ad hexon, HBcAg and HBsAg derived from the plasmid p173 encoding the AdHBV vector construct. Prior to epitope prediction, the plasmid sequence was sequenced and confirmed by Antje Malo.

6.3.1 Protein sequence of Ad hexon

MATPSMMPQWSYMHISGQDASEYLSPGLVQFARATETYFSLNNKFRNPTVAPTHDV
TTDRSQRLTLRFIPVDREDTAYSYKARFTLAVGDNRVLDMASTYFDIRGVLDRGPTF
KPYSGTAYNALAPKGAPNPCEWDEAATALEINLEEEDDDNEDEVDEQAEQQKTHVF
GQAPYSGINITKEGIQIGVEGQTPKYADKTFQPEPQIGESQWYETEINHAAGRVLKKT
TPMKPCYGSYAKPTNENGGQGILVKQQNGKLESQVEMQFFSTTEATAGNGDNLTPK
VVLYSEDVDIETPDTHISYMPTIKEGNSRELMGQQSMPNRPNYIAFRDNFIGLMYYNS
TGNMGVLAGQASQLNAVVDLQDRNTELSYQLLLDSIGDRTRYFSMWNQAVDSYDP
DVRIIENHGTEDELPNYCFPLGGVINTETLTKVKPKTGQENGWEKDATEFSDKNEIRV
GNNFAMEINLNANLWRNFLYSNIALYLPDKLKYSPSNVKISDNPNTYDYMNKRVVA
PGLVDCYINLGARWSLDYMDNVNPFNHHRNAGLRYRSMLLGNGRYVPFHIQVPQKF
FAIKNLLLLPGSYTYEWNFRKDVNMVLQSSLGNDLRVDGASIKFDSICLYATFFPMA
HNTASTLEAMLRNDTNDQSFNDYLSAANMLYPIPANATNVPISIPSRNWAAFRGWAF
TRLKTKETPSLGSGYDPYYTYSGSIPYLDGTFYLNHTFKKVAITFDSSVSWPGNDRLL
TPNEFEIKRSVDGEGYNVAQCNMTKDWFLVQMLANYNIGYQGFYIPESYKDRMYSF
FRNFQPMSRQVVDDTKYKDYQQVGILHQHNNSGFVGYLAPTMREGQAYPANFPYPL
IGKTAVDSITQKKFLCDRTLWRIPFSSNFMSMGALTDLGQNLLYANSAHALDMTFEV
DPMDEPTLLYVLFEVFDVVRVHRPHRGVIETVYLRTPFSAGNATT

6.3.2 Protein sequence of HBcAg

MDIDPYKEFGATVELLSFLPSDFFPSVRDLLDTASALYREALESPEHCSPHHTALRQAI
LCWGELMTLATWVGVNLEDPASRDLVVSYVNTNMGLKFRQLLWFHISCLTFGRETV
IEYLVSFGVWIRTPPAYRPPNAPILSTLPETTVVRRRGRSPRRRTPSPRRRRSQSPRRRR
SQSRESQC

6.3.3 Protein sequence of HBsAg

MENITSGFLGPLLVLQAGFFLLTRILTIPQSLDSWWTSLNFLGGTTVCLGQNSQSPTSN
HSPTSCPPTCPGYRWMCLRRFIIFLFILLLCLIFLLVLLDYQGMLPVCPLIPGSSTTSTGP
CRTCMTTAQGTSMYPSCCCTKPSDGNCTCIPIPSSWAFGKFLWEWASARFSWLSLLV
PFVQWFVGLSPTVWLSVIWMMWYWGPSLYSILSPFLPLLPIFFCLWVYI

6.4 Sequence alignments of HBcAg and pp65 protein

6.4.1 Sequence alignment of HBc_C18 peptide with pp65 protein

```
Alignment of Sequence_1:  [C18 Peptide] with  Sequence_2: [pp65 Protein-Seq.xprt]
Similarity : 9/10 (90,00 %)
Seq_1  1     ------------------------------------------------------------  0
Seq_2  1     MESRGRRCPEMISVLGPISGHVLKAVFSRGDTPVLPHETRLLQTGIHVRVSQPSLILVSQ  60

Seq_1  1     ------------------------------------------------------------  0
Seq_2  61    YTPDSTPCHRGDNQLQVQHTYFTGSEVENVSVNVHNPTGRSICPSQEPMSIYVYALPLKM  120

Seq_1  1     ------------------------------------------------------------  0
Seq_2  121   LNIPSINVHHYPSAAERKHRHLPVADAVIHASGKQMWQARLTVSGLAWTRQQNQWKEPDV  180

Seq_1  1     ------------------------------------------------------------  0
Seq_2  181   YYTSAFVFPTKDVALRHVVCAHELVCSMENTRATKMQVIGDQYVKVYLESFCEDVPSGKL  240

Seq_1  1     ----FLPSDFFPFV----------------------------------------------  10
                 :|:||::::
Seq_2  241   FMHVTLGSDVEEDLTMTRNPQPFMRPHERNGFTVLCPKNMIIKPGKISHIMLDVAFTSHE  300

Seq_1  11    ------------------------------------------------------------  10
Seq_2  301   HFGLLCPKSIPGLSISGNLLMNGQQIFLEVQAIRETVELRQYDPVAALFFFDIDLLLQRG  360

Seq_1  11    ------------------------------------------------------------  10
Seq_2  361   PQYSEHPTFTSQYRIQGKLEYRHTWDRHDEGAAQGDDDVWTSGSDSDEELVTTERKTPRV  420

Seq_1  11    ------------------------------------------------------------  10
Seq_2  421   TGGGAMAGASTSAGRKRKSASSATACTSGVMTRGRLKAESTVAPEEDTDEDSDNEIHNPA  480

Seq_1  11    ------------------------------------------------------------  10
Seq_2  481   VFTWPPWQAGILARNLVPMVATVQGQNLKYQEFFWDANDIYRIFAELEGVWQPAAQPKRR  540

Seq_1  11    ----------------------  10
Seq_2  541   RHRQDALPGPCIASTPKKHRG  561
```

6.4.2 Sequence alignment of HBcAg protein with pp65 protein

```
Alignment of Sequence_1:  [HBc aus Translation p173] with  Sequence_2: [pp65
Protein-Seq.xprt]

Similarity : 122/183 (66,67 %)

Seq_1  1     ------------------------------------------------------------  0

Seq_2  1     MESRGRRCPEMISVLGPISGHVLKAVFSRGDTPVLPHETRLLQTGIHVRVSQPSLILVSQ  60


Seq_1  1     ------------------------------------------------------------  0

Seq_2  61    YTPDSTPCHRGDNQLQVQHTYFTGSEVENVSVNVHNPTGRSICPSQEPMSIYVYALPLKM  120


Seq_1  1     ------------------------------------------------------------  0

Seq_2  121   LNIPSINVHHYPSAAERKHRHLPVADAVIHASGKQMWQARLTVSGLAWTRQQNQWKEPDV  180


Seq_1  1     ------------------------------------------------------------  0

Seq_2  181   YYTSAFVFPTKDVALRHVVCAHELVCSMENTRATKMQVIGDQYVKVYLESFCEDVPSGKL  240


Seq_1  1     ------------------------------------------------------------  0

Seq_2  241   FMHVTLGSDVEEDLTMTRNPQPFMRPHERNGFTVLCPKNMIIKPGKISHIMLDVAFTSHE  300


Seq_1  1     ----------------------MDI-DPYKEFGATVELLSFLPSDFFPSVRDLLDTASA  36
                                   |   :: ::: ||||: ::|:::::  : :|   :
Seq_2  301   HFGLLCPKSIPGLSISGNLLMNGQQIFLEVQAIRETVELRQYDPVAALFFFDIDLLLQRG  360


Seq_1  37    LYREALESPEHCSPHHTALRQAILCWGELMTLATWVGVNLEDPASRDLVVSYVNTNMGLK  96
             :  : :: ::: ::     | :::: ::::  :|  :::::::: ::|:  ::   :  ::
Seq_2  361   PQYSEHPTFTSQYRIQGKLEYRHTWDRHDEGAAQGDDDVWTSGSDSDEELVTTERKTPRV  420


Seq_1  97    FRQLLWFHISCLTFGRETVIEYLVSFGVWIRTPPAYRPPNAPILSTLPETTVVRRRGRSP  156
             ::::::: :| : :::::::::::  : : ::|::: :::: :::  ::: ::::   : :
Seq_2  421   TGGGAMAGASTSAGRKRKSASSATACTSGVMTRGRLKAESTVAPEEDTDEDSDNEIHNPA  480


Seq_1  157   RRRTPSPRRRRSQSPRRRRSQSRESQC---------------------------------  183
             :  :| : ::  ::: : ::: :::|:
Seq_2  481   VFTWPPWQAGILARNLVPMVATVQGQNLKYQEFFWDANDIYRIFAELEGVWQPAAQPKRR  540


Seq_1  184   ----------------------  183

Seq_2  541   RHRQDALPGPCIASTPKKHRG  561
```

7 Acknowledgement

I would like to express my gratitude and thanks to Ulrike Protzer for the opportunity to work in the institute of virology on such an interesting topic and for providing guidance and supervision. Furthermore, I would like to thank Iris Antes and Mathias Heikenwälder as members of my thesis committee for comment and advice.

My thanks and appreciations also go to Hicham Bouabe, Lynette Henkel, Bastian Höchst, Eva Loffredo-Verde and Andreas Moosmann for helpful collaborations. Furthermore, I would like to thank Matthias Schiemann for advice with diverse computer issues.

I would like to extend my sincere thanks to Theresa Asen, Marvin Festag, Antje Malo and Natalie Röder for their support during mouse experiments and virus production. Furthermore, I would like to thank the following people for their kind support and help directly and indirectly to complete this work: Kerstin Ackermann, Christian Bach, Tanja Bauer, Julia Beneke, Romina Bester, Christoph Blossey, Jan-Hendrick Bockmann, Felix Bohne, Nina Böttinger, Claudia Breit, Xiaoming Cheng, Wen-Min Chou, Christina Dargel, Claudia Dembek, Michael Dudek, Knud Esser, Uwe Friedrich, Hanaa Gaber, Familie Graf, Julia Graf, Julia Hasreiter, AG Heikenwälder, Clemens Jäger, Kathrin Kappes, Nina Körber, Miriam Lekic, Thomas Michler, Martin Mück-Häusl, Andreas Muschaweckh, Doris Pelz, Oliver Quitt, Carolina Russo, Beate Schittl, Katrin Singethan, Daniela Stadler, Raindy Tedjokusumo, Frank Thiele, Andrea Weicht, Clara Wende, Jochen Wettengel, Karin Wisskirchen, Yuchen Xia and Ke Zhang.